Advances in Colloid and Interface Science 205 (2014) 275–318

Contents lists available at ScienceDirect

Advances in Colloid and Interface Science

journal homepage: www.elsevier.com/locate/cis

Anionic biopolyelectrolytes of the syndecan/perlecan superfamily: Physicochemical properties and medical significance

G. Siegel [a,b,*], M. Malmsten [b,a], E. Ermilov [a]

[a] Charité — University Clinic Berlin, 10117 Berlin, Germany
[b] University of Uppsala Biomedical Center, 751 23 Uppsala, Sweden

ARTICLE INFO

Available online 25 January 2014

Keywords:
Syndecan/perlecan physicochemistry and molecular biology
Lipoprotein binding receptor
Blood flow sensor
Smooth and heart muscle rhythmogenesis
Cation binding
Tumour invasion and metastasis

ABSTRACT

In the review article presented here, we demonstrate that the connective tissue is more than just a matrix for cells and a passive scaffold to provide physical support. The extracellular matrix can be subdivided into proteins (collagen, elastin), glycoconjugates (structural glycoproteins, proteoglycans) and glycosaminoglycans (hyaluronan). Our main focus rests on the anionic biopolyelectrolytes of the perlecan/syndecan superfamily which belongs to extracellular matrix and cell membrane integral proteoglycans. Though the extracellular domain of the syndecans may well be performing a structural role within the extracellular matrix, a key function of this class of membrane intercalated proteoglycans may be to act as signal transducers across the plasma membrane and thus be more appropriately included in the group of cell surface receptors. Nevertheless, there is a continuum in functions of syndecans and perlecans, especially with respect to their structural role and biomedical significance. HS/CS proteoglycans are receptor sites for lipoprotein binding thus intervening directly in lipid metabolism. We could show that among all lipoproteins, HDL has the highest affinity to these proteoglycans and thus instals a feedforward forechecking loop against atherogenic apoB100 lipoprotein deposition on surface membranes and in subendothelial spaces. Therefore, HDL is not only responsible for VLDL/IDL/LDL cholesterol exit but also controls thoroughly the entry. This way, it inhibits arteriosclerotic nanoplaque formation. The ternary complex 'lipoprotein receptor (HS/CS-PG) – lipoprotein (LDL, oxLDL, Lp(a)) – calcium' may be interpreted as arteriosclerotic nanoplaque build-up on the molecular level before any cellular reactivity, possibly representing the arteriosclerotic primary lesion combined with endothelial dysfunction. With laser-based ellipsometry we could demonstrate that nanoplaque formation is a Ca^{2+}-driven process. In an in vitro biosensor application of HS-PG coated silica surfaces we tested nanoplaque formation and size in clinical trials with cardiovascular high-risk patients who underwent treatment with ginkgo or fluvastatin. While ginkgo reduced nanoplaque formation (size) by 14.3% (23.4%) in the isolated apoB100 lipid fraction at a normal blood Ca^{2+} concentration, the effect of the statin with a reduction of 44.1% (25.4%) was more pronounced. In addition, ginkgo showed beneficial effects on several biomarkers of oxidative stress and inflammation.

Besides acting as peripheral lipoprotein binding receptor, HS/CS-PG is crucially implicated in blood flow sensing. A sensor molecule has to fulfil certain mechanochemical and mechanoelectrical requirements. It should possess viscoelastic and cation binding properties capable of undergoing conformational changes caused both mechanically and electrostatically. Moreover, the latter should be ion-specific. Under no-flow conditions, the viscoelastic polyelectrolyte at the endothelium — blood interface assumes a random coil form. Blood flow causes a

Abbreviations: aFGF, acidic fibroblast growth factor; ALP, alkaline phosphatase; ATIII, antithrombin III; AVP, arginine vasopressin; bFGF, basic fibroblast growth factor; BP_{dias}, diastolic blood pressure; BP_{sys}, systolic blood pressure; CAM, cell adhesion molecule; cAMP, adenosine 3′,5′-cyclic monophosphate; cA-PK, cAMP-dependent protein kinase; CD, cluster of differentiation; cGMP, guanosine 3′,5′-cyclic monophosphate; cG-PK, cGMP-dependent protein kinase; CREA, creatinine; CS, chondroitin sulfate; CS-P, multi-chain chondroitin sulfate peptidoglycan; DS, dermatan sulfate; EDHF, endothelium-derived hyperpolarizing factor; EDRF, endothelium-derived relaxing factor; EGF, epidermal growth factor; ESA, excited-state absorption; FBP, fructose-6-phosphate; FGF, fibroblast growth factor; FGFR, fibroblast growth factor receptor; FN, fibronectin; F6P, fructose-6-phosphate; Fru-2,6-P_2, fructose-2,6-bisphosphate; GAG, glycosaminoglycan; Gal, galactose; GalN, D-galactosamine; GalNAc, *N*-acetylgalactosamine; GlcA, D-glucuronic acid; GlcN, D-glucosamine; GlcNAc, *N*-acetylglucosamine; GM-CSF, granulocyte-macrophage colony-stimulating factor; GPI, glycosylphosphatidylinositol; GPx, glutathione peroxidase; HA, hyaluronic acid, hyaluronan; HDL, high-density lipoprotein; HMG-CoA, β-hydroxy-β-methylglutaryl coenzyme A; HOMA-IR, homeostasis model assessment of insulin resistance; HS, heparan sulfate; hs-CRP, high-sensitivity C-reactive protein; HS-PG, heparan sulfate proteoglycan; IAA, monoiodoacetate; IDL, intermediate-density lipoprotein; IdoA, L-iduronic acid; IFN, interferon; Ig, immunoglobulin; IGF-1, insulin-like growth factor; IL, interleukin; 8-*iso*-$PGF_{2\alpha}$, 8-*iso*-prostaglandin $F_{2\alpha}$; KS, keratan sulfate; L1, long interspersed nuclear element; LDL, low-density lipoprotein; LIF, leukaemia inhibitory factor; Lp(a), lipoprotein(a); MAG, myelin-associated glycoprotein; MIP-1β, macrophage inflammatory protein-1β; MMP, matrix metalloproteinase; MPO, myeloperoxidase; mRNA, messenger ribonucleic acid; NADPH, reduced nicotinamide adenine dinucleotide phosphate; NCAM, neural cell adhesion molecule; NMR, nuclear magnetic resonance; NO, nitric monoxide; oxLDL, oxidized low-density lipoprotein; PARP, proline- and arginine-rich protein; PDGF, platelet-derived growth factor; PFK, phosphofructokinase; PGF, prostaglandin F; PGI_2, prostacyclin; PKC, protein kinase C; PLC, phospholipase C; PSCP, pump-supercontinuum-probe; PTKR-SF, protein tyrosine kinase receptor superfamily; RET, resonant energy transfer; ROS, reactive oxygen species; SOD, superoxide dismutase; TGF, transforming growth factor; TIMP, tissue inhibitor of metalloproteinase; TIRF, total internal reflection fluorescence; URAC, uric acid; VLA, very late antigens (integrin α_1-α_6); VLDL, very low-density lipoprotein; Xyl, xylose.

* Corresponding author at: Charité — University Clinic Berlin, Institute of Physiology, Charitéplatz 1, D-10117 Berlin, Germany. Tel.: +49 30 450 528 521; fax: +49 30 450 528 920.
E-mail address: guenter.siegel@charite.de (G. Siegel).

http://dx.doi.org/10.1016/j.cis.2014.01.009

conformational change from the random coil state to the directed filament structure state. This conformational transition effects a protein unfurling and molecular elongation of the GAG side chains like in a 'stretched' spring. This configuration is therefore combined with an increase in binding sites for Na^+ ions. Counterion migration of Na^+ along the polysaccharide chain is followed by transmembrane Na^+ influx into the endothelial cell and by endothelial cell membrane depolarization. The simultaneous Ca^{2+} influx releases NO and PGI_2, vasodilatation is the consequence. Decrease in flow reverses the process. Binding of Ca^{2+} and/or apoB100 lipoproteins (nanoplaque formation) impairs the flow sensor function.

The physicochemical and functional properties of proteoglycans are due to their amphiphilicity and anionic polyelectrolyte character. Thus, they potently interact with cations, albeit in a rather complex manner. Utilizing $^{23}Na^+$ and $^{39}K^+$ NMR techniques, we could show that, both in HS-PG solutions and in native vascular connective tissue, the mode of interaction for monovalent cations is competition. Mg^{2+} and Ca^{2+} ions, however, induced a conformational change leading to an increased allosteric, cooperative K^+ and Na^+ binding, respectively. Since extracellular matrices and basement membranes form a tight-fitting sheath around the cell membrane of muscle and Schwann cells, in particular around sinus node cells of the heart, and underlie all epithelial and endothelial cell sheets and tubes, a release of cations from or an adsorption to these polyanionic macromolecules can transiently lead to fast and drastic activity changes in these tiny extracellular tissue compartments. The ionic currents underlying pacemaker and action potential of sinus node cells are fundamentally modulated. Therefore, these polyelectrolytic ion binding characteristics directly contribute to and intervene into heart rhythm.

Contents

"Als Gott das Universum schuf, war seine geringste Sorge, es so zu schaffen, daß wir es verstehen."

[Albert Einstein]

1. Preface

Dear Björn, this is a Festschrift in your honour. The statement by Einstein provides a premise according to which you have aligned your life and scientific work. You went and go as always to the understanding of things. In science, that may be relatively simple. Origins, causalities, correlations, and associations must be explored. Nowadays we say, mechanistic explanations have to be found. In spite of all these supreme efforts much remains hidden from us. This, we have to bear. It seems much more difficult to come to a self-conception which is the prerequisite of understanding others. Often, that takes years. During a one-year sabbatical 1976 in your institute in Lund, I was lucky to experience this intellectual field

of tension and way of thinking that had a lasting impact on my own scientific development until today.

When years later, walking in Fontane's footsteps we visited castle "Rheinsberg" [1], where the young Prussian crown prince Friedrich (Frederick II, the Great) spent his happiest and most carefree years, and we subsequently roamed through meadows and forests in the March of Brandenburg, we strenuously discussed how one could investigate the viscoelastic properties and conformation of the biopolyelectrolyte perlecan flow- and ion-dependently. Your suggestion, first to begin with ellipsometry, led me to Martin Malmsten, first to Stockholm (Ytkemiska Institutet), then to Uppsala (Biomedical Center). Viewed from a distance, the outcome appears quite good. By a closer look we have to concede that fundamentals in our understanding are still missing.

We hope for your further help, since you directly and indirectly contributed to everything that I am dealing with on the following pages. For all this, I would like to express my appreciation to you, and also for the many years of friendship.

2. Introduction

Building upon that time, in which we investigated for the first time the ion binding properties of CS-P with $^{23}Na^{+}$ Fourier transform NMR, it shall be specially highlighted that the quadrupole relaxation method can constitute a very general experimental approach to the problem of ion binding in biological systems [2]. CS-P belongs to the group of glycoconjugates of the extracellular matrix which again can be subdivided into the components structural glycoproteins and proteoglycans. The extracellular space around the cells occupies a considerable portion of tissue volume. In the structured meshwork of the extracellular matrix there are three basic forms of complex macromolecules. The texture of the interstitial connective tissue is composed of proteins, glycoconjugates, and carbohydrate polymers, among which collagens, structural glycoproteins, and proteoglycans have been identified as major components. Proteoglycans, GAGs (essentially HA), and structural glycoproteins form a large group of polysaccharide-rich and/or protein-rich macromolecules that are located in the strongly hydrated matrix ground substance, in basement membranes, at the cell surfaces, and even in subcellular compartments. Some are of importance for cell–matrix interactions and their changes in pathological processes, such as invasion and tumour metastasis [3]. The main components of the fibre proteins, collagen and elastin, are embedded in the hydrated polysaccharide gel of the ground substance. They are responsible for biomechanical stability and elasticity as well as for tissue development. A remarkable diversity in form and function of the different tissues arises from the large variability in their macromolecular organization [4]. The matrix can calcify and thus form bones and teeth; as a rope-like structure it can impart tensile strength to tendons; and as a transparent cornea it forms the front of the eye. The matrix thus plays an active role in the behaviour of the cells with which it interacts. It affects and controls development, generation, motion, form, and metabolic functions [5].

While in vertebrates proteins such as collagen serve as structure-forming biopolymers, in arthropodes and plants this function is assumed by the polysaccharides chitin and cellulose. The fibrils of these polymers are virtually embedded as "reinforcements" into a matrix, which in the vertebrate body is represented by GAGs usually linked covalently to protein in the form of proteoglycans, and in plants by pectins, alginic acids, and carrageenans, being likewise acidic polysaccharides [6]. Within the composite "connective tissue", these acidic polysaccharides are designated as intercellular ground and cement substance. They are copolymers of hexuronic acid residues, therefore having a common glycan backbone. The plant products are used in medicine, chemistry, and the food industry as bacterial growth media, in gel electrophoresis and chromatography, in the production of ice cream, jam, and pudding as well as in emulsifiers and thickeners.

In the present review, we would like to restrict ourselves to properties and functions of the syndecan/perlecan superfamily of extracellular matrix, merely not to extend the topic too much. On the other hand, the fact shall be taken into account that these polyanionic macromolecules belong to the best conserved proteins ever and – due to their strategic location in cell membrane, endo- and epithelial basement membrane and in the extracellular matrix – are involved in all important life functions. Furthermore, they play a decisive role in microevolutionary and molecular biological development of life-threatening diseases such as tumourigenicity. Therefore, in the following we will focus – besides on general physicochemical and molecular biological properties – in an overview on their significance for ion binding, as flow sensor and lipoprotein receptor in the circulation as well as their participation in carcinogenesis and metastasization.

3. Molecular structure, functional diversity and self-assembly of proteoglycans: an overview

The physicochemical behaviour of the syndecan/perlecan superfamily as compared to neutral polysaccharides is essentially changed through the carboxyl group in C-6 typical of uronic acids. In the cell and basement membrane, they act as ion exchangers on account of their polyelectrolyte nature; furthermore, they influence the transmembrane ion transport and membrane potential [7]. Their high degree of polymerization causes an exceptional hygroscopicity and swelling capacity, so that they can take up several times their weight in water. Thus, they regulate the water content of connective tissue. In the liquid state, GAG molecules have an extended conformation through the electrostatic repulsion of their carboxylated and sulfated groups. As proteoglycans, they produce very viscous solutions that are converted into gels depending on the concentration in free acid groups, pH value, and cationic strength and valency [6]. When there are numerous free, unesterified acid groups, divalent ions such as Ca^{2+} can elicit gelatinization through physical cross-linking of adjacent chains. Gel formation is additionally promoted by the hydrophobic interaction of methyl groups of neighbouring chains and by esterification of the polysaccharides at C-4 and C-6 with sulfuric acid. The hydrated polysaccharide gels are characterized mechanically by a high compressive strength, and the interspersed collagen fibres by a high tensile strength. Therefore, the physiological properties of GAGs and their proteoglycans include [7–11]:

- A high hydrodynamic volume,
- The ability to bind cations,
- The specific interaction with partner molecules.

The pathobiochemical importance of proteoglycans is expressed in changes of their macromolecular structure and tissue distribution pattern during [5,12,13]:

- Progression of age,
- Connective tissue diseases,
- Genetic defects of their metabolism.

After several biophysical properties of proteoglycans had been attributed to the GAG chains, the sequence analysis of protein cores at the cDNA and protein level proved that specific functional features are conferred by distinct protein *and* carbohydrate domain structures. All core proteins contain GAG substitution domains that may vary from one to more than a hundred. Many proteoglycans carry two types of side chains, and their size and ratio may change with development, ageing, or disease [13,14]. Different variants of the same proteoglycan are expressed in cells at different developmental stages. Additional functional domains of the protein core mediate a linkage to the cell surface either by a transmembrane domain or a GPI anchor, to matrix macromolecules, or to other interrelative proteins such as growth factors and CAMs. Interactions with the extracellular matrix regulate the

activities of growth factors and restrict their diffusion and range of action [3]. The manifold biological roles of proteoglycans include:

- Simple mechanical support functions,
- Modulation of diffusion, activity, and stability of various cytokines,
- Effects on cell adhesion, motility, and proliferation,
- Influence on differentiation and tissue morphogenesis.

The binding of protein ligands to GAG chains causing this variety of processes depends upon charge interactions and high-affinity binding sites of specific saccharide recognition sequences [14,15]. It should be emphasized, however, that only the concerted action of both GAG and protein moiety culminates in the entire function.

3.1. Classification and macromolecular structure

In proteoglycans a central protein core, the molecular mass of which can be anything between 10 and 600 kDa, is associated with a variable number of GAG side chains in covalent binding to a macromolecule. Proteoglycans found ubiquitously associated with cell surfaces, intracellularly in secretory granules, and incorporated into extracellular matrices are classified by their post-translationally modified GAG moiety. In contrast to the ramified *N*- and *O*-linked oligosaccharides found on secreted and cell surface glycoproteins, GAGs are unbranched polysaccharide chains consisting of disaccharide repeat units. These are composed of two types of monosaccharides such as GlcN or GalN and either GlcA or IdoA or galactose units (in KS) that are arranged in a strictly alternating fashion constituting linear polymers [3]. Since GAG components can be variably *N*- and *O*-sulfated, and C-5 epimerized from GlcA to IdoA during post-translational modifications, these copolymers reveal substantial sequence heterogeneity both within and between individual polysaccharide chains [15]. Additionally, the modification process may be interrupted at various stages. The openness of proteoglycan structures, especially their GAG chains, to extensive modulation during cellular expression provides versatile sequences that can encode considerable information. Little is currently known about the significance of GAG sequences, but it appears that select sequences vary during cellular responses to suit different biological needs [3,14]. Sulfation and/or carboxylation of amino and simple sugars condition the strongly negative charge of GAGs and proteoglycans, their acidic reaction and anionic polyelectrolyte character.

The biosynthesis of HS/heparin is accomplished through polymerization of [β-D-glucuronic acid $\xrightarrow{\beta 1,4}$ *N*-acetyl-β-D-glucosamine $\xrightarrow{\alpha 1,4}$]$_n$ disaccharides that then undergo the following chemical modifications to a variable extent:

- *N*-deacetylation/*N*-sulfation,
- C-5 epimerization of GlcA to IdoA,
- 2-*O*-sulfation of IdoA,
- 3-*O*-and/or 6-*O*-sulfation of GlcN,
- 2-*O*- or 3-*O*-sulfation of GlcA.

The final GAG chains are highly diverse and comprise 30 different disaccharide sequences [15]. In HS, extended block structures of GlcNAc and GlcA units with no or little sulfate alternate with *N*-sulfated, copiously modified sequences, resulting in a particularly extensive versatility [16]. The identification of the antithrombin III-binding sequence found on heparin containing a pentasaccharide with a unique pattern of epimerization and sulfation demonstrated the functional importance of a selected motif within a GAG chain [15]. This structure is important for the anticoagulant and antiproliferative activity of heparin/HS. HS differs from heparin in that it is less modified and thus less sulfated. Furthermore, HS is found in all tissues and linked to various core proteins, while heparin is a constituent of the single proteoglycan serglycin in mast cells. The X-ray diagrams of the HS Na^+ and Ca^{2+} salts differ from each other. From the layer plane spacing it follows that the Na^+ salt is a left-handed 2_1-helix with an identity period of 1.86 nm, whereby a disaccharide unit has a height of 0.93 nm projected onto the axis [17]. Thus, it is a very extended conformation. The axial advance can be diminished through a conformational change induced by Ca^{2+} ions, so that the pitch of turns becomes shorter [18]. Numerous intrachain hydrogen bonds between neighbouring saccharide rings stabilize the helix. Heparin also exhibits a 2_1-helix conformation with an identity period of 1.68 nm [6]. The twofold-screw conformation represents the mean conformation of these biopolymers. The very tight arrangement of sulfate groups along the heparin molecule strongly supports ionic interactions. Therefore, the potent basic protamine is its antagonist.

CS and DS are both derived from the parent polymer of [β-D-glucuronic acid $\xrightarrow{\beta 1,3}$ *N*-acetyl-β-D-galactosamine $\xrightarrow{\beta 1,4}$]$_n$, the disaccharides of which may be subjected to 2-*O*-sulfation of GlcA and 4-*O*- or 6-*O*-sulfation of GalNAc. Since the GalNAc residues remain acetylated, the structural diversity is limited to nine different disaccharide units [14,15]. Generally, in a CS chain, regions with 4-*O*-sulfation are succeeded either by regions with 6-*O*-sulfation, sections with no sulfate, or domains with both 4-*O*- and 6-*O*-sulfation. DS is peculiar in that some GlcA residues are C-5 epimerized to IdoA, which may then be 2-*O*-sulfated. The glycosidic bond is also changed to α(1 → 3). The GAG is called DS if one or more IdoA residues are interspersed in a CS chain. Ordered conformations from the Na^+ salts of CS and DS were obtained by X-ray diffraction showing a layer-line spacing of 2.88 nm (3_2-helix) and 2.82 nm (3_2-helix), respectively [17,19]. The difference in axial rise can be attributed to the C-5 epimeric L-IdoA carboxyl group, which in DS is no longer equatorially but axially positioned. The altered conformation may be responsible for the higher cation-binding affinities in DS chains, as substantiated by measuring relaxation rates with NMR methods [9].

3.2. Functions of proteoglycans

The biological role of proteoglycans is diverse with regard to their structures and functions. The functional properties of protein cores and GAG chains are expressed in specific interactions between these moieties and other macromolecules. In principle, several operational mechanisms of GAGs and proteoglycans can be differentiated:

- Self-association and allo-association into aggregates,
- Electrostatic binding to positively charged protein domains,
- Specific binding to proteins via GAG or protein consensus sequences,
- Concerted actions of GAG and protein moieties in matrix binding, cell adhesion, and cytoskeleton reorganization.

It has only been possible to partly trace back the molecular basis for the various functions to distinct modular protein and carbohydrate structures. The interaction between the core protein of the small interstitial matrix proteoglycan decorin and collagen affects collagen fibrillogenesis [20–22]. Both decorin and biglycan bind fibronectin as well as TGFβ [23], the latter being a pleiotropic cytokine involved in tissue development, remodelling, and wound repair. Furthermore, the core proteins of the HS class, including the large basement membrane proteoglycan perlecan, can associate with fibronectin-binding domains [24]. The ability of aggrecan, versican, and CD44 to bind HA designates a further core protein-mediated function. Versican may constitute a link between extracellular matrix HA and the cell membrane. Its N-terminal G1 domain interacts with HA, and its C-terminal CAM-like region with the cell surface [25,26].

The polyanionic and hydrophilic GAG chains, on the other hand, have a strong influence on tissue hydration and elasticity, i.e., they dominate the physical properties of the proteoglycans. Their negative fixed charges attracting countercations, especially Na^+, provide for osmotic hydration of the matrix. Negatively charged molecules are repulsed by the GAG chains, forming porous hydrated gels. These exclude

other macromolecules from the water-filled compartments, which can, however, be permeated by low molecular solutes and migrated by cells. Thus, pericellular compartments with concentrated proteoglycans and ions may influence spatiotemporally controlled reaction rates and concentration-dependent interactive physical processes [7,14]. Under physiological ion concentrations and pH, the specific binding of GAGs to proteins such as

- proteases and antiproteases,
- growth factors and other cytokines,
- matrix proteins and glycoconjugates,
- cell adhesion molecules,
- lipoproteins, and lipases

allows proteoglycans to intervene in cell and tissue development in numerous ways [3,15,27]. For some GAG-binding proteins, high-affinity constants of log K_a 6–9 L/mol were determined.

The potent anticoagulant activity of heparin/HS through the protease inhibitor antithrombin III (ATIII) is based upon thrombin inhibition, which is more efficient in the presence of the GAG. The anticoagulant effect of DS functions in a similar way via heparin cofactor II [28], which binds tightly to DS via the GAG hexasaccharide [−IdoA(2-OSO_3)-GalNAc(4-OSO_3)-]$_3$ consensus sequence [15]. ATIII binding requires the pentasaccharide recognition sequence [−GlcNAc(**6-OSO_3**)-GlcA-GlcN**SO_3**(**3-OSO_3**)-IdoA(2-OSO_3)-GlcN**SO_3**(6-OSO_3)-] in heparin, whereby the GlcN 3-*O*-sulfate group is selectively incorporated as a marker component into the ATIII-binding region through a specific 3-*O*-sulfotransferase [29,30]. The other sulfate groups shown in bold type also promote the interaction between heparin and antithrombin. The strong reaction acceleration is supported by the simultaneous presence of both protease and protease inhibitor on the same scaffolding GAG chain. The antiproliferative effect is achieved by various HS/heparin-related GAGs with differing chain lengths and degrees of *N*-acetylation/sulfation which interfere at different sites. While nuclear HS oligosaccharides are involved in the regulation of transcription factor activity and gene expression reducing cell division [31,32], the antiproliferative influence of heparin on vascular smooth muscle cells and of HS, synthesized by vascular endothelial cells and associated with ATIII, may additionally result in a nonthrombogenic blood vessel surface [33].

Many growth and differentiation factors are bound and modulated by proteoglycans, such as syndecan/perlecan, decorin, and CD44-like molecules. Both GAG and core protein moieties participate in these interactions [34]. The growth factors and other cytokines are

- complexed with cell surface-binding proteins on endothelial cells, promoting leukocyte extravasation in inflammation (MIP-1β; IL-8) [35],
- stored and sequestered on extracellular matrices available for rapid release during matrix injury or tissue repair (TGFβ; FGF; PDGF; LIF; IL-1) [36], or
- localized to stromal cell layers in bone marrow-stimulating hematopoiesis (GM-CSF; IL-3; SCF) [37].

Since many growth factors contain basic domains interacting with GAG chains, the extracellular matrix entraps and stores these molecules as they are secreted by cells [3]. The storage provides a spatially controlled source of these factors, restricting their diffusion and effective range [27]. The potency of cytokines to affect

- cell proliferation, differentiation, and movement,
- leukocyte migration and function,
- hematopoietic cell numbers,
- temperature regulation,
- acute phase responses,
- tissue remodelling and cell survival

in nano- to picomolar concentrations requires a strict regulation of cytokine production and action on the level of gene expression, processing of precursor forms, sequestration, and receptor modulation. Thus, many cytokines and prostaglandins act to inhibit the production of other cytokines and their receptors, e.g., TGFβ, which is a broad-spectrum inhibitor of cytokine expression [38]. The interaction of TGFβ with the decorin core protein neutralizes the activity of the TGFβ [23]. The homologous proteoglycan biglycan binds to TGFβ as well modulating the subsequent association of this growth factor with signal-transducing receptors [39]. Since TGFβ promotes expression of decorin/biglycan core proteins and regulates biosynthesis of the GAG side chains, the ability of decorin to block this action is indicative of its potential role in this negative feedback control. Basic FGF, readily bound to the HS chain of proteoglycans and sequestered in the extracellular matrix and basement membrane, is thought to be involved in the modulation of cell proliferation, motility, differentiation, and angiogenesis as well as in the protection from proteolytic plasmin degradation [40–42]. Plasmin, plasminogen activator, heparin, and tissue heparitinases can release matrix-bound bFGF in a form that is still biologically active [42,43]. Moreover, association of bFGF with cell membrane syndecan is essential for bFGF to bind to and activate its transmembrane cell surface receptor tyrosine kinase [44]. Without activation by HS side chains, bFGF exists in a conformation that cannot interact with its high-affinity receptor. Association with HS proteoglycan on the cell surface converts bFGF to a receptor-compatible configuration, giving it the ability to bind to the receptor (Fig. 1). Syndecan does not operate itself as the signal-transducing receptor, but as a coreceptor for bFGF. Thus, modulation in HS expression of this proteoglycan is an essential form of FGF receptor activity regulation. Moreover, the HS component has been shown to bind different growth factors including bFGF, aFGF, GM-CSF, IL-3, and IFNγ [34].

Matrix assembly and cell adhesion to multidomain matrix proteins and glycoconjugates bearing specific GAG recognition sequences can be mediated by secreted and cell surface proteoglycans via their GAG chains. The presence of IdoA units substantiates the superior HS over CS binding ability. While HS/heparin proteoglycans, including the small core protein forms, interact with laminin-binding sites in the basement membrane [27], the hybrid HS/CS syndecans bind to tenascin. Both heparan/heparin and heparan/chondroitin sulfate classes can associate with the fibronectin-binding domains FN-C/H I,II at N-terminal FNI or C-terminal FNIII repeats [45]. Binding of CS chains, however, sterically hinders the interaction of the fibronectin cell attachment site with its cell surface receptor VLA-5 [46]. Vitronectin is a cell-adhesive glycoprotein found in blood plasma and the extracellular matrix that modulates coagulation and complement processes [47]. A polycationic stretch with

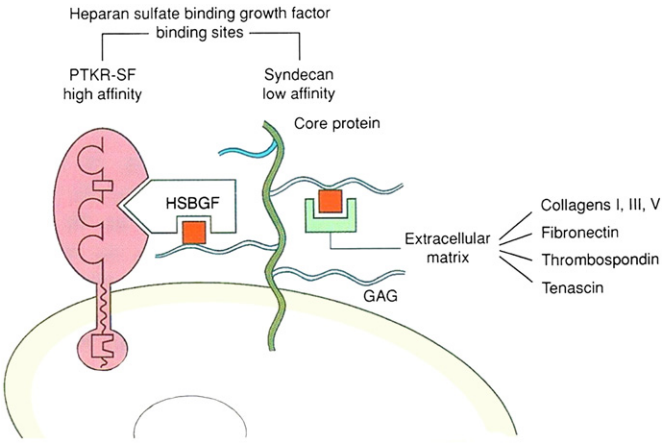

Fig. 1. Interactions of heparan sulfate/heparin-binding growth factor (HSBGF) with membrane-integrated proteoheparan sulfate (syndecan) and of HSBGF associated with a member of the protein tyrosine kinase receptor superfamily (PTKR-SF), according to the Yayon model [44]. Syndecan serves as a low-affinity receptor for HSBGF, having different binding sites at the glycosaminoglycan (GAG) moiety for HSBGF and certain matrix proteins (collagen, fibronectin, thrombospondin, tenascin). HSBGF bound to the low-affinity receptor is presented to the signal-generating, high-affinity PTK receptor (from [5,265]).

a highly charged basic domain is located at the C-terminal portion of the molecule and constitutes the major HS/heparin-binding domain at the hemopexin tandem repeat II. This basic consensus sequence supporting strong ionic interactions provides the epitope for GAG binding. Vitronectin, which undergoes a profound conformational transition when it interacts with heparin, prevents this GAG from catalysing the thrombin-antithrombin III complex formation [48]. Proteoglycans mediate the adhesion between platelet and extracellular matrix glycoprotein thrombospondin and cells. Its globular heparin high-affinity binding domain PARP at the N terminus constitutes the ligand to cell surface syndecan [49–51]. This module has been implicated in thrombospondin-conferred disruption of focal contacts and regulation of proliferation through actin cytoskeleton reorganization by the integral membrane core protein of syndecan [52]. Two heparin-binding regions are located on von Willebrand factor, a large multimeric plasma glycoprotein. Epitope mapping yielded collagen, proteoglycan, and two platelet receptor-binding domains (GPIb-IX and GPIIb-IIIa) mediating platelet aggregation and linkage to the subendothelium at sites of vascular injury [53]. Finally, GAG-binding matrix proteins include the fibrillar and nonfibrillar collagen types I–VI. Whereas basement membrane collagen type IV associates with heparan and heparin sulfate proteoglycan [54], collagen types I and II preferably interact with the protein cores of decorin and fibromodulin [55].

The function of homophilic cell–cell adhesion molecules, such as NCAM and MAG, can be regulated by binding to other molecules on the same cell surface [56]. For CAM-mediated overall membrane–membrane apposition of neural and non-neural cell types to occur, a distinct heparin-binding site on the NCAM Ig-2 domain must be occupied by syndecan [57]. This association induces a conformational change in the NCAM adheron through interaction with the proteoheparan sulfate GAG chains, which in turn promotes the adhesion of the homophilic binding domain. L1 interacts with NCAM in an assisted homophilic-binding mechanism which potentiates the adhesive properties of L1 in a carbohydrate-dependent manner [58].

Several lipoproteins and lipases involved in uptake and catabolism can associate with integral membrane HS/CS proteoglycans. Cholesterol and other lipids are transported in the body fluids by lipoproteins to their target sites. Hepatocytic syndecan has a twofold effect on the cell surface [3]:

- Facilitation of lipoprotein binding via apolipoprotein B and E interactions,
- Immobilization of the soluble enzymes lipoprotein and hepatic/pancreatic triglyceride lipases.

Atheroma formation in the vascular wall is preceded by endothelial dysfunction (primary lesion) [59] and extracellular preatheromatous lipid deposition ("fatty streak") in the intima and inner media. Physiologically, small and smallest lipoproteins, such as VLDLs, IDLs, LDLs, and HDLs, are steadily transported from the blood into the vascular interstitium within large endothelial transport vesicles [60]. This transendothelial lipoprotein transport is the prerequisite for a primarily extracellular lipidosis [61]. LDL and IDL known to be especially atherogenic are concentration-dependently stored in extracellular matrices and basement membranes of the intima. With progressive intima sclerosis, the amount of CS/HS proteoglycans identified as essential LDL-binding components increases [62,63]. Stretches of basic amino acid-rich residues within apoB and apoE constituting the predominant protein moiety of LDL display a high electrostatic binding affinity to proteoglycans [64,65]. LDL binding to proteoglycans, to which primary atherogenic importance is attached, is inhibited by HDL.

3.2.1. Perlecan

Perlecan and related proteoglycans are ubiquitous and integral basement membrane components. This modular proteoglycan has evolved from ancient ancestors by gene duplication and exon shuffling [66]. Perlecan consists of an elongated multidomain and multiglobular protein core and three N-terminally attached HS side chains. Proteoglycan structure is diversified by post-translational modifications in the GAG chains that vary in size depending on the cell source. HS binding to laminin and collagen type IV, core protein binding to entactin, and limited self-assembly mediated by NCAM-like sequences help perlecan integrate into basement membranes [27]. Perlecan functions include cell adhesion via β_1-integrins, control of charge-selective glomerular ultrafiltration, storage of growth factors (cf. Chapter 3.2 and Fig. 1), and binding of serine protease inhibitors [67]. Moreover, incorporation of perlecan into basement membranes endows a high negative charge density to the microenvironment in close vicinity to excitable cell membranes (see Chapter 5.1.5.2).

Stretches of basic amino acid-rich residues within apoB, apoA and apoE constituting the predominant protein moiety of LDL and HDL display a high electrostatic binding affinity to proteoglycans. The large protein core of perlecan – with a molecular mass of 467 kDa and a length of 80 nm – carries three HS chains of 30–70 kDa which are 100–170 nm in length and covalently attached to Ser–Gly consensus sequences clustered at the N terminus [68]. (Other studies favour a C-terminal location [69]). This major HS-attachment domain I is considered to be a putative lipoprotein binding site for reasons of electrostatic attraction [5]. Perlecan belongs to the low buoyant density class of HS proteoglycans with high protein content (75–80%). Electron microscopy after rotary shadowing revealed six large globular domains with small connecting rods resembling pearls ("perles") on a string. The perlecan core protein displays a remarkable homology to sections in the laminin A chain and can be divided into five distinct domains composed of five protein repeats in different combinations [70,71] (Fig. 2). Domain I at the N terminus is considered to be the major HS-binding site. Immediately adjacent to domain I, domain II contains four copies of LDL receptor repeats and one Ig repeat (NCAM module) [27]. Also such motifs in perlecan are thought to mediate LDL binding for reasons of core protein receptor module — lipoprotein ligand interactions [72]. Interestingly, the expression of the proteoglycan in endothelial cells is modulated by LDL [73].

These membrane and subendothelial LDL binding sites in the connective tissue matrix are preferential locations for the generation of arteriosclerotic plaques, particularly when free oxygen radicals induce lipid peroxidation to oxLDL. Full-blown arteriosclerotic plaques as clinically detected by spiral computer tomography and magnetic resonance imaging basically contain lipoproteins associated with proteoglycans of high diversity and versatility and complexly aggregated with high amounts of calcium [74]. Therefore, the replica in nanoscale dimensions of the heterotrimeric aggregational complex consisting of proteoglycan receptor, lipoprotein and calcium presumably portrays the very earliest stages of an arteriosclerotic plaque, which remains undiscovered even with the most up to date clinical diagnostics. This so-called primary lesion impresses merely as endothelial dysfunction. The formation of the proteoglycan – lipoprotein – calcium complex (Figs. 5,6,9) may be initiated by cooperative Ca^{2+}-binding to the proteoglycanic GAG chain inducing a diminution of the axial rise of its left-handed 2_1-helix through a conformational change, so that the pitch of turns is compressed [17,75,76]. Simultaneously, the cooperativity of this dual complex may be amplified by allosteric lipoprotein docking to that shortened conformation supported by the higher charge density and fitting stereospecificity. Thus, the heterotrimeric complex would become rather stable.

Domain III of perlecan exhibits marked homology to the laminin short arms [55]. It is composed of 14 eight-Cys EGF repeats that can be divided into three subdomains, each starting with a globule. Domain IV includes 21 consecutive Ig repeats with a low NCAM homology. The C-terminal domain V resembles the C-terminal G domain of the laminin A chain. Two six-Cys EGF repeats are each interspersed among three homologous globular repeats (GR-1,2,3) that may provide a cell-binding site recognized by β_1-integrins [27]. Moreover, the asterisks at domain V of Fig. 2 denote approximate positions of further putative HS attachment sites and thus additional locations for lipoprotein binding. This domain classification suggests that the perlecan core protein is one of

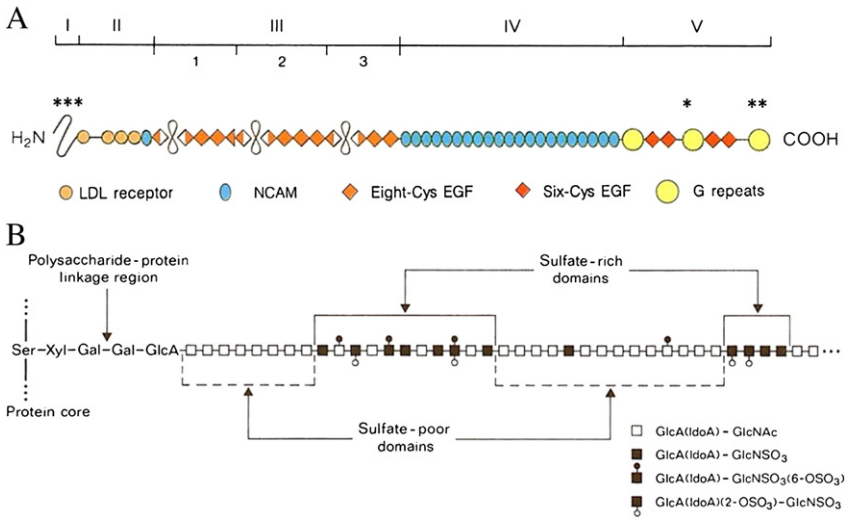

Fig. 2. Domain structure, core protein modules, and disaccharide sequence in an HS side chain of the large basement membrane proteoglycan perlecan. A. Major domains are identified by Roman numbers and subdomains by Arabic numbers. Asterisks denote approximate positions of putative HS attachment sites. The protein modules include low-density lipoprotein (LDL) receptor, neural cell adhesion molecule (NCAM), eight-Cys epidermal growth factor (EGF), six-Cys EGF, and G repeats. EGF-like repeats with eight cysteines and EGF globules (loops) are homologous to those of laminin. NCAM denotes motifs with a single disulfide bridge typical for the immunoglobulin superfamily. G domains are globules homologous to those in the laminin A chain. B. HS chains are covalently bound to the protein core via a Xyl-Gal-Gal-GlcA polysaccharide-protein linkage region. The size of the domains rich and poor in sulfate, respectively, was experimentally determined (from [5]).

the most versatile single-chain multidomain polypeptides. cDNA clones hybridize to a 14-kb mRNA message encoding this core protein. Restriction fragment length polymorphism patterns indicated a single-copy gene. It has been localized to human chromosome 1p35–36.1 [77].

3.2.2. Syndecan

Syndecan is a polymorphic, membrane-intercalated, HS/CS hybrid proteoglycan abundant on epithelial and induced mesenchymal cells during embryogenesis and in adult tissues [78]. Through its HS side chains it binds extracellularly to various interstitial matrix components and to bFGF [79]. Syndecan can alter the conformation and presentation of the growth factor to its FGF receptor protein [44,80]. Its intracellular domain interacts with the actin cytoskeleton (see chapter 6.3), resulting in the formation or elimination of focal cell adhesions [15]. Therefore, syndecan is involved in the cellular regulation of shape and tissue organization [3,79].

The syndecan core protein (33 kDa) contains a large N-terminal, cysteine-free ectodomain, a hydrophobic transmembrane domain, and a short C-terminal cytoplasmic domain (Fig. 3) [81]. Several isoforms have been identified, but their transmembrane and cytoplasmic domains are highly conserved between the four family members (Table 1). The cytoplasmic domains of all syndecan family members can be divided into three regions: a membrane proximal constant (C1) region, a variable (V) region, and a carboxyl-terminal constant (C2) region. The C2 region has a consensus sequence for binding proteins with class II PDZ domains and such an association would result in the formation of an adhesive/signalling complex [82,83].

The ectodomain of the syndecan family contains a characteristic protease-susceptible basic dipeptide adjacent to the cell membrane. Five potential GAG linkage sites are found in extracellular regions close to and distant from the cell membrane carrying two to four HS and CS chains in variable composition. TGFβ effects expression of a CS-rich syndecan that results both from a higher number of chains and from an increase in chain length [84]. While thrombospondin fails to bind syndecan with a regular complement of HS and CS, the CS-rich syndecan is specifically bound. These results demonstrate that ligand specificity is encoded in the GAG substitution pattern. This pattern is recognized by a variety of extracellular ligands that cross-link and associate with syndecan: collagen types I, III, and V, fibronectin, laminin, and thrombospondin [79,85]. Furthermore, cytokines modulate the GAG pattern during differentiation and tissue development. Information about the actual microenvironment of a cell can be transferred via the binding of matrix elements to the cell surface. Since the cytoplasmic tail contains three conserved tyrosine residues [78], which provide

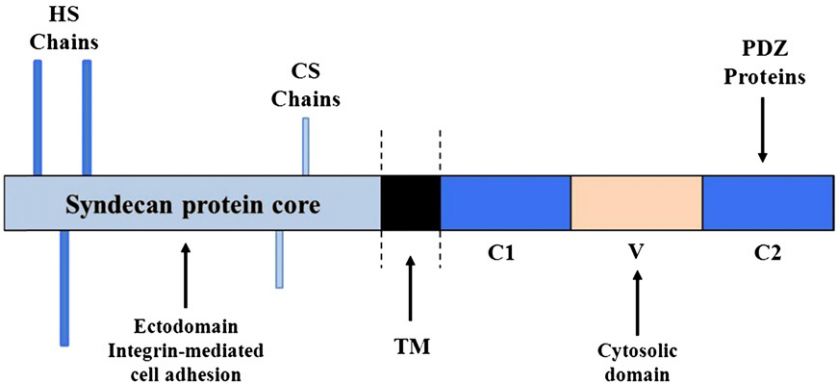

Fig. 3. Domain structure of the syndecan protein core. TM, transmembrane domain; C1 and C2, conserved regions of the cytosolic domain; V, variable region of the cytosolic domain (from [13,87]).

Table 1
Main proteoglycans of basement and cell surface membranes. Acronyms and chromosomal location refer to human genes (from [13,55,82]).

Proteoglycan location	Proteoglycan type	Acronym (access to gene bank)	MW [kDa] core protein	GAG chain		Chromosomal location
				Type	Number	
Basement membrane	Collagen XVIII	COL-18A1	2451 aa[a]	HS	2	21q22.3
	Perlecan	HSPG2	470	HS	3	1p35–36.1
Cell surface	Syndecan-1	SDC1	32	HS/CS	3/2	2p24.1
	Syndecan-2	SDC2	22	HS	3	8q22–24
	Syndecan-3	SDC3	46	HS/CS	4/2	1p22.3
	Syndecan-4	SDC4	22	HS/CS	3/1	20q12–13

[a] Number of amino acids.

potential phosphorylation sites for protein kinases, syndecan has been called a coreceptor collaborating with integrins in signal transduction [14]. Chromosomal locations of human syndecans are presented in Table 1 [82,86].

Examples of the various functions of syndecans include [13]:

- Syndecans can immobilize ligands, present them to a specific receptor, prevent their degradation, and contribute to the dimerization of growth factors [87]. The interaction between FGF-2 and HS is required for binding of FGF-2 to its high-affinity tyrosine kinase receptor FGFR-1 [88].
- Syndecans bind lipoproteins and can mediate uptake, lysosomal delivery and degradation of the lipoproteins independent of specific lipoprotein receptors [88].
- Syndecans are crucially involved in the regulation of circulation. Based on their viscoelastic and ion binding properties they are implicated in flow-dependent vasodilatation conditioned by shear stress-induced conformational changes [89,90].
- Syndecans bind proteases and protease inhibitors. The interaction of the protease thrombin and its inhibitor ATIII that controls blood coagulation is implicated in wound healing processes [91,92].
- The protein core of syndecans can promote the adhesion of fibroblasts and B-lymphoid cells. Furthermore, the SDC4 cytoplasmic domain may be involved in the activation of Rho kinases.
- Syndecans are shed from the cell surface membrane by enzymatic cleavage of the core protein [88]. The enzyme responsible was identified as a TIMP-3 sensitive MMP. Shedding can be accelerated by exogenous proteases like thrombin and plasmin. Shed syndecans have been found in serum and in body fluids during wound healing and cancer [93].
- Syndecans supply attachment sites for viruses.

3.3. Supramolecular matrix organization and functional heterogeneity

In the following sections, the functional heterogeneity of extracellular matrix structures is discussed in the light of some examples, the focus of which are basement membranes with their supramolecular organization occurring ubiquitously in the body [94]. Whether we consider the control of extracellular ion concentrations close to the cell membrane or the molecular filtration processes in the kidney, it is always the physicochemical or cell biological scaffolding and recognition properties of the basement membrane which play the decisive functional role, with alternating accentuation of the physiological versatility of this complex structure. The basement membrane is also the strategic site at which cells traverse this surface, subbase, and interfacial structure: In inflammatory processes they do so under complete control, and in tumour invasion and metastasis they do so by avoiding and excluding the control systems.

3.3.1. Basement membrane

We have already discussed the basal lamina as an archetypal example of extracellular matrix, common to practically all multicellular animals and an essential feature of epithelial tissues. Basement membranes or basal laminae are specialized extracellular matrices with tissue support, molecular sieving, and cell regulatory functions [54,66]. They play a decisive role not only in cell differentiation during embryogenesis and wound repair, but also in cell behaviour and in hereditary and acquired diseases. Between tissue compartments, they function as passive selective molecular sieves and impede the pervasion of inflammatory and metastatic tumour cells. Basement membranes are produced by epithelial, endothelial, and mesenchymal cells. They underlie all epithelial and endothelial cell sheets and tubes, and they surround muscle, fat, and Schwann cells [95]. Even though their composition varies in different tissues, major constituents of these flexible thin mats (40–120 nm thick) sandwiched between a cell layer and a thick collagenous stroma are the following:

- Various forms of type IV collagen,
- The large HS proteoglycan perlecan,
- The glycoprotein laminin,
- The glycoprotein entactin.

The supramolecular architecture of these matrices is created by self-assembly processes and specific heterophilic interactions between the protein, glycoprotein, and proteoglycan protomers [27] (Fig. 4). The primary polygonal network is formed by N-terminal, C-terminal, and lateral association of type IV collagen chains; the secondary polymer meshwork is self-assembled by laminin through terminal-domain associations. Entactin and perlecan moor and stabilize the framework. While entactin bridges the laminin centre and type IV collagen triple-helical regions, the HS proteoglycan binds laminin and type IV collagen via its GAG chains. Furthermore, perlecan self-assembly through core protein interactions polymerizes dimers and oligomers. The primary supramolecular structure and shape can be modified and regulated by variations in composition, isoform substitution, and exogenous heparan/heparin sulfate to meet different developmental, tissue-specific, and physiological needs [54]. While most basement membranes underlay epithelial cells with an electron-lucent (lamina lucida) and an electron-dense (lamina densa) layer connected to the underlying stroma through anchoring fibrils of type VII collagen [96], the corneal endothelial basement membrane lacks a lamina lucida and contains hexagonal lattices.

3.3.1.1. Molecular self-assembly. Basement membrane self-assembly from its components polymerizes protomers to homologous oligo- and polymers, involving covalent stabilizations and cross-links. Type IV collagen can assemble into a stable three-dimensional network using the following mechanisms:

- Unification of C-terminal globule pairs to form linear dimers [97],
- Binding of four N-terminal ends to each other to form an end-overlapped 7S domain [98],
- Dimer self-interaction by lateral associations with superhelix formation [99].

In the dimeric globular domain, corresponding cysteines of the monomers are completely disulfide exchanged. Tetramer size complexation of

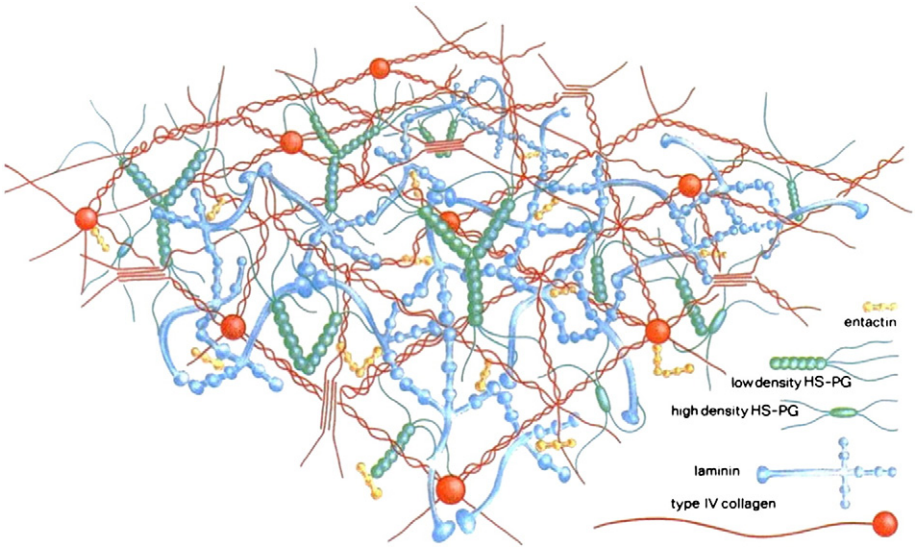

Fig. 4. Three-dimensional model of basement membrane architecture. The basement membrane is formed by specific interactions between the proteins type IV collagen, laminin, and entactin as well as the proteoglycans perlecan (low-density heparan sulfate proteoglycan, HS-PG) and high-density HS-PG. Type IV collagen and laminin constitute double polymer networks. Entactin bridges collagen and laminin with additional laminin-to-collagen interactions. HS-PG complexes, anchored in the network, interact with laminin and collagen through its polyanionic chains (from [5]).

the 7S domain overlap formation requires maximal hydrophobic contact of the four ends, resulting in antiparallel interactions of correct axial and azimuthal orientation [100]. Finally, lateral associations forming an irregular polygonal network necessitate the presence of dimeric C-terminal globular domains. After assembly, the collagen C and N termini with superhelix formation become stabilized by covalent cross-links, and the superhelices by covalent end interactions of their laterally associated filaments.

The different structural domains of laminin serve different architectural functions, cell attachment, spreading, growth, and differentiation [101]. Furthermore, functional multiplicity is guaranteed by laminin diversity. Laminins are a family of large glycoproteins that are distributed ubiquitously in basement membranes [55]. Above a critical concentration (60 nmol/L), laminin forms polymers through a cooperative nucleation/propagation-type assembly. An initial temperature-dependent oligomer-forming step is followed by a Ca^{2+}-dependent polymer-forming step [54]. A Ca^{2+}-induced conformational change in laminin activates the polymerization [102]. End-to-end interactions between short arms and long arms are essential for laminin aggregation into dimers and oligomers (Fig. 4). In basement membranes, the following conditions are fulfilled, giving laminin polymers important architectural features [54]:

- Laminin concentration is high enough to permit arm contacts between all neighbouring molecules.
- Laminin shows gelation properties that are similar in the absence or presence of other matrix components.
- Laminin-rich basement membranes lacking collagen exist and are produced by tumours.

Antibody studies have provided evidence for proteoglycans specific for basement membranes and clearly distinguishable from proteoglycans bound to the cell membrane. The distinction is significant, since both types of proteoglycans are predominantly substituted with HS chains and occur simultaneously in adjacent anatomic compartments [27]. A low-density (large-core protein) and high-density (small-core protein) HS proteoglycan and proteoglycans carrying either HS and/or CS side chains are typically found in basement membranes. The protein core of the most prominent, low-density proteoglycan perlecan can also self-assemble into dimers and oligomers [54]. At physiological pH and ionic strength, the C-terminal poles opposite the HS linkage site can bind to each other, forming larger structures of dimers and trimers (Fig. 4). The anionic biopolyelectrolyte chains confer charge-dependent selective filtration properties to basement membranes [103].

3.3.1.2. Heterophilic interactions and supramolecular architecture. Complex protein, glycoprotein, and proteoglycan protomer associations with each other form the heterologous supramolecular architecture of basement membrane matrices. Strong protomer interactions result in high local concentrations of matrix components, allowing weaker interactions to contribute to the final structure and to meet functional needs [54]. Thus, the two major polymeric arrays of type IV collagen and laminin are interwoven by entactin high-affinity bridges and by low-affinity direct interactions between the ends of laminin arms and the type IV collagen chain 140 nm proximal to its C-terminal globule [104]. Both perlecan and HS small-core proteoglycan bind laminin at high-affinity, long-arm and low-affinity, short-arm binding sites. The binding to laminin and collagen IV occurs through HS chains, whereas the association with the central globular domain of entactin results from interaction of the perlecan core protein [105]. Ternary complexes can also form between laminin, entactin, and type IV collagen contributing to the final basement membrane architecture [106]. Proteoglycan linkage with type IV collagen has been localized to the globular NC1 domain and two collagen chain regions. Furthermore, locally secreted HS can modulate and rearrange both polyanionic charge distribution and laminin/collagen IV polymerization.

The tight arrays of perlecan and several other proteoglycan polyanionic chains surrounded by a hydrational mantle provides a size- and charge-selective permeability barrier. Early permeation models treated the basement membrane as a sheet penetrated by pores 5–10 nm in diameter. In contrast to the pore concept, later investigations on glomerular basement membranes, which are thought to act as a compressible ultrafilter separating the blood from the urinary space, confirmed the fibre matrix hypothesis with quasi-elastic heteropolymeric mesh-like architecture [107,108]. Permeant molecules are hindered by collisions with the matrix fibres rather than being constrained by the rigid dimensions of pores. Even though the type IV collagen and laminin mesh does not contribute a sieve tight enough to exclude proteins, the HS chains enveloped in a hydrational shell provide selective charge sieving in that they leave only a minor space of free water for the molecular passage [54]. Clarification of the molecular mechanism of this process calls, however, for a great effort.

Diabetic nephropathy and autoimmune glomerulonephritis indicate the correlation between a reduction in perlecan mRNA and an impaired filtration control associated with proteinuria [103,109]. Furthermore, high glucose levels decrease the proteoglycan synthesis in mesangial cells [110], which underscores the prominent role of proteoglycans in filtration.

4. Lipoprotein binding

After this overview of the essential physicochemical and molecular biological properties of syndecan–perlecan proteoglycans, examples of certain specific functions shall be presented, starting with lipoprotein binding (cf. chapter 3.2) and its clinical relevance. At the beginning, we would like to specially emphasize that arteriosclerotic plaque formation, which together with its clinical sequelae cardiac infarction and stroke amounts to still 50% of all deaths, does not so much depend upon the absolute blood lipoprotein concentrations of LDL and HDL but rather on their ratio LDL/HDL [111]. A quotient above four increases mortality dramatically. Even more decisive, mainly based on their strongly aggregational features, are the concentrations of oxLDL and Lp(a). Therefore, the ratio oxLDL/LDL as well as Lp(a) levels should be in the focus of future treatment targets. But first of all, we would like to devote ourselves to the protection of the vascular wall by HDL.

4.1. HDL, a feedforward forechecking loop

The polyanionic and hydrophilic GAG chains dominate the physical properties of proteoglycans such as endothelial and vascular smooth muscle cell membrane syndecans and vascular matrix and basement membrane perlecan. Both these macromolecules belong to a class of transmembrane and interfacial matrix polyelectrolytes that control and regulate the transendothelial and paracellular trafficking of blood lipids at the strategic boundary layers of blood–cell (glycocalyx), cell–cell (paracellular adhesive ground and cement substance) and cell–matrix (basal lamina and subbase matrices) barriers, almost exclusively in the high pressure system of the peripheral arterial vascular tree [5]. HDL, on the other hand, is the counter partner in this system of internalization and diffusion control for lipoprotein entry into the vascular wall. Based on stereochemical and chiral conformity with its proteoglycan receptor, HDL owns by far a higher affinity compared with LDL, and thus mounts, together with the proteoglycan pattern, an effective and fussy forechecking impediment. The mode of interaction among the lipoproteins at the receptor site is thought to be dominated by competition [112].

Under pathophysiological conditions, e.g., high LDL or low HDL concentrations, even at physiological Ca^{2+} levels, this feedforward loop may be sensitively impaired allowing the initiation of an increased LDL binding and thus the formation of an extracellular pre-atheromatous lipid deposition on the endothelial cell, in the intima and inner media. This can calcify and build up the first stages of an arteriosclerotic nanoplaque [113]. This ternary complex 'lipoprotein receptor (HS-PG) – LDL – calcium' may be interpreted as arteriosclerotic nanoplaque formation on the molecular level before any cellular reactivity, possibly responsible for the arteriosclerotic primary lesion [114]. On the one hand, nanoplaque deposition on endothelial and vascular smooth muscle cell membranes may constitute primary lesion formation responsible for endothelial dysfunction correlated with blunted NO and PGI_2 production. On the other hand, it could interfere with the communication both between cells and between extracellular and intracellular space. Signals can be transferred by direct cell–cell contact, by diffusible factors, and also through interactions between cells and extracellular matrices. Extracellular nanoplaque deposition at the transmembrane proteoglycan receptor ligand-binding part may induce a conformational change in the intracellular receptor domain, which forwards the signals from the outside either through direct contacts with the cytoskeleton or through the activation of signalling cascades (see chapter 3.2). Such signals can influence almost every aspect of cellular motility, differentiation and functional phenotype.

Thus, the interfacial behaviour of lipoproteins and their protein components is of interest in numerous biophysical and biochemical processes, as well as in biomedical applications. The deposition of lipoproteins, notably LDL, at the surface of endothelial cell membranes and connective tissue matrices in blood vessels constitute one of the initial steps in arteriosclerosis [115,116]. Not only LDL, but also modified LDL, VLDL, IDL and Lp(a) are known risk factors for arteriosclerosis, particularly at high Ca^{2+} concentrations [117–119]. In contrast, HDL has not only been shown to be able to prevent arteriosclerosis, but also to reverse it [120]. Naturally, arteriosclerosis is much more complex than this and after the initial lipoprotein deposition, numerous processes, such as oxidation, glycosylation, calcification, post-translational modification, and bacterial or viral infection may occur, involving not only the endothelium, monocytes and smooth muscle cells, but also cell surfaces and extracellular matrices [5,16,114,121]. Nevertheless, the initial deposition step is a surface-related phenomenon.

In order to learn more about the interfacial behaviour of lipoproteins, we performed investigations on the adsorption of lipoproteins at two different surfaces, i.e., one hydrophobic, and one where the hydrophobic surface was further modified through adsorption of HS-PG, the latter substrate thus mimicking the surface receptors exposed to lipoproteins in the blood stream or on their paracellular pathway (Fig. 5) [116,122]. In order to obtain information of some biological relevance, an important aspect of the present investigations was to perform these experiments at close to in vivo conditions. The results obtained with this simple model are correlated to the role of lipoproteins in the clinical situation. Furthermore, the use of the model system for screening of candidate drugs to arteriosclerosis in a biosensor application was tested for statins, ω3 fatty acids and antioxidants [112,114,123,124].

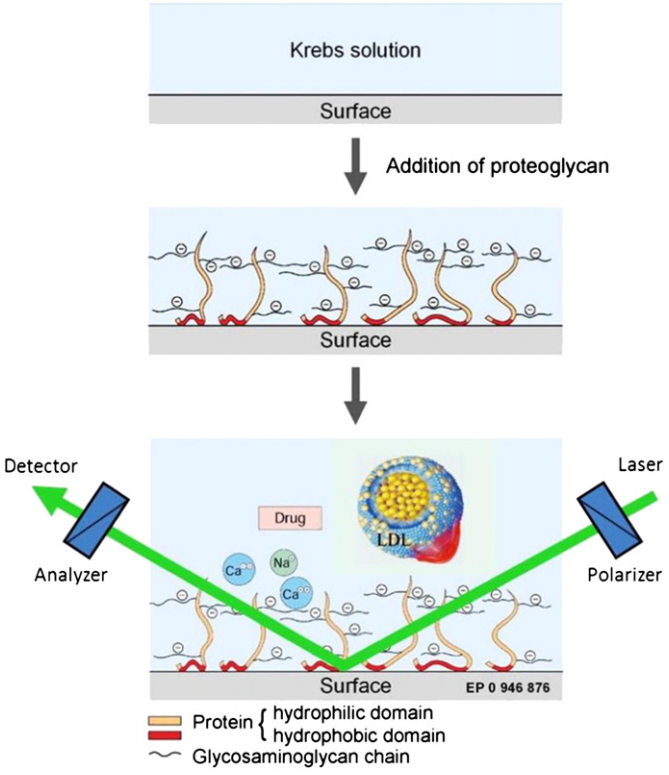

Fig. 5. Monomolecular coating of a methylated silica surface with proteoheparan sulfate molecules and their interaction both with Ca^{2+} and Na^{+} ions and lipoprotein particles in blood substitute solution (not to scale). Furthermore, the influence also of pharmaceuticals can be tested in this laser-based biosensor model (EP 0 946 876) (from [134]).

4.2. Adsorption of lipoproteins at HS-PG modified surfaces

Shown in Fig. 6 is the adsorption of LDL at methylated silica coated with HS-PG. As can be seen, the adsorption is limited in the absence of Ca^{2+}, at least for a considerable time. In the presence of the physiological serum concentration of Ca^{2+}, on the other hand, the deposition is strongly accelerated. Parallel studies on the colloidal stability of LDL in the presence of Ca^{2+} indicated that deposition at the proteoglycan-coated surface is not due to Ca^{2+}-induced flocculation of LDL [125], but rather due to some other mechanism, e.g., partial screening of repulsive lipoprotein – lipoprotein and lipoprotein – surface interactions of an electrostatic nature [126], or formation of lipoprotein – polyanion – metal ion aggregates, known to form in this type of system, and indeed used practically for isolation of serum proteins.

The interaction between HDL and the adsorbed proteoglycan layer is somewhat complex, as the total adsorbed amount actually decreases slightly upon the addition of HDL. This could mean that the proteoglycan is displaced to some extent by HDL and that the latter adsorbs at the methylated silica surface to a smaller extent than the proteoglycan. Another possibility could be that part of the preadsorbed proteoglycan is effectively solubilized by the HDL, presumably through the hydrophobic anchoring moiety of the former. The solubilization of hydrophobic solutes by HDL is indeed part of its physiological role and is well documented [127]. However, given the very fast kinetics of the process ($\approx$500 s), it seems unlikely that there are any major reorganizations of the adsorbed layer, since these usually take much longer times ($\approx$hours) for mixed protein systems [128]. Instead, most of the proteoglycan is likely to remain adsorbed, whereas the amount HDL present in the mixed adsorbed layer is more uncertain.

However, it is suggested from Fig. 6 that HDL is indeed present in the adsorbed layer, and more importantly, that it is able to at least partially hinder any further LDL deposition, even at high Ca^{2+} and LDL concentrations. This is a very interesting observation as it matches expectations from clinical investigations, the latter showing the beneficial effect of HDL on arteriosclerosis [120,129]. Therefore, an interpretation of the results is that HDL removes some of the preadsorbed HS-PG, presumably by solubilization, and also binds to the proteoglycan, thereby preventing the binding (attractive interaction) between the polysaccharide chains and LDL. Indeed, such a high-affinity binding site for HDL has been suggested from previous investigations [130]. From these experiments we could conclude that HDL has a four times higher affinity constant to HS-PG as compared to LDL. Translated into practical medicine this means that a person whose HDL blood concentration is 50 mg/dL could cope with an LDL concentration of 200 mg/dL without needing medication, if this person has no further cardiovascular risk factors (e.g., smoking, diabetes, etc.).

Lipoprotein binding to HS-PG preadsorbed from a Ca^{2+}-free Krebs solution at methylated silica resulted in a reduction of the adsorbed amount when HDL was added (Figs. 6,7). This effect may involve competitive adsorption or desorption of some of the HS-PG molecules, possibly by a hydrophobic interaction between the hydrophobic protein domain of the latter and the HDL hydrophobic domain. Furthermore, HDL binding to HS-PG was only slightly increased by stepwise additions of Ca^{2+} ions. The adsorbed layer thickness (δ_{el}) showed no change upon addition of HDL to the preadsorbed proteoglycan receptor (Fig. 7B). Maybe that after the strong interaction between HS-PG and HDL a compaction of the proteoglycan — HDL building blocks takes place, which appears in combination with a simultaneous fall in adsorbed amount (Fig. 7A). Therefore, in contrast to LDL, there were no indications of a Ca^{2+}-induced aggregational effect [122]. The adsorbed layer thickness practically did not change upon Ca1 and Ca2 additions, although in the absence of proteoglycan coating, particle size and adsorbed amount significantly increased with Ca2 incubation [112]. In the presence of

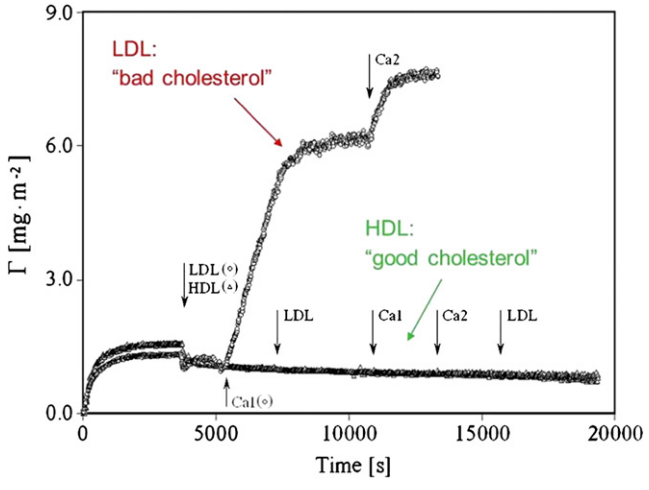

Fig. 6. Comparison of the Ca^{2+}-induced LDL deposition at methylated silica coated with HS-PG in the absence (○) and presence (△) of HDL addition (0.75 mmol/L) prior to the LDL addition (1.5 mmol/L). At time zero, proteoheparan sulfate (0.1 mg/mL) was adsorbed at hydrophobic silica from a Ca^{2+}-free Krebs solution (○, △). The arrows indicate addition of 1.25 mmol/L LDL, 2.52 mmol/L Ca^{2+} (Ca1) and 7.56 mmol/L Ca^{2+} (Ca2), respectively (○) or of 0.75 mmol/L HDL, 1.5 mmol/L LDL, 2.52 mmol/L Ca^{2+} (Ca1), 7.56 mmol/L Ca^{2+} (Ca2) and 1.5 mmol/L LDL, respectively (△). The pH was 7.30 (from [112,116,125]).

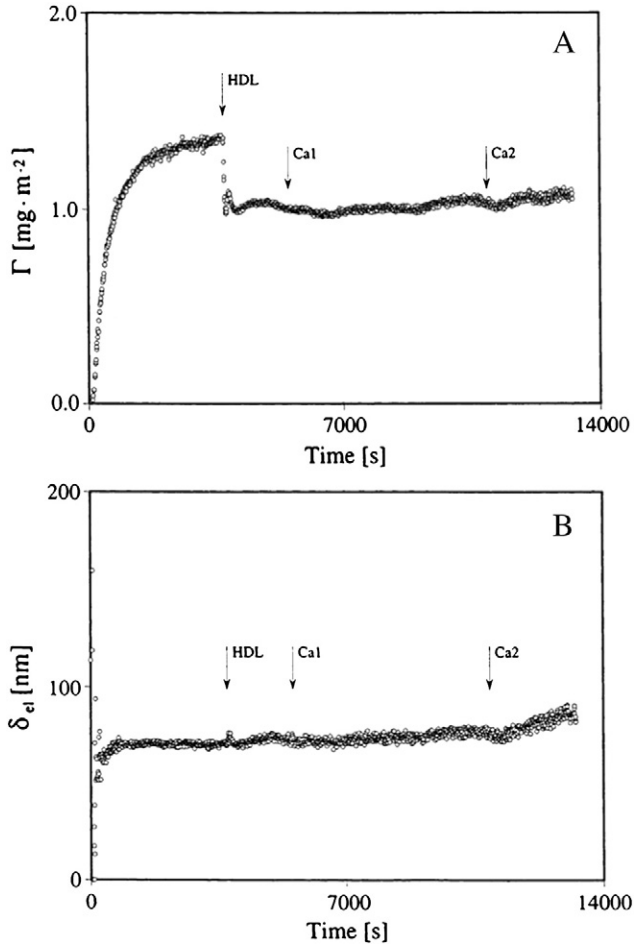

Fig. 7. (A) Total adsorbed amount versus time. At time zero, proteoheparan sulfate (0.1 mg/mL) was adsorbed at hydrophobic silica from a Ca^{2+}-free Krebs solution. The arrows indicate the addition of 0.75 mmol/L HDL, 2.52 mmol/L Ca^{2+} (Ca1) and 7.56 mmol/L Ca^{2+} (Ca2), respectively. The pH was 7.28. (B) Adsorbed layer thickness versus time for proteoheparan sulfate (0.1 mg/mL) at methylated silica from Ca^{2+}-free Krebs solution. The arrows indicate the addition of 0.75 mmol/L HDL, 2.52 mmol/L Ca^{2+} (Ca1) and 7.56 mmol/L Ca^{2+} (Ca2), respectively. The pH was 7.28 (from [112]).

proteoglycan coating, specific effects could not be observed with Ca^{2+} additions lower than 17.64 mmol/L. Thus, this experiment clearly highlights the antiatherogenic effect of HDL.

Given the fact that Lp(a) is a known risk factor for arteriosclerosis [131], it is interesting to study its adsorption at a surface coated with HS-PG. As can be seen from Fig. 8, there is indeed an additional adsorption upon the addition of Lp(a) after HS-PG preadsorption. Quantitatively, this additional adsorption is relatively small, but this could be expected from the flexible nature of the proteoglycan coating, which in turn, could be expected to result in a weaker attractive adsorption driving force of hydrophobic and van der Waals nature, and at the same time partially oppose the adsorption through a steric repulsive interaction. Naturally, the interpretation of these results in terms of absolute adsorbed amounts of the two components is precluded by the absence of information as to the interfacial exchange caused by the Lp(a) postadsorption. This can, at least in principle, be investigated, e.g., with TIRF spectroscopy as done previously by the authors for a number of systems and conditions [132]. However, this means labelling of the components, which can hardly be done without destroying these sensitive systems. On the other hand, since previous studies have shown the interfacial exchange to be limited for protein adsorption at the presently used hydrophobic surface for a number of systems [132,133], the extent of interfacial exchange is expected to be rather limited. This is also supported to some extent by the fast adsorption upon the addition of Lp(a).

Lipoprotein binding to HS-PG preadsorbed from a Ca^{2+}-free Krebs solution at methylated silica resulted in no additional adsorbed amount for LDL during the first 20 min (cf. also Fig. 6). Thereafter, with LDL aggregation, the adsorbance could increase to 14 mg/m^2 within 1.5 h. In contrast, oxLDL steadily reduced the adsorbed amount of the HS-PG/oxLDL complex to 0.7 mg/m^2 within 2 h [122,134,135]. Furthermore, it was striking that after oxLDL addition, the scatter in the measurement rose significantly. Possibly by its intervention as an oxygen free radical, oxLDL seems to bind strongly to HS-PG and to alter its polyanionic GAG binding sites through breaking up the linkage β-D-glucuronic acid β(1 → 4) to *N*-acetyl-β-D-glucosamine as well as to change its protein backbone through peroxidation. The consequence is a dramatic increase in smaller, negatively charged particles (rise in scattering) that desorb from the silica surface. Altogether, this experiment impressively illustrates how sensitive this biosensor assay functions, also as useful approach for further risk stratification in arteriosclerosis. Furthermore, the strong risk factors oxLDL and Lp(a) show immediate nanoplaque build-up upon slightest Ca^{2+} additions.

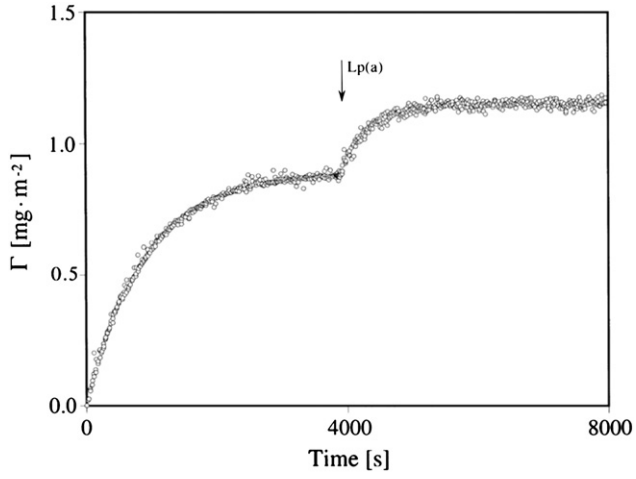

Fig. 8. Adsorption of proteoheparan sulfate at methylated silica from Krebs solution as well as subsequent adsorption of lipoprotein(a) at the proteoglycan-coated surface (from [125]).

4.3. Clinical trials in cardiovascular high-risk patients

In a number of investigations [116,123,131,134,136–139], a good correlation has been observed between in vivo biomarkers and risk factors, on one hand, and lipoprotein risk factor deposition to HS-PG under accelerated in vitro conditions [114]. While the latter could most realistically be performed with endothelial cells adhered to methylated silica surfaces for ellipsometry and microscopy, analogous results were found and already described with simpler and more robust endothelial model surfaces, in which HS-PG was simply adsorbed to methylated silica surfaces (cf. Fig. 5) [140]. With a study in metabolic syndrome patients treated with *Ginkgo biloba* (EGb 761: Rökan novo®, Spitzner Arzneimittel, Ettlingen; Tebonin®, Schwabe Pharmaceuticals, Karlsruhe, Germany), we wanted to evaluate the applicability of the molecular model for nanoplaque formation in the clinical situation. Although there was no change in bulk lipid concentrations after ginkgo medication in the patients, it is demonstrated in Fig. 9 how nanoplaque generation can be reduced. The lipid docking mechanism to HS-PG changed after drug treatment, and the figure shows how the first gradual and then steep increase in nanoplaque formation and size was largely blocked by treatment with ginkgo. Since nanoplaque formation is a

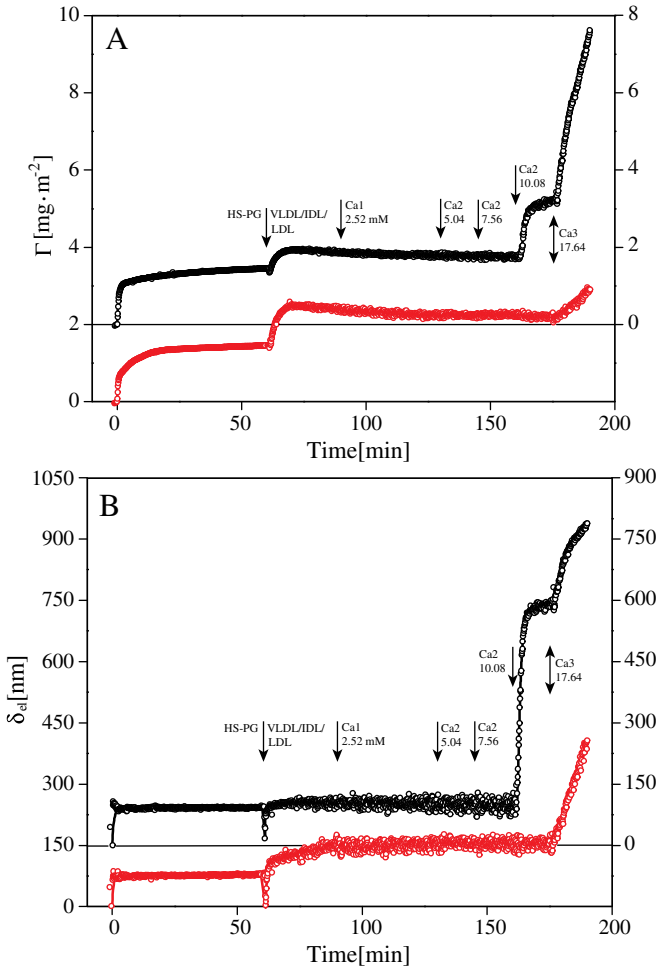

Fig. 9. Total adsorbed amount (A) and layer thickness (B) versus time. At time zero, HS-PG (0.1 mg/mL) was adsorbed on hydrophobic silica from a Ca^{2+}-free Krebs solution. The first arrow indicates the addition of the plasma VLDL/IDL/LDL fraction at its in vivo concentration from a metabolic syndrome patient either untreated (○, black curve) or after 2 months treatment with daily 2 × 120 mg *Ginkgo biloba* extract (○, red curve). Total Ca^{2+} concentrations in solution are indicated at the arrows. The thick, solid lines were computed by an iterative parameter fit of the nonlinear allosteric-cooperative, simple saturative or exponential kinetics to the experimental points using an algorithm for least-squares estimates [215]. The pH was 7.38 (○) and 7.20 (○), respectively (from [114,137]).

Ca^{2+} driven process, a complete Ca^{2+} titration curve was measured. As one can easily see, the stepwise increase in adsorbed amount and layer thickness upon Ca^{2+} additions of 10.08 and 17.64 mmol/L in the baseline measurement is strongly reduced after ginkgo treatment. Calculating the percent reduction in nanoplaque formation and size at each Ca^{2+} concentration used, the mean value of all experimental points during the Ca^{2+} period in question was related to the mean value of all experimental points during the VLDL/IDL/LDL binding period ($[Ca^{2+}] = 0$ mmol/L). The extent of average inhibition in nanoplaque formation (nanoplaque size) was for the different Ca^{2+} concentrations [mmol/L]: *2.52* –14.3%; $p < 0.004$ (−23.4%; $p < 0.001$); *5.04* –16.2%; $p < 0.001$ (−30.4%; $p < 0.001$); *7.56* –20.0%; $p < 0.001$ (−34.0%; $p < 0.001$); *10.08* –26.7%; $p < 0.001$ (−43.2%; $p < 0.001$); *17.64* –54.1%; $p < 0.001$ (−71.1%; $p < 0.001$).

In the present metabolic syndrome study, changes in nanoplaque formation were well correlated to changes in oxLDL/LDL ratio ($r = 0.83$; $p < 0.0210$). That is why we searched for further biomarkers and actuators of oxidative stress and inflammation which could evoke changes in oxLDL/LDL ratio and nanoplaque formation. Before discussing specific correlations between the biomarkers, their averaged changes after ginkgo therapy shall be provided: SOD +17.7% ($p < 0.009$), GPx +11.6% ($p < 0.001$), oxLDL/LDL −21.0% ($p < 0.002$), MPO −29.6% ($p < 0.013$), 8-*iso*-$PGF_{2\alpha}$ −39.8% ($p < 0.002$), IL-6 −12.9% ($p < 0.041$), Lp(a) −26.3% ($p < 0.001$), hs-CRP −39.3% ($p < 0.004$), ALP −14.8% ($p < 0.003$), CREA −11.3% ($p < 0.001$), URAC −10.6% ($p < 0.004$), insulin −9.4% ($p < 0.042$), HOMA-IR −14.0% ($p < 0.024$). Since ΔoxLDL/LDL is strongly correlated with Δ8-*iso*-$PGF_{2\alpha}$ ($r = 0.99$; $p < 0.0001$), which is a potent vasoconstrictor besides MPO [141] and which is likewise tightly correlated to ΔMPO ($r = 0.90$; $p < 0.0003$), an association between blood pressure and oxLDL/LDL was to be expected. In fact, Fig. 10 shows that changes of the diastolic and systolic blood pressure are closely coupled with changes of the oxLDL/LDL quotient.

Previous clinical trials reported a blood pressure lowering effect of statins in hyperlipidemic hypertensive patients who were not taking any antihypertensive drugs [142] and who had already received antihypertensive therapy [143–145]. The mechanisms of the reduction of blood pressure by statins in these patients included the activation of endothelial nitric oxide synthase [146], the downregulation of angiotensin II type 1 receptors [147], and a reduction in the vascular production of ROS [59]. ROS generation does not only play a decisive role in hypertension, but also in lipid peroxidation [148], inflammation [149], atherogenesis [150] and cardio–cerebro-vascular events [124,151–153]. Therefore, we found that changes in BP_{dias} and BP_{sys} were closely linked to changes in oxLDL/LDL ratio (Fig. 10). Moreover, BP_{dias} was lowered significantly by 5.2 ± 2.3 mmHg ($p < 0.0479$), while BP_{sys} did not change. The correlations depicted in Fig. 10 show significant positive linearities allowing for 17 mmHg regulation breadth. This means that in the oxLDL/LDL range concerned here, the metabolic syndrome patients could in principle have varied their oxLDL/LDL quotient and thus their blood pressure by 17 mmHg in total through simple measures like lifestyle changes [114].

In the next study, we will demonstrate how nanoplaque generation can be prohibited or blunted, and furthermore that we can use this model in a high throughput screening of possible candidate drugs against arteriosclerosis in a biosensor application. Within a large clinical trial we tested the lipid fractions of high-risk patients with dyslipoproteinemia and type 2 diabetes mellitus before and after a long-term medication (two months) with fluvastatin (Locol®, Novartis Pharma, Nürnberg, Germany), an HMG-CoA reductase inhibitor and therefore a lipid lowering substance. Here, the results with the whole lipoprotein fraction of VLDL/IDL/LDL in its natural blood concentration of the patients are presented. Fig. 11 shows nanoplaque formation (A) and size (B), averaged from seven high-risk patients, in function of the Ca^{2+} concentration, where the initial amounts for the dimeric complex of proteoglycan receptor and VLDL/IDL/LDL in Ca^{2+}-free solution were normalized to common starting values. On a first glance one recognizes a clear reduction both in nanoplaque formation and size after long-term fluvastatin therapy for all Ca^{2+} concentrations used. Importantly, with normal blood serum Ca^{2+} of 2.52 mmol/L, nanoplaque build-up (size) increased by +43.8% (+26.0%), whereas it was significantly reduced after fluvastatin medication by −19.0% (−6.5%) in relation to the 0 mmol/L Ca^{2+} starting value. These reductions are represented quantitatively in Fig. 12. In normal Ca^{2+} concentration, new plaques were formed to a roughly 45% less extent, nanoplaque size was reduced by 25% [154]. That nanoplaque formation and build-up are Ca^{2+}-driven processes is underscored by the fact of a steadily increasing reduction with rising Ca^{2+} concentration.

Summarizing, it shall be stated that the pleiotropic effects of statins described so far, such as plaque stabilization [117], antiinflammatory effects [155], reduction of thrombus formation [156] and removal of endothelial dysfunction [157], is joined by a further pleiotropic effect, that possibly has decisive prophylactic and therapeutic importance for

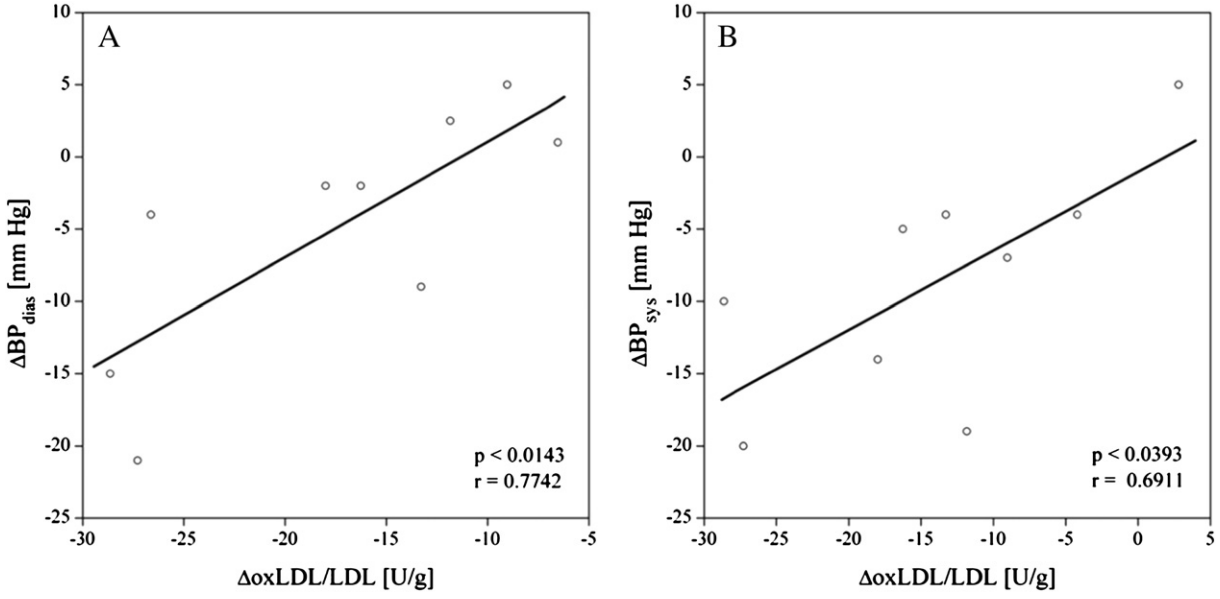

Fig. 10. Significant correlations between changes in BP_{dias} (A) as well as BP_{sys} (B) and changes in oxLDL/LDL ratio from metabolic syndrome patients treated with ginkgo extract for two months (from [114]).

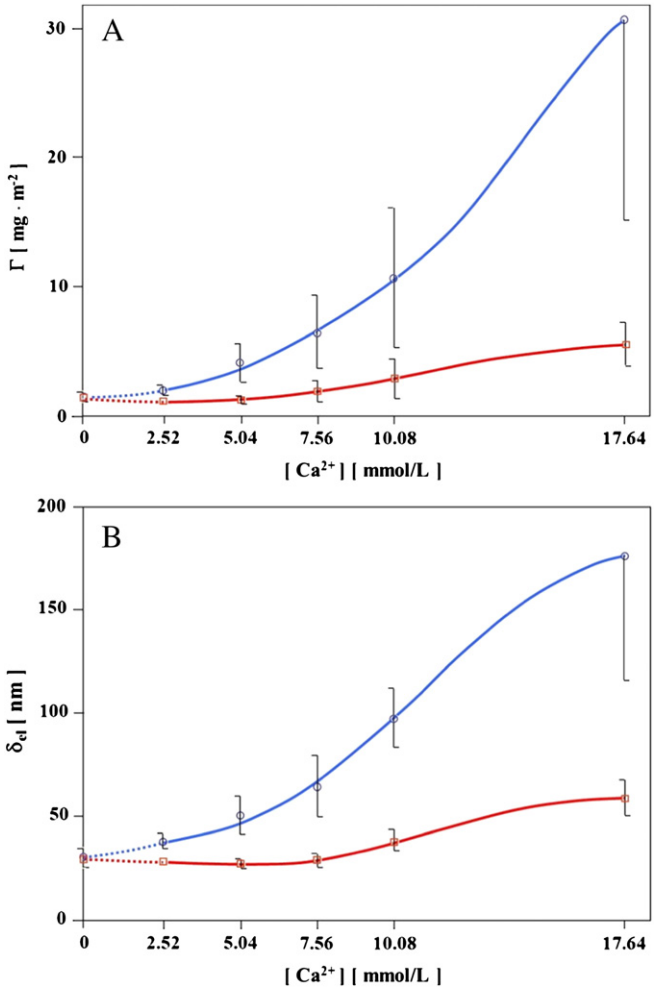

Fig. 11. Nanoplaque formation and size in seven high-risk patients before (blue curve) and after 2-month fluvastatin therapy (red curve). Total adsorbed amount (A) and adsorbed layer thickness (B) are presented in dependence on the Ca^{2+} concentration of the Krebs solution. Adsorbed amounts and layer thicknesses were normalized to a common mean value of the VLDL/IDL/LDL incubation periods (zero Ca^{2+} concentration). Symbols reflect the mean values of all experimental points during the Ca^{2+} period in question of either untreated patients (○) or after 2 months treatment with daily 80 mg fluvastatin (□) (from [154]).

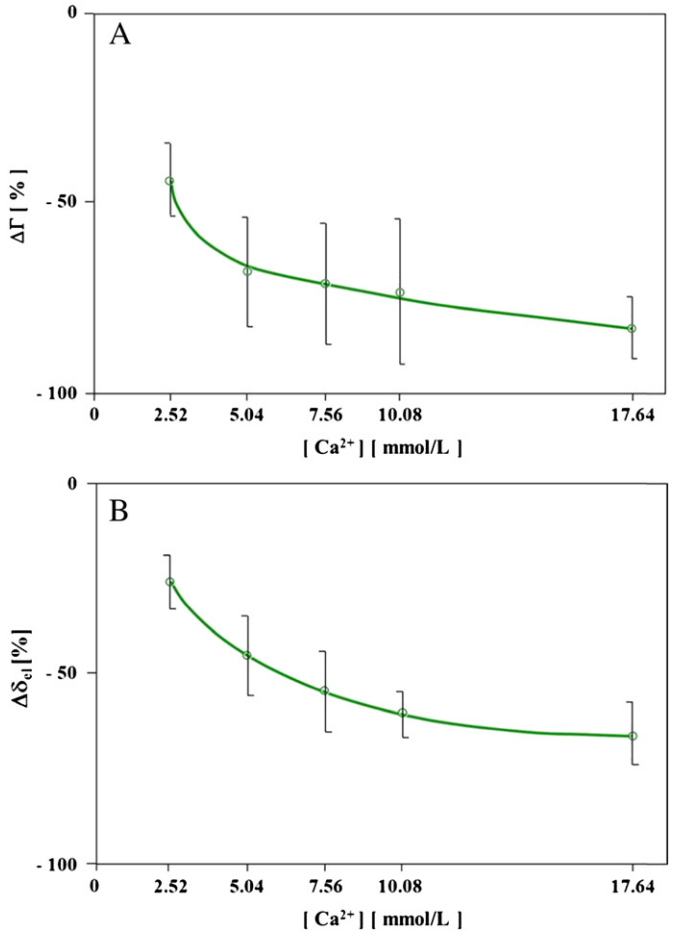

Fig. 12. Reduction in Ca^{2+}-induced changes of adsorbed amount (A) and layer thickness (B) by fluvastatin as derived from the curves in Fig. 11. The reductions upon application of the VLDL/IDL/LDL fractions taken from the same patients treated with one fluvastatin tablet for two months daily intake (○) were calculated in ratio to the control values of the untreated patients (from [154]).

the lowering of cardiovascular risk under fluvastatin with respect to myocardial infarction and stroke. According to our conception, fluvastatin could acutely intervene in the deranged control circuit at the blood – endothelium – matrix interface and assist HDL in its vasculoprotective effect from an increased LDL uptake and formation of ternary proteoglycan receptor – lipoprotein – calcium nanoplaques [123]. Therefore, both HDL and fluvastatin are able not only to prevent the build-up of the heterotrimeric complex but also to partly disintegrate such a primary lesion nanoplaque. Concluding, we believe that the presented model system can be of some use in clinical investigations to estimate the potency of substances against arteriosclerotic nanoplaque formation, as well as in a high throughput screening of candidate drugs against arteriosclerosis in a biosensor application.

With respect to the lipoprotein fractions used in our experiments, the question arises whether these concentrations are relevant within the scenario studied. On the one hand, HS-PGs are integral constituents of the plasma membrane of endothelial cells (e.g., syndecans) and, on the other hand, of the extracellular matrices (e.g., perlecan, fibroglycan). In the first case, our model is adequately suited because we used the lipoprotein fractions at their natural patient blood concentration, and these could interact with the proteoglycan receptor. For the second case, it should be critically mentioned that the lipoprotein ratio applied probably does not correspond to the in vivo relations in the extracellular matrix of the vessel wall. Based on different sizes of the lipoprotein particles and since molecular sieving takes place at the endothelial barrier, the lymph/plasma concentration ratios vary from 0.03 for VLDL sized particles to 0.3 for HDL sized particles [158]. These ratios indicate that blood concentrations are likely to be much higher than concentrations in the extracellular matrix of the vessel wall. Since we wanted to exemplarily show with our experiments that nanoplaque formation and size can be restricted by ginkgo and fluvastatin treatment, the results should be correlated with the in vivo situation.

5. Flow sensing, rhythmogenesis and self-oscillations in the cardiovascular system

After this section on lipoprotein binding, further pleiotropic effects of proteoglycans shall be discussed. Within the following paragraph, attention is expressly paid to the flow- and shear stress-dependent conformational changes of syndecan/perlecan and their importance for blood flow regulation as well as cardiovascular rhythmogenesis and autorhythmicity (see chapter 3.2). The introduction is opened by some general considerations of the autonomic and biochemical regulation of blood vessels.

5.1. Vascular susceptibility to physical factors

Sympathetic neuroeffector transmission by the release of noradrenaline causes a tonic depolarization and closure of inward-rectifier K^+

channels in arterioles. Therefore, in vivo blockade of the sympathetic nerve impulses results in some membrane hyperpolarization. Removal of the vascular endothelium, on the other hand, leads to smooth muscle depolarization of several millivolts and to vasoconstriction. The basal tone can thus be influenced by the release of vasoactive substances from the endothelium [159,160]. These effects are amplified when physical factors directly change membrane ionic conductances and secretory activities of endothelial cells [161]. For example, the release of dilative PGI_2 increases significantly with pulsatile transmural pressure or the occurrence of hypoxic conditions. This reaction is enhanced in response to an increase in blood flow with associated shear stress. However, the rise in shear forces reduces the release of the potent constrictor endothelin, thus promoting vasodilatation. Therefore, the response of vascular smooth musculature to physical effector influences is a balanced interplay between hyperpolarizing-vasodilatory (PGI_2, NO) and depolarizing-vasoconstrictory factors (noradrenaline, endothelin) superimposed on blood vessel basal tone.

5.1.1. Endothelium-derived relaxing factor (NO)

Furchgott and Zawadzki [162] observed an acetylcholine-induced vasorelaxation mediated by a factor released from the endothelium (EDRF). As well as acetylcholine, the vasoactive substances noradrenaline, angiotensin II, serotonin, histamine, bradykinin, adenine nucleotides, thrombin, arachidonic acid, and leukotrienes can release EDRF after interaction with their endothelial receptor. EDRF is a short-lived radical with a half-life counted in seconds and has been identified as NO.

NO is formed in endothelial and smooth muscle cells from L-arginine or arginine derivatives by a NADPH-dependent, Ca^{2+}-activated enzyme. Endothelium-derived NO directly stimulates a soluble guanylyl cyclase in smooth muscle and platelets augmenting intracellular cGMP. This leads, on the one hand, to a relaxation of vascular smooth musculature, and on the other hand to an antiaggregatory and antiadhesive activity for platelets.

5.1.2. Prostacyclin

Both effects are shared by the eicosanoid PGI_2, which is formed in endothelial and vascular smooth muscle cells from membrane-bound arachidonic acid by the enzyme cyclooxygenase. PGI_2 is also chemically unstable ($t_{1/2}$, approximately 3 min) following cleavage of its furan ring with subsequent formation of 6-keto-$PGF_{1\alpha}$, which is excreted in the urine. PGI_2 generation is stimulated by a number of substances including the following:

- Bradykinin
- Choline esters
- Arachidonic acid
- Thrombin
- Trypsin
- Platelet-derived growth factor
- Epidermal growth factor
- Interleukin-1
- Adenine nucleotides.

PGI_2 generation is inhibited by:

- Glucocorticosteroids
- Lipocortin
- Low-density lipoproteins.

Unlike EDRF, PGI_2 displays its vasodilating and platelet-inhibiting effect by activation of adenylyl cyclase. Both substances behave concertedly and synergistically and are coreleased from the endothelial and vascular smooth muscle cells. This coupled release is mediated by a PLC-linked common transduction mechanism and activation of PKC. Additionally, an increase in cytosolic Ca^{2+} is required. Endothelin also causes the release of PGI_2 and EDRF, thereby restricting its own vasoconstrictor and pressor activity.

5.1.3. Stimulation of adenylyl and guanylyl cyclase

PGI_2 and EDRF/NO relax vascular smooth muscle cells by an elevation of the cyclic nucleotides cAMP and cGMP, respectively. In analogy to the effect of adrenaline on the β_2-adrenoreceptor, PGI_2 stimulates adenylyl cyclase after interaction with its specific membrane receptor [159]. While EDRF released to the vascular lumen is inhibited by haemoglobin blocking guanylyl cyclase, the abluminal EDRF/NO diffusion to the subendothelial muscle cell layer leads directly to the stimulation of guanylyl cyclase. The therapeutic relaxant effect of the NO-containing agents sodium nitroprusside and nitroglycerin is also mediated by this enzyme. The increase in either cAMP or cGMP activates cA-PK or cG-PK, respectively, which phosphorylate at least Ca^{2+} (inhibition) and K_{Ca} channels (activation) and the sarcolemmal Ca^{2+} pump (stimulation) [163,164]. The signal transduction chain begins with the elevation in cyclic nucleotides and is identical in all steps to the effect of β_2-receptor agonists, whereby membrane hyperpolarization with a closure of voltage-sensitive Ca^{2+} channels can be considered as the chief cause of vasodilatation. Since it was shown that NO free radicals cause a hyperpolarization of vascular smooth muscle, suggesting that they activate K^+ conductances, the demand for another EDRF which brings about vasodilatation exclusively via hyperpolarization seems to be hardly necessary (EDHF). The observation that cGMP by itself and via cG-PK-induced phosphorylation acts on K_{Ca} channel gating supports this view.

5.1.4. Pressure and shear stress

Driven by the cardiac muscle, the blood flow through the arterial tree of conduit and resistance arteries results in both pressure and shear stress, which influence the vascular wall. Shear stress is a tangential force that is generated by friction between the blood and the endothelial cell membrane [165]. While pressure effects membrane depolarization, the response an endothelial cell makes to shear stress is generally the opposite one, i.e. hyperpolarization with activation of the inward-rectifier K^+ channel. Experimentally, intraluminal saline infusion may cause either a decrease or an increase in the active wall tone of resistance arteries and of small veins. When wall tone is high, the predominant vascular response is dilatation or a decrease in tension. When wall tone is low, the response is contraction or an increase in tension. Consequently, intraluminal flow does not change wall force at an intermediate tension level. Thus, flow tends to shift active wall tone towards this intermediate set point [166]. The balance point is the result of the interaction of these dilator and constrictor responses to flow modified by a variety of other influences. Electrophysiologically, the set point of the vascular smooth muscle cells was determined to be approximately −52 mV. With a more positive membrane potential, the voltage response to shear stress was hyperpolarization, and with a more negative membrane potential, depolarization. It has been shown experimentally that the membrane potential varies between −53 mV and −23 mV when the blood pressure is altered within the range of 40–120 mmHg [167]. Since in arterial blood vessels with normal blood pressure values of the membrane potential of about −48 mV or more positive were found, flow dilatation is the commonly observed response [168].

Flow-dependent dilatation is reduced after removal of the endothelium. As already mentioned, shear stress leads to an increase in K^+ conductance of the endothelial cells and thus to their hyperpolarization. Hyperpolarization raises the inward driving force ($V-E_{Ca}$) for Ca^{2+} ions, which pass the endothelial cell membrane through a nonselective cation channel and stimulate NO synthase [161]. EDRF/NO and coreleased PGI_2 diffuse to the subjacent vascular smooth muscle cells and elicit here the cascade of cG-PK- and cA-PK-dependent reactions, including a membrane hyperpolarization of the muscle cells. The resulting flow dilatation can be so powerful that it reverses the wall force increase caused by stretch, noradrenaline, histamine, serotonin, $PGF_{2\alpha}$ or AVP.

5.1.5. Flow sensor function

Increase in blood flow induces vasodilatation, decrease in blood flow effects vasoconstriction, a fundamental circulation law reads.

Superimposed to this, an increase in blood pressure causes a transmembrane Ca^{2+} inward current via depolarization of the vascular smooth muscle cell membrane which leads to contraction. In a negative feedback circle, the Ca^{2+} influx effects a stimulation of the Ca^{2+}-activatable K^+ channel, the open state probability of which increases. The resulting membrane hyperpolarization produces vasorelaxation. This smooth muscle relaxation is supported by the blood flow velocity augmented through the preceding vasoconstriction. Via enhanced shear forces at the blood–endothelium interface, the increased flow rate leads to a flow-dependent vasodilatation. All the three mechanisms are feedback-coupled and adapt the vascular width to the actual circulation demands. The heart as a pump supplies the driving force for the variation in flow.

As yet the mechanochemical and mechanoelectrical signal transduction pathway which causes hyperpolarization of the endothelial cell membrane in reply to shear stress has not been determined. Shear stress results from the surface drag of the flowing blood on the intimal surface. At this strategic point, polyanionic macromolecules such as proteoglycans and acidic glycoproteins of the endothelial and smooth muscle cell membrane, in the glycocalyx, and/or the extracellular matrix seem to assume a flow sensor function [169,170]. Based upon their viscoelastic properties, flow can induce a "mechanical distortion" in the form of a conformational change of these specific surface molecules, which is again reversed with a decrease in flow. Support comes from the observation that flow dilatation occurs only above a distinct mechanical threshold of shear stress (τ, 1.3 N/m^2) [171]. Therefore, it requires a certain energy to accomplish the conformational change of the sensor molecules. Moreover, they are polyanions as a result of their sulfated, carboxylated, or sialic acid-containing residues. These flow sensor molecules are thus endowed with a high and also specific cation-binding capacity (Na^+, Ca^{2+}), which is apparently involved in the electrical transformation of the signal [170]. Finally, it should be emphasized that these biopolyelectrolytes are multiply anchored in basement membranes, extracellular matrix, and cytoskeleton.

5.1.5.1. Proteoglycan viscoelasticity. Since the Na^+-dependence of flow-induced dilatation in resistance arteries was reported, such a sensor molecule has to fulfil certain mechanochemical and mechanoelectrical requirements [172]. It should possess viscoelastic and cation binding properties capable of undergoing conformational changes caused both mechanically and electrostatically. Moreover, the latter should be ion-specific.

Viscoelasticity is not restricted to a few macromolecular substances, rather it is a property which all such substances attain above their specific softening temperature, provided that they have not already disintegrated. The anionic biopolymers of proteoglycans that are found in vascular connective tissue, and also in the cell membrane of endothelial and smooth muscle cells, belong to this group of substances [173,174]. If biopolyelectrolytes are subjected to externally applied strain for some time, the stretched molecules will gradually shift and assume their inherent shape in their new position. This phenomenon, whereby the internal stress of the system returns to equilibrium by a change in places of the molecules, is called relaxation. This happens in every flowing liquid, only that in normal, low viscosity liquids relaxation occurs instantaneously so that the elastic recoil is not observed. The viscoelastic substances may therefore be classified as highly viscous liquids. Alternatively, they may be considered as liquids with large relaxation constants because with short periods of deformation they will exhibit elastic properties and with extended periods of external pressure they will show flow characteristics. A typical characteristic is the large difference between the G-moduli of a single substance. The relaxation time depends strongly on structural parameters, e.g., minor changes in the degree of cross linking with any one chain.

The viscoelastic deformation is, in terms of solid body physics, an intramolecular relaxation because it is a flow phenomenon. A cross linked biopolyelectrolyte can be transformed from a randomly coiled to an oriented state by stretching it. With increasing shear stress, the intramolecular and macroscopic viscosity decreases. This is plausible when one considers that the external force applied stretches the polymer chains to a greater or lesser extent (coil deformation). This reduction in entropy induces elastic recoil. The speed of an unrestricted viscoelastic recoil is a measure of the intramolecular viscosity, which can be correlated with this limited flow process consisting of a conformational change in polymer chains. As such it is dependent on the primary chain structure and the temperature.

Fig. 13 demonstrates the results of a competition experiment with a multi-chain chondroitin 4-sulfate-polypeptide complex (CS-P) which was derived from native connective tissue. In this investigation the static and dynamic binding properties of Na^+ ions were studied. The influence on $R_{2_{ex}}$ of an increasing Ca^{2+} concentration and of elastic energy stored and lost per unit volume of the solution under non-stationary shearing conditions by shaking was measured. It appears that this increase of up to 3.75 mmol/L Ca^{2+} in the solution after it has been added and shaken does not lead to a reduction in $R_{2_{ex}}$ but regularly to a fast and drastic elevation. Only with 6.25 mmol/L $[Ca^{2+}]_o$ competition behaviour appears. The transverse relaxation rate falls. After the addition of Ca^{2+}, the 'envelope curve' initially shows an increase and above 3.75 mmol/L $[Ca^{2+}]_o$ a decrease in $R_{2_{ex}}$ [175]. This curve confirms earlier findings on CS-P [176–178] and native vascular connective tissue [179]. It could be interpreted as a conformational change of the macromolecules which is due to a cross linking between different chains owing to the strong ability of Ca^{2+} to build complexes. This aggregation is expected to affect both τ_c (reduction of the local mobility) and $p_B\chi^2$ (higher local charge density, increased field gradients). As we have discussed earlier, not only are Ca^{2+} ions bound to the polyanions but also Na^+ ions. These are allosterically-cooperatively bound, in fact to a specific site. A second binding site remains purely competitive and prevails with higher Ca^{2+} concentrations (cf. 6.25 mmol/L $[Ca^{2+}]_o$) [180]. It is clear therefore, that Na^+ ions are only bound within a relatively small range of $[Ca^{2+}]_o$. Above this range they will be released again.

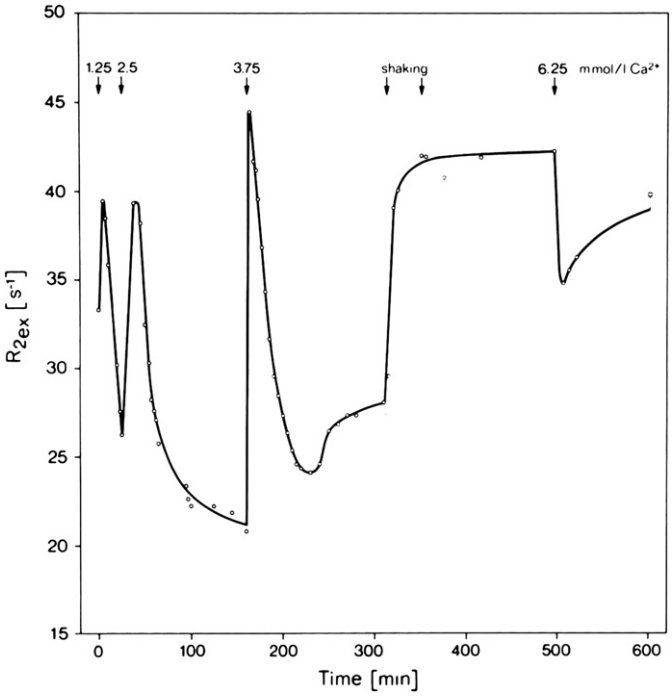

Fig. 13. Time dependence of $^{23}Na^+$ excess transverse relaxation rate for 0.2 mol/L (monosaccharide units) CS-P at pH 12.2 with a sodium concentration of 0.3 mol/L. Additions of Ca^{2+} ions and/or shaking of the sample (at the arrows) caused an increase in $R_{2_{ex}}$ (decrease with 6.25 mmol/L Ca^{2+}) and then a spontaneous decrease in $R_{2_{ex}}$ (increase with 6.25 mmol/L Ca^{2+}) (from [169]).

5.1.5.2. Proteoheparan sulfate as flow sensor at the endothelium–blood interface. Fig. 13 further shows that with a constant Ca^{2+} concentration the simple shaking of the solution leads to an increase of $R_{2_{ex}}$. At these low excitation frequencies (similar to physiological frequencies), aggregated CS-P can store much more energy than single-chain peptidoglycan monomers. This indicates that aggregation of proteoglycans greatly enhances network formation. The extent of the network formation in proteoglycan solutions is augmented by both an increase in concentration (0.1 mol/L CS-P) and the proportion of proteoglycan present as aggregates (Ca^{2+} ions). However, the initial network organization, existing in these highly aggregated solutions, is particularly sensitive to disruption at low shear rates. This means that with increasing shear rate ('shaking') the CS-P solution showed shear thinning, a decrease in viscosity which is a macroscopic manifestation of the net loss of the number of intermolecular interactions during shearing [175]. Thus, shear thinning involves the disruption of the network structure formed by aggregates and at the same time an increase of formerly occluded ion binding sites [181]. Therefore, the 'shaking' in Fig. 13 effects an increase in $R_{2_{ex}}$, which is also an expression of an augmented Na^+ binding to the anionic polyelectrolyte.

From Fig. 14B, the conclusion can be drawn that the sudden changes of τ_c induce intra- or intermolecular cross-linking leading to conformational transitions of the polyelectrolytes and to molecular associations. Such a higher molecular network formation is coupled with an

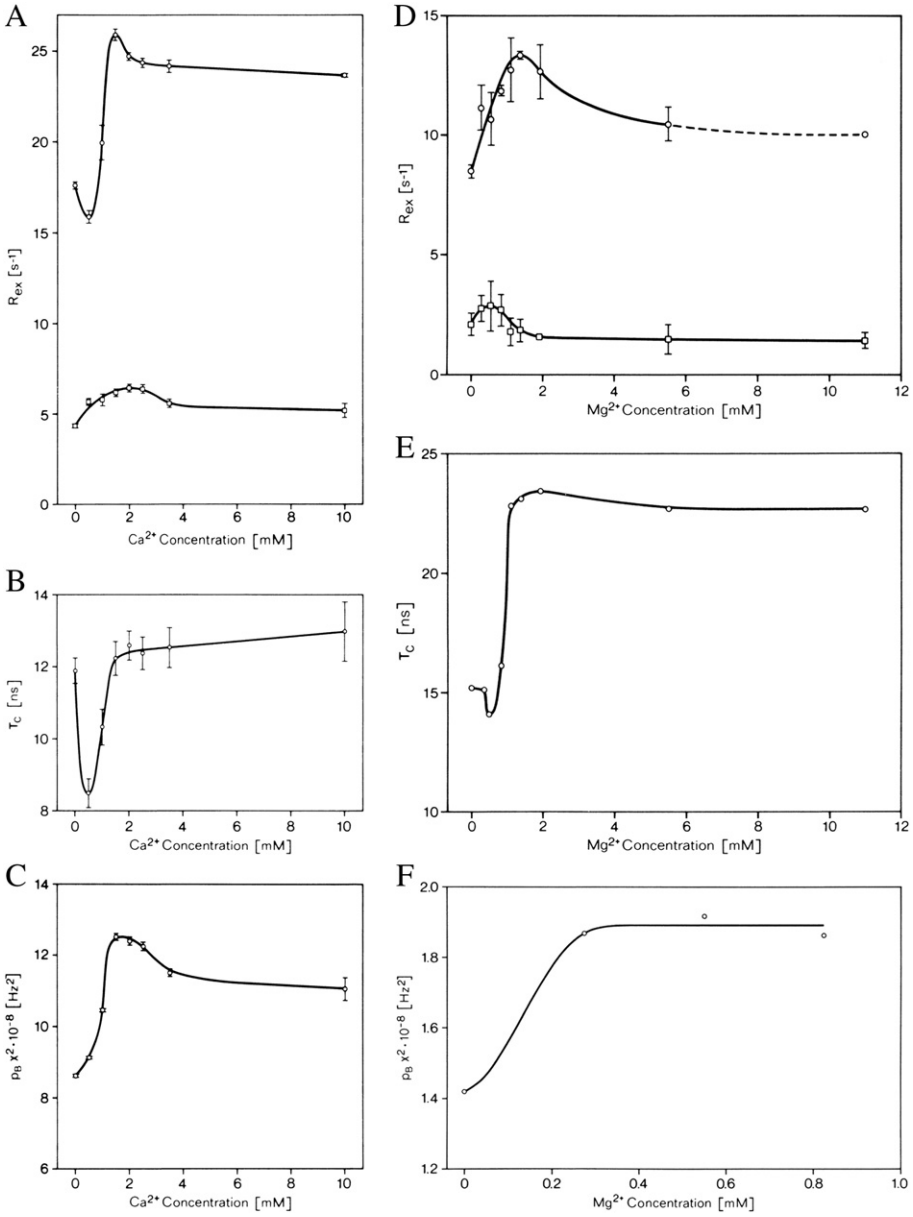

Fig. 14. (A) $^{23}Na^+$ excess longitudinal (□) and transverse relaxation rates (○), $R_{1_{ex}}$ and $R_{2_{ex}}$, in dependence on different Ca^{2+} concentrations of a normal Krebs solution ($[Na^+]_o$ = 151.2 mmol/L) containing native vascular connective tissue at pH = 7.3. For 0.5 mmol/L < $[Ca^{2+}]_o$ < 2 mmol/L the ratio $R_{1_{ex}}/R_{2_{ex}}$ is indicative of a conformational transition in the connective tissue polyanions. In addition, the initial rise of the longitudinal relaxation rate signifies allosteric, cooperative Na^+ binding to the matrix macromolecules. (B) Correlation time for Na^+ ions bound to native vascular connective tissue. The ratio $R_{1_{ex}}/R_{2_{ex}}$ was used in the calculation of τ_c. (C) $p_B\chi^2$, the product of the fraction of bound Na^+ and the squared quadrupolar coupling constant. (D) The $^{39}K^+$ excess longitudinal (□) and transverse relaxation rates (○), $R_{1_{ex}}$ and $R_{2_{ex}}$, in dependence on different Mg^{2+} concentrations of a 1.17 mmol/L K^+-Krebs solution containing native vascular connective tissue at pH = 7.0. For $[Mg^{2+}]_o$ < 1.38 mmol/L the ratio $R_{1_{ex}}/R_{2_{ex}}$ is indicative of a conformational transition in the connective tissue polyanions. In addition, the initial rise of the longitudinal relaxation rate signifies allosteric, cooperative K^+ binding to the matrix macromolecules. (E) Correlation time for potassium ions bound as a function of the Mg^{2+} concentration of the Krebs solution. The ratio $R_{1_{ex}}/R_{2_{ex}}$ was used in the calculation of τ_c. (F) $p_B\chi^2$, the product of the fraction of bound K^+ and the squared quadrupolar coupling constant, as a function of the Mg^{2+} concentration of a 1.17 mmol/L K^+-Krebs solution (from [169,180]).

increased viscosity for solutions with ideal statistic coils according to the Einstein–Kuhn [182–184] viscosity law

$$[\eta] = \frac{2.5\sqrt{M}}{K^0_{\rho[\eta]}} = K^0_{[\eta]}\sqrt{M} \quad (1)$$

The degree of the rise in viscosity, $(\eta_{rel} - 1)/c = \eta_{sp}/c$, is a function of the molecular weight M in such systems. This is based on the characteristic property of coils that their density decreases as their molecular weight increases. One might conclude from this that the $R_{2_{ex}}$ increase with elevated Ca^{2+} concentrations (Fig. 14A) could be due to this rise in viscosity. This, however, is most unlikely because Fig. 13 demonstrates that the disruption of the network structure with concomitant shear thinning also leads to a dramatic increase in $R_{2_{ex}}$. Therefore, greater viscosity cannot be held responsible for the increase in Na^+ binding.

The deformation of structures, originating in the intermolecular associations of macromolecules, by shear stress – just as the creation of such structures by coil deformation – is an event which can proceed with different speeds. The time constant derived from Fig. 13 has a mean value of 4 min. Since $R_{2_{ex}}$ abruptly rises with shaking, this time constant allows the intervention in cardiovascular control.

The viscoelastic recoil is expressed in the relaxation time, which is a measure of the viscous retardation effect after a sudden application of a constant load on a viscoelastic substance. Ideally, elastic solids, with no internal viscous or frictional dissipations, have zero retardation times. The mean time constant for $R_{2_{ex}}$ relaxation after the addition of Ca^{2+} ions and shaking, as determined from the protocol in Fig. 13, was 25 min. Since the decrease in $R_{2_{ex}}$ and therefore the energy dissipation in the solution start once shaking ceases, this property, which is combined with a fall in the bound Na^+ fraction, may also be of importance for cardiovascular control.

In rabbit ear resistance arteries, Bevan and Joyce [160] reported on a sodium dependent, flow-induced dilatation which is endothelium-independent and a function of the rate of infusion. The authors hypothesized that this flow-dilatation is the result of a sodium dependent mechanism in vascular smooth muscle. It seems that their observation neither involves Na^+ pump activity, nor fast Na^+ channels, nor Na^+-Ca^{2+} exchange nor Na^+–H^+ exchange. HS-PG, a viscoelastic, anionic polyelectrolyte, has been described as a constituent of the vascular smooth muscle cell membrane [173,174]. The polymer seems to be located at circumscribed sites in the membrane, probably in the vicinity of the Na^+ channel or it takes part in the channel's molecular structure. The protein core is integrated into the cell membrane while the GAG side chains protrude into the extracellular space (Fig. 15). It is quite possible that this proteoglycan, appearing only occasionally (low local concentration), acts as a flow sensor [185].

In flowing viscous solutions containing molecular coils, these coils will align with the direction of flow. One of the contributing factors to this alignment with flow of molecular coils is any deviation from the perfect sphere. Alignment is more pronounced in diluted solutions of high molecular polymers. This may contribute to a reduction in viscosity, the effect being greater for a steeper flow gradient. This is because the coils in the structurally viscous solutions tend to link layers of flow. Linkage is least when the coils are aligned. When a flow gradient exists, not only are the coils aligned with the direction of the current but also they become elongated. Inevitably, this results in a more or less pronounced parallel orientation of chain segments. These segments are, of course, not covalently cross-linked but auxiliary valency associations are formed. This conformational change from a random coil to a streamlined filament structure, depending on the flow gradient, is accompanied by an increase of binding sites for counterions. In blood, these are predominantly Na^+ ions. When the flow is reduced, the viscoelastic recoil forces become effective which then cause a decrease of Na^+ binding due to a conformational change. The corresponding time constants have already been discussed. Moreover, the τ_c values in

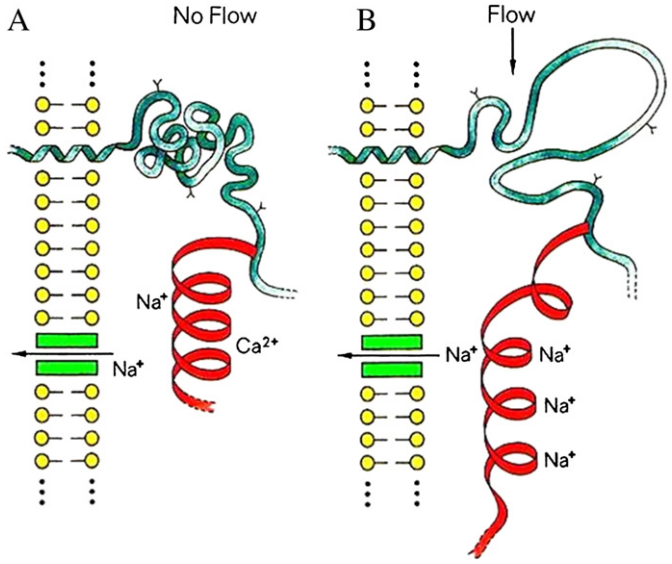

Fig. 15. Schematic representation of proteoheparan sulfate as a flow sensor at the endothelium–blood interface. (A) Under no-flow conditions, the viscoelastic polyelectrolyte assumes a random coil form, whereby most of the polyanionic sites undergo intramolecular hydrogen bonding. The random coil with only one GAG side chain is shown. This is a left-handed 2_1-helix with an identity period of 1.86 nm, whereby a disaccharide unit has a height of 0.93 nm projected onto the axis. Thus, it is a very extended conformation. The height can also be diminished through a conformational change induced by Ca^{2+} ions, so that the pitch of turns becomes shorter. The protein core of a proteoheparan sulfate macromolecule has globular and helical domains. The hydrophobic, helical section of the protein core is anchored in the membrane of an endothelial cell. (B) Blood flow causes a conformational change from the random coil state to the directed filament structure state. This conformational transition effects a protein unfurling and molecular elongation of the GAG side chains, i.e., the pitch of turns increases like in a 'stretched' spring. This configuration is therefore combined with an increase in binding sites for Na^+ ions. Counterion migration of Na^+ along the polysaccharide chain is followed by transmembrane Na^+ influx into the endothelial cell and by endothelial cell membrane depolarization (from [185]).

Fig. 14B may also be related to counterion migration along a polysaccharide chain or some motion within the chain [176]. If HS-PG is in the immediate vicinity of the Na^+ channel, or is involved in its formation, then not only Na^+ binding but also transmembrane Na^+ flux is plausible.

5.1.5.3. Sensor conformation and sensitivity to sodium. The finding of a Ca^{2+}-initiated conformational change in the blood flow sensor was confirmed by surface force, ellipsometry and pump–supercontinuum-probe measurements [18,186–188]. The effects of electrolytes on the adsorption of HS-PG and HS, the electrolyte-dependent conformation of HS-PG adsorbed at hydrophobic surfaces and the interaction forces between such surfaces was investigated. It was found that HS-PG adsorbs at hydrophobic silica surfaces, the adsorbed amount increasing strongly on addition of $CaCl_2$. HS does not adsorb at either hydrophobic or hydrophilic silica surfaces, even in the presence of excess salt. Thus, the adsorption of HS-PG at hydrophobic surfaces occurs via its hydrophobic protein moiety, which acts as an anchor for this macromolecule. At the endothelial cell membrane, the hydrophobic domain of the protein core is integrated in the hydrophobic interior of the cell membrane, while the hydrophilic domain of the protein core together with the polyanionic HS side chains protrudes into the blood stream. Thus, we have a model for the in vivo scenario, since the orientation of the sensor macromolecule at the present hydrophobic model surface is expected to be similar to that in the endothelial cell membrane. In fact, by previous surface force measurements, we have shown that HS-PG orients at hydrophobic surfaces in accordance to this conception [18].

In Fig. 16, the forces between HS-PG layers adsorbed at hydrophobic surfaces are represented in solutions of different cation species. The force curves observed are composed of one distant slowly decaying regime and one proximal hard wall regime at distances of separation

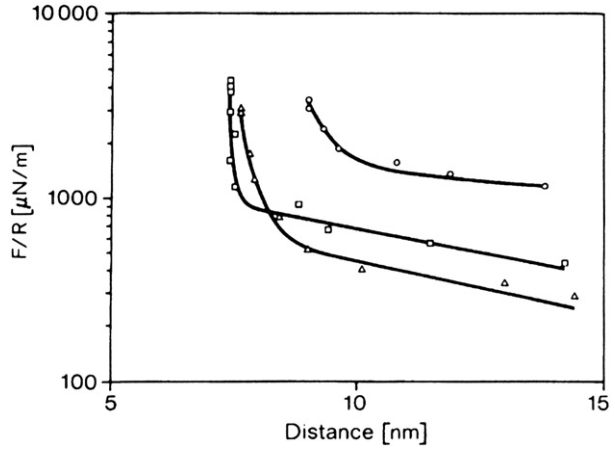

Fig. 16. Comparison of the forces obtained between proteoheparan sulfate layers adsorbed at hydrophobic surfaces as a function of the distance of separation at different excess electrolyte concentrations. The forces were measured on approach in 0.1 mmol/L NaCl (○), 1.25 mmol/L $CaCl_2$ (□), and 2.5 mmol/L $CaCl_2$ (Δ) (from [18,189]).

smaller than 10 nm. The forces in the distant regime were reversible on approach and separation. On addition of $CaCl_2$, the range of the distant regime interaction was diminished. The decay length is reduced from 24.8 nm in 0.1 mmol/L NaCl over 8.3 nm in 1.25 mmol/L $CaCl_2$ to 7.6 nm in 2.5 mmol/L $CaCl_2$. At these Ca^{2+} concentrations, the Debye lengths are 5 and 3.5 nm, respectively. Steric rather than simple double-layer forces dominate the observed interaction. Electrostatic interactions are still important since they strongly influence the conformation of the HS side chains and thus the range of interlayer forces. The distance of separation at the onset of the proximal repulsive regime is reduced with Ca^{2+} as well. For example, a force of 1000 μN/m is encountered at 18.04 nm in 0.1 mmol/L Na^+, while the corresponding values at 1.25 and 2.5 mmol/L Ca^{2+} are 7.64 and 8.08 nm, respectively. These results reflect the displacement of the proximal hard wall from 8.53 over 7.25 to 7.28 nm on the addition of Ca^{2+}. Although the screening of the electrostatic repulsion contributes to this decrease, it cannot account for the whole effect. Instead, as was the case with the distant force regime, a contraction of the GAG chains in the presence of Ca^{2+} ions is likely to cause this effect.

This observation was supported by PSCP experiments in the 280–700 nm spectral range (Fig. 17). We analyzed the results of these PSCP measurements with femtosecond time resolution to investigate the ultrafast dynamics of tryptophan as reference substance, HS-PG Na^+ salt, and HS-PG after Ca^{2+} addition. The measured broadband transient absorption spectra revealed indications of excited state absorption, stimulated emission and resonant energy transfer. The results for tryptophan in Krebs solution confirmed the solvation dynamics reported recently by fluorescence up-conversion measurements, but also provided novel information about the ESA signal evolution. Comparing the data obtained with tryptophan to those with HS-PG, qualitative differences in the broadband absorption features were apparent. An exponential decay with a time constant of 24 ps attributed to RET, presumably from tryptophan residues to the GAG side chains, was obtained in addition to the short term solvation dynamics. Moreover, the difference in absorption by adding Ca^{2+} to the probe was investigated. Upon Ca^{2+} binding to HS-PG, a conformational transition of the protein proven supplementarily in surface force and ellipsometry measurements, probably changed the resonant energy transfer and hence the absorption spectrum [187,188]. A minor decrease of the HS-PG signal was found that evolved in the minute range after addition, but was blue-shifted and vanished within 1 ps after the UV excitation. These small but clearly visible features, which were only visible due to the high spectral and temporal resolution of the PSCP technique, provide a first insight into the molecular formation of nanoplaques at blood vessel interfaces.

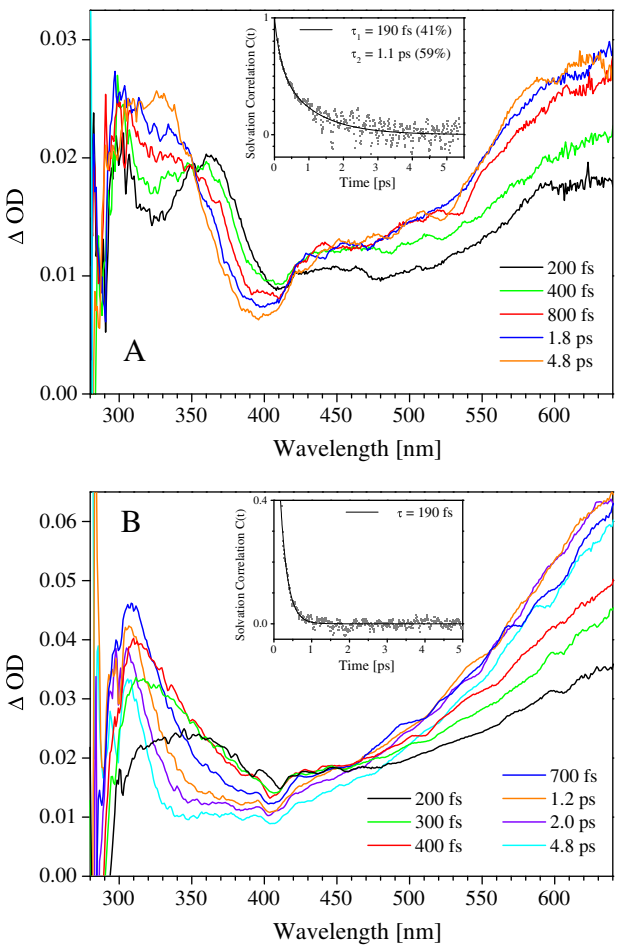

Fig. 17. (A) Transient PSCP spectra of tryptophan in Krebs solution for the wavelength range 280 ≤ λ ≤ 640 nm following laser excitation at 282 nm. Inset: Solvent correlation function $C(t) = (\nu(t) - \nu(\infty)) / (\nu(0) - \nu(\infty))$ produced from the transient optical density signal, where $\nu(t)$ is the maximum of the optical density around 350 nm at time t. The position of the maxima was determined by fitting log-normal functions through the spectra. A two-exponential function was fitted through the points. (B) Analogous PSCP spectra of HS-PG in Krebs solution. Inset: Solvation correlation function constructed from the peak evolution, predominately caused by ESA showing only a fast one-exponential decay (from [188]).

In future, studies on the proteoglycan — lipid interaction utilizing this approach may enhance our understanding of atherogenesis.

Taking these investigations together, this means that Ca^{2+} ions can influence, via such a conformational change, the extent of Na^+ binding to the sensor molecule and thus the signal transduction. Since presumably less Na^+ ions are bound after shortening of the HS chains, Ca^{2+} ions are apparently able to adjust the sensitivity of the sensor. These surface force, ellipsometry and femtosecond spectroscopy measurements on native HS-PG, adsorbed at a hydrophobic surface or in solution, proved to be extremely Ca^{2+}-sensitive in adsorption, conformation and Na^+ binding [18,186]. First of all, some fundamental lines of concept on the adsorption of anionic biopolyelectrolytes should be considered. The adsorption of the sensor macromolecule to a hydrophobic silica surface is possible via its hydrophobic protein moiety. It is supported by electrostatic screening of the highly charged polyelectrolyte. Therefore, general electrostatic effects would be expected to strongly influence the interfacial behaviour of proteoglycans. The adsorption should be higher at a higher electrolyte concentration, since the electrolyte will screen the electrostatic double-layer interactions, such as the repulsive image–charge interaction between the proteoglycan charges and the low dielectric constant hydrophobic surface, and the intralayer repulsive interactions between similarly charged

segments of the adsorbed proteoglycan. Since the electrostatic interplay counteracts adsorption, its screening will promote adsorption.

From Fig. 18, it follows that not only the effects of divalent ions may be subdivided into an electrostatic and a non-electrostatic contribution. The same seems to apply for monovalent ions. Both Na^+ and K^+ result in an adsorbed amount of HS-PG decreasing with increasing electrolyte concentration. Furthermore, the effects of the two monovalent cations are of different magnitude. And finally, while the effect of Na^+ is essentially instantaneous ($k_{Na^+} > 10^{-1}\ s^{-1}$), the effect of K^+ is much slower ($k_{K^+} = 4.2{\cdot}10^{-3}\ s^{-1}$). These effects of the monovalent cations are not easy to understand. Although both promote adsorption of HS-PG due to electrostatic reasons (screening of the repulsive intralayer electrostatic and image — charge interactions), both cause a decrease in the adsorbed amount at high concentrations in the presence of divalent cations, thus opposing the effects of the latter. From previous studies, we have inferred that similar effects occur for the HS chains in the absence of the protein core [186]. Thus, the GAG moieties are likely to be responsible for these unexpected electrolyte influences. These cation-specific effects seem to form the basis for the biological function of these systems.

HS-PG is able to change its conformation both through intervening shear forces and through the action of cations. The former mentioned configurational transition is based upon the viscoelastic properties of these macromolecules, the latter upon the anionic polyelectrolyte characteristics. Therefore, the coil – helix and helix – coil phase conversions seem to be tightly linked to the protein moiety, while the fine adjustment of the flow sensor could additionally be determined by the cation composition of its microenvironment. Hence, this has decisive influence on signal transduction. In the surface force and ellipsometry investigations, a contraction by 8.9 nm of the sensor macromolecule appeared under the influence of a physiological external Ca^{2+} concentration. Na^+ ions, on the other hand, induced a molecular extension by 13.7 nm. For the following considerations, we take the $^{23}Na^+$ NMR results on HS, the GAG side chain, into account [189]. The bound Na^+ fraction, $p_B\chi^2$, decreases between 0 and 1.25 mmol/L $[Ca^{2+}]_o$, i.e., in the physiological range of the freely ionized, non-protein-bound Ca^{2+} fraction in the blood. This would mean that the Ca^{2+}-elicited shortening of the biosensor leads to a restriction in Na^+ binding, while the Na^+-elicited elongation promotes the Na^+ binding. When a rough estimate with the Bjerrum length for Na^+ is allowed here, 12 Na^+ ions would be released into the blood by tightening of the 'helical spring'. On the other hand, stretching of the spring by sodium would make an additional binding of 19 Na^+ ions feasible [177,190,191]. This means that Na^+ ions intensify the sensitivity of the flow sensor to Na^+ in an autocatalytic process and thus promote the signal transduction [cf. 192]. Ca^{2+} ions would lower the susceptibility for Na^+ to be adsorbed. And finally, the idea that Na^+ ions are primarily sensed by HS-PG is supported by the determination of a very small time constant for Na^+. All the Na^+ effects observed occurred practically momentaneously.

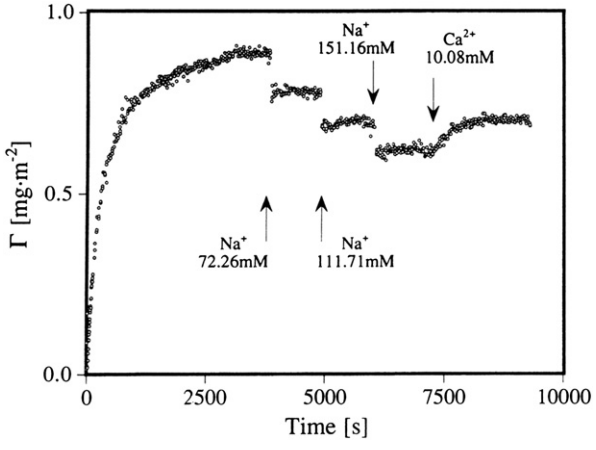

Fig. 18. Adsorption of proteoheparan sulfate from Na^+-deficient (32.81 mmol/L) Krebs solution at methylated silica. The first, second and third arrow indicates addition of Na^+ to a final concentration of 72.26 mmol/L, 111.71 mmol/L and 151.16 mmol/L, respectively, corresponding to a $C_{s,tot}$ (1:1) of 76.95 mmol/L, 116.40 mmol/L and 155.85 mmol/L, respectively. $C_{s,tot}$ (2:1) was 3.62 mmol/L. The fourth arrow indicates the addition of Ca^{2+} to a final concentration of 10.08 mmol/L (from [90,189]).

5.1.5.4. Flow sensing upon lipoprotein binding. The binding of lipoproteins to the HS-PG receptor (flow sensor) changed its conformation through an increased or decreased nanoplaque formation with the result of a change in polarization of endothelium and vascular smooth muscle cell membranes and in the smooth muscle cell tension based on modifications of the signal transduction chain elicited by the intracellular domain of the HS-PG molecule [122]. While LDL led to membrane depolarization, vasoconstriction and lowering of cGMP levels in the smooth muscle cells of human coronary arteries (Fig. 19), the cardiovascularly protective HDL effected the opposite, thus supporting the flow sensor activity in its regulating and adapting mechanisms to the requirements of a functioning circulation. Fig. 19A shows the stepwise decrease in wall tension with increasing flow rate from 3 mL/min ($T = 2.000$ g) to 100 mL/min ($T = 1.287$ g). The addition of 100 mg/dL LDL to the blood substitute solution reduced tension from 2.000 g to 1.796 g when increasing the flow rate (Fig. 19B). This means that in this case the flow-dependent dilatation was impaired by 71.4% through LDL-application, or, utilizing the Laplace equation, perfusion would have been reduced by 48% [185].

After this comment, the importance of a functioning flow sensor for the regulation of organ perfusion is evident. Disturbances in the electrolyte and lipid metabolism, an endothelial dysfunction, hypertension or arteriosclerosis may affect the sensor properties. For example, the flow-dependent dilatation reverses to flow-dependent constriction with increasing degree in arteriosclerosis (Fig. 20). An estimate shows that the increase of blood flow under in vivo conditions with a medium grade of arteriosclerosis is reduced to one fifth. This fact has deleterious consequences especially under hypoxia [193], in bypass operations and heart transplantations. The hypoxic dilatation, which is normally further amplified via an increase in blood flow, is restricted in a double sense in the arteriosclerotic vessel or even completely abolished. The drastic change of flow-dependent dilatation in arteriosclerosis (Fig. 20) has presumably three reasons: (i) The diminished NO and PGI_2 synthesis and release in endothelial and vascular smooth muscle cells [189], (ii) a dysfunction of the HS-PG sensor. An oversulfatation in certain domains of the molecule could result in an augmented Ca^{2+} binding and thus an impairment of the signal transduction through a Na^+ binding reduced by Ca^{2+} competition, and (iii) oversulfatation would promote LDL binding.

5.1.5.5. Flow-dependent vasodilatation and ξ-potential. The particularly interesting question arises regarding how the flow-dependent relaxation comes about. The exact signal transduction pathway is as yet unknown. It should be pointed out, however, that the shear-stress-dependent and conformation-dependent Na^+ binding to HS-PG conforms to the strictly serum-Na^+-linked flow-induced vasodilatation [172]. The interaction with Ca^{2+} ions also agrees. The following possibilities provide a theory for signal transduction which should ultimately lead to an influx of Ca^{2+} ions into the endothelial cell:

(1) The conformational change of HS-PG to the unfurled filament state, connected with increased Na^+ binding, leads to counterion migration along the polysaccharide chain. Since the flow sensor is put up like an umbrella over unspecific, voltage-dependent ion channels in the endothelial cell membrane (mainly conducting Na^+), a transmembrane Na^+ passage subsequently follows. The Na^+ inward current depolarizes the endothelial cell membrane enhancing the Ca^{2+} permeability [161]. Ca^{2+}

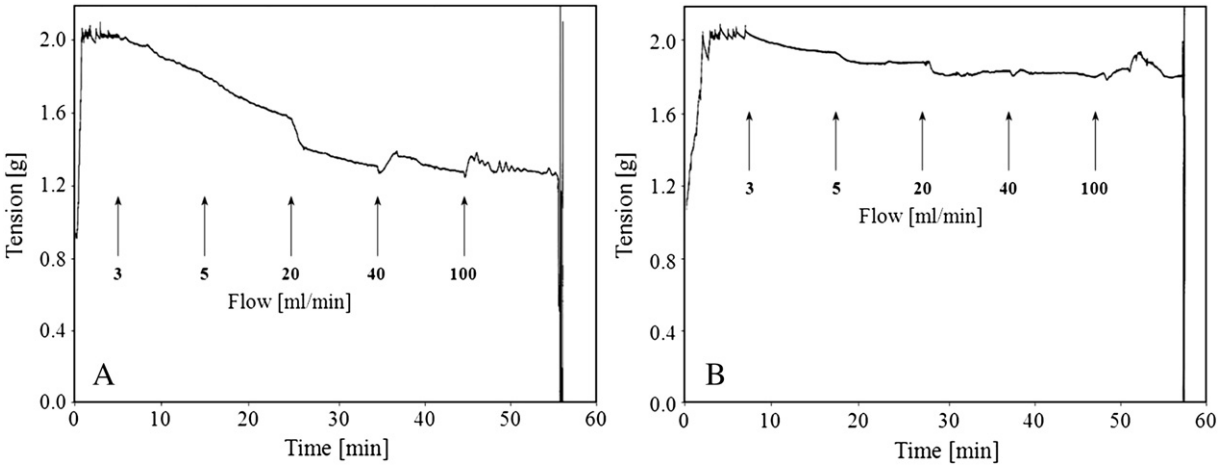

Fig. 19. (A) Flow-dependent relaxation in a normal human coronary artery segment in Krebs solution. Every 10 min, the flow rate was changed to a higher value (arrows). (B) Flow-dependent relaxation in a normal human coronary artery segment (same artery as in A) in Krebs solution with 100 mg/dL LDL-cholesterol. Every 10 min, the flow rate was changed to a higher value (arrows) (from [185]).

ions flowing into the cell stimulate the Ca^{2+}-activated NO-synthase which produces NO. NO diffuses to the subjacent smooth muscle cells and relaxes them via membrane hyperpolarization.

(2) Since the polyanion HS-PG is instrumental in the formation of the cell membrane negative fixed charges (glycocalyx) and/or the Na^+ leakage channel, a change in the ξ-potential is inevitable when Na^+ ions are bound (reduction of the negative fixed charges). The result is a membrane hyperpolarization which, in turn, leads to a Ca^{2+} inward current into the cell driven by an increased electrochemical gradient ($V\text{-}E_{Ca}$) for Ca^{2+} ions. The following reaction steps are identical to those outlined in (1).

The key to vasorelaxation is the transmembrane Ca^{2+} influx into the endothelial cells which then synthesize NO. In the second case, a change in ξ-potential through Na^+ binding to the flow sensor results directly in a membrane hyperpolarization and thus an increase in the driving force for Ca^{2+}. This simple possibility will now be discussed in more detail.

An electric potential is usually generated at the boundary between two phases of electrolytes. The potential at the interface is the Nernst potential (Ψ_s) (Fig. 21). When suspended in an electrolytic solvent, a charged particle, such as a living cell, will attract ions of unlike signs around its membrane. Therefore, a so-called ion atmosphere around the cell will be created in the immediate vicinity of the cell, where ions of the opposite sign prevail and ions of the same sign are repulsed. This electrical double layer is not static but is a diffuse layer because of the thermal motion. Gouy [194] and Chapman [195] developed a theory to describe these phenomena (Ψ_0). It connects the surface potential and the charge density at the surface using the following equation.

$$\sigma = \pm\left\{2\varepsilon_0\varepsilon_r RT\sum_n C_{n\infty}[\exp(-z_n F\Psi_0/RT)-1]\right\}^{1/2} \quad (2)$$

This concept was changed by Stern [196], who introduced a layer of immobilized ions around the charged particle. In our case the Stern layer was equivalent to the cell glycocalyx involving the glycoproteins and the proteoglycan of heparan sulfate. By measuring the electrophoretic mobility of a charged particle one can derive the potential at the surface of the shear layer, the ξ-potential. The Gouy–Chapman potential and the ξ-potential are almost identical because the shear layer is not very thick. Thus, surface potential was mostly measured using electrophoresis.

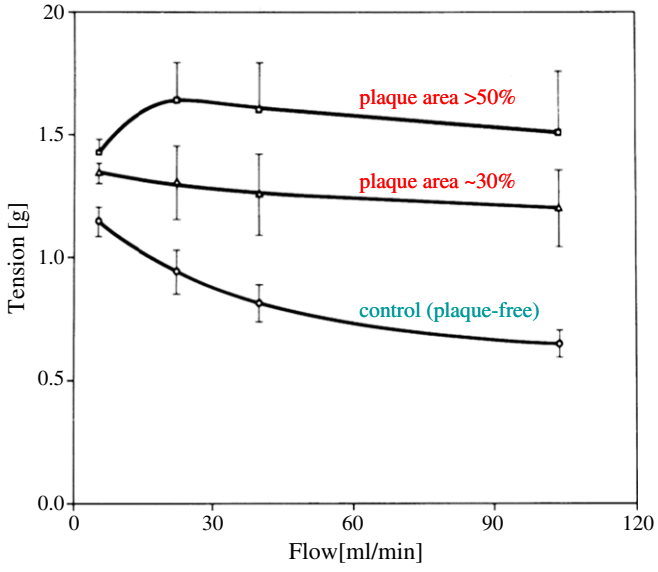

Fig. 20. Blood flow-dependent relaxation in normal human coronary arteries (○) and in arteriosclerotic coronary arteries (Δ) with a plaque area of around 30%. Coronaries with a plaque area >50% (□) show a flow-dependent vasoconstriction (from [185]).

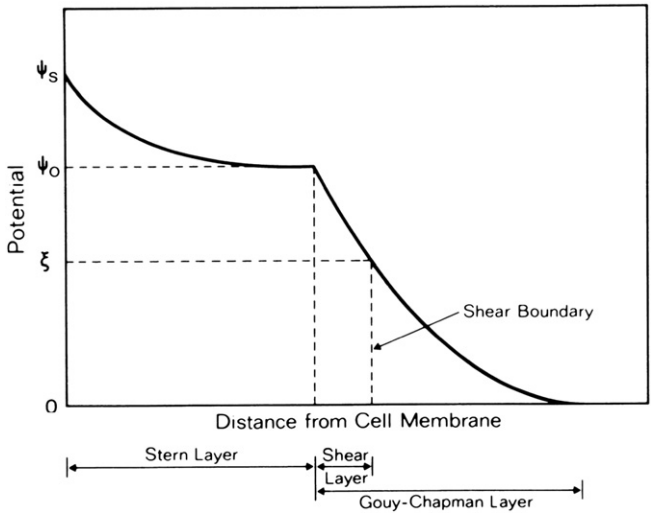

Fig. 21. Potential distribution at the cell membrane. Since shear boundary and boundary of the Stern layer are almost identical, the Gouy–Chapman potential Ψ_0 equals the ζ-potential for a thin zone of shear (from [198]).

The consequence of all these theories is that the local concentration of ions around the cell largely depends on the membrane surface potential.

$$C_0 = C_\infty \exp(-zF\Psi_0/RT) \quad (3)$$

The local concentration of ions with opposite signs to the surface potential will be higher than in the bulk solution. For ions with the same sign the opposite is true. Borst–Pauwels [197] made extensive studies on yeast cells which confirm this. Although the ξ-potential is determined empirically and the molecular bases of the different layers which result in the potential distribution in Fig. 21 are unknown, predominantly Na^+ ions come into question as countercations at the endothelium–blood interface. Their concentration is about 35 times higher than that of the next cation (K^+). These findings support the hypothesis that proteoglycans, integrated into the cell membrane, fulfil the mechanochemical and mechanoelectrical requirements of a flow sensor [198]. Moreover, the flow sensor can only achieve its function as a signal transducer if the serum Na^+ concentration is maintained. Should this not be the case, the sensor function and consequently vasodilatation are limited. A rise in peripheral resistance and hypertension may result.

5.1.6. Coordination of responses

In view of the diverse effector influences present in the complex scenario of vascular regulation, the central role of the membrane potential of the vascular smooth muscle cells can be *prima facie* regarded as the basic mechanism of integration or coordination of the responses. The level of the membrane potential in vivo is greatly influenced by intramural pressure and the rate of intraluminal flow. Pressure and flow, which cooperate in an integrative fashion in the myogenic response, might be regarded as the final vascular effectors ensuring circulatory homeostasis [199]. During physiological adjustments, the influence exerted by neurotransmitters, endothelial-derived factors, and other locally produced and systemically circulating substances may enhance or diminish the myogenic response. These effector influences will again be modified by the changes in flow that they cause. Thus, the primary regulating effect is caused by flow.

5.2. Vascular rhythmogenesis and autorhythmicity

Rhythms and oscillations are an expression of the temporal organization of living systems. We are familiar with countless rhythmic phenomena in the living world: yearly and monthly rhythms, day-and-night rhythms, respiratory and circulatory rhythms, and the rhythms of rapid-firing neurons, all of which man is subject to. Vascular smooth muscle, like cardiac muscle, originates ontogenetically from the vascular muscle tube. Thus, it is not surprising that in principle all vascular smooth muscle and sinus node cells are capable of rhythmicity, which manifests itself as periodic alterations of membrane potential and tone. In the microcirculation, these events are referred to as "vasomotion", whereas the term "slow wave activity" [200] is used for small and conduit arteries, veins, and lymphatic vessels [201]. Sinus node cells generate "pacemaker potentials" in the frequency range 0.001–0.004 Hz. These expressions designate the same phenomenon.

We can differentiate between two types of genesis for mechanical oscillations. In vascular smooth muscle, mechanical waves have been described in terms of electrical oscillations of the membrane potential (graded de- and hyperpolarization). On the other hand, it was observed in a few vessels that the depolarized part of a more or less distinct slow wave with superimposed action potentials can be paralleled by the phases of an increase in tension [200]. These action potentials are preceded (genuine pacemaker cells) or not (transmitted excitation) by a depolarizing prepotential resembling that found in sinoatrial node cells. This classification involves different ionic bases for slow wave (pacemaker) and action potential activity. While the wave potentials, which may not necessarily be slow, are probably due to a periodically changing cellular metabolism [202], voltage- and time-dependent ionic channels are responsible for the action potential activity.

5.2.1. Oscillatory diameter changes

In vivo microscopic observations of arterioles practically always reveal oscillatory changes in diameter. This vasomotion is responsible for the periodic variance in spatial blood flow and flow velocity. The absence of temporal fluctuations is regarded as a pathophysiological state lacking autoregulation. Therefore, the rhythmogenic properties of vascular smooth muscle are closely coupled to a functioning circulation. The oscillatory activity is nonrandom, but only seldom exactly periodic. The spectral analysis of frequencies often shows two or three relatively broad peaks, which are frequently coordinated as integral multiples to a basic frequency [202]. At the macroscopic level, these observations are equivalent to the electrical and mechanical oscillations (slow waves) in small and more rarely in conduit arteries and in veins (e.g., pial arteries, portal vein). An exact comparison of the wave crests and troughs between voltage and tone suggests that periodic changes in the membrane potential precede the changes in force by 40 ms. This confirms the existence of a tight electromechanical coupling even under these nonstationary conditions [203,204]. Oscillations in membrane potential of up to ±5 mV allow the open probability of voltage-sensitive Ca^{2+} channels to alternate rhythmically. Thus, vascular tone also varies periodically [205]. However, the finding that the oscillations can be inhibited by K^+ and Ca^{2+} channel blockers does not permit us to conclude that the origin of the oscillation lies in the interplay between potential-dependent K^+ and Ca^{2+} channels.

5.2.2. Rhythmogenic properties of vascular smooth muscle

Temporal fluctuations in microvascular voltage, diameter, and flow velocity exhibit characteristics of a low-order, though highly complex, nonlinear dynamic system [165]. The system may be dominated by only a few control points [206]:

- Allosteric-cooperative enzymes
- Smooth muscle membrane potential
- Intracellular Ca^{2+} levels
- Contraction kinetics
- Concentrations of extracellular regulatory substances.

The number of dominating processes is not a specific integer. In such a complex system, there are also secondary control mechanisms. In the following, three prominent control points shall be exemplarily discussed which, as negatively feedback-coupled, nonlinear synergetic order parameters, are functionally interwoven [207,208]: (1) PFK; (2) Na^+/K^+-ATPase, and (3) flow sensor (syndecan/perlecan proteoglycan) conformation.

As early as the 1950s, Edith Bülbring [209] discovered the dependence of the electromechanical properties of intestinal smooth muscle on the glycolytic metabolism. It has already been known for some years now that glycolysis, cell respiration, and cellular transport processes can be oscillatory. The cause of the oscillations is the periodically varying effectiveness of regulatory enzymes and transport proteins. Oscillation is observed when enzymes show nonlinear kinetics, when the biochemical or biophysical systems are simply or multiply feedback coupled, and when they are far from equilibrium and thermodynamically open [202].

5.2.2.1. Phosphofructokinase. A great number of feedback coupled processes on the cellular and subcellular level might play a causal, a dominating, or only a mediating role in the oscillatory phenomena. We are already familiar with two of these rather secondary processes, namely the interaction between potential-dependent K^+ and Ca^{2+} channels and between pressure-induced vasoconstriction and flow-induced vasodilatation. In the following a model will be outlined that incorporates the observations made by Bülbring [209]. Since measurements of

enzyme activity have shown a high glycolytic capacity of vascular smooth musculature and cardiac sinus node (Table 2), and since IAA blocked the electromechanical oscillations completely, PFK might be a glycolytic entry enzyme which controls the energy-supplying metabolism and has multiple feedback [204,210]. In the upper part of the glycolytic pathway, the allosteric enzyme PFK converts F6P and ATP to FBP and ADP, respectively. For an analysis of the regulatory properties of PFK based upon experimental data, the enzyme system of Fig. 22 is proposed, where two effectors were considered: FBP as an allosteric activator and ATP as inhibitor of the enzyme [202]. The sum of ADP and ATP concentrations was kept constant. For the reconstitution of ATP from ADP in the lower part of the glycolytic pathway and in other biochemical cell reactions, an overall rate representing these different reactions was used and chosen to be equal to the rate of removal of the product FBP. The input rate for F6P was constant and corresponded to physiological values in vascular smooth muscle. A computer programme [211] designed for solving kinetic problems in chemistry was utilized for studying the PFK system with the two substrates rate law formulated for the concerted model of Monod, Wyman, and Changeux [212].

$$\begin{aligned}
&\alpha_i = \frac{S_i}{K_{R,S_i}};\quad \gamma_i = \frac{P_i}{K_{R,P_i}};\quad q = \frac{V_{T,\max}}{V_{R,\max}};\quad c_i = \frac{K_{R,i}}{K_{T,i}};\quad (i = 1,2)\\
&V = V_{R,\max}\cdot v(\alpha_1,\alpha_2,\gamma_1,\gamma_2)\\
&v = \left(g_R\cdot\alpha_1\alpha_2\cdot R^{n-1} + q\cdot L\cdot g_T\cdot c_1\alpha_1\cdot c_2\alpha_2\cdot T^{n-1}\right)\Big/\left(R^n + L\cdot T^n\right)\\
&R = 1+\alpha_1+\alpha_2+g_R\cdot\alpha_1\alpha_2\\
&T = 1+c_1\alpha_1+c_2\alpha_2+g_T\cdot c_1\alpha_1\cdot c_2\alpha_2\\
&L = L_0\prod_i\left(\frac{1+c_{M,i}\cdot\mu_i}{1+\mu_i}\right)^m;\quad \mu_i = \frac{M_i}{K_{R,M_i}};\quad c_{M,i} = \frac{K_{R,M_i}}{K_{T,M_i}}
\end{aligned} \tag{4}$$

S_i, P_i, M_i denote substrates, products and modifiers, respectively; g_R, g_T are the affinity coefficients for the two possible states of enzyme configuration.

It has been shown for PFK isolated from vascular smooth and cardiac muscle of the dog that the enzyme exists as a tetramer [213]. Furthermore, a distinction between the number n of functional subunits converting substrates to products and the number m of subunits with identical binding sites for effectors seemed to be reasonable, since it is known from X-ray diffraction studies on a bacterial PFK that two protomers are necessary to bind one molecule of substrate, while on the other hand each of the four subunits seems to be able to bind the effectors [214]. This led to the assumption $n = 2$ and $m = 4$ for our calculations. The influence of effectors on v was formulated in the term L under the simplifying hypothesis that the effectors ATP and FBP bind to different allosteric centres and act independently. This assumption is justified, as the exact mechanism is not yet known.

The coefficients g_R and g_T and the ratio q were evaluated by a computer fit from curves as shown in Fig. 23 using an algorithm for least squares estimates of non-linear parameters [215]. For the subsequent

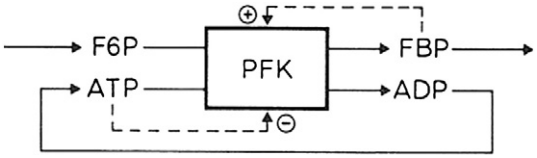

Fig. 22. Enzyme model for PFK activity and glycolytic oscillations (from [210]).

simulations the mean values $g_R = 0.98$, $g_T = 36.97$, $q = 0.145$ of two independent sets of experimental data on PFK activity were applied. The rest of parameters was determined by experiments:

	$L_o = 2.6\cdot 10^5$	$V_{R,max} = 0.050$ mM/s
For the substrates:	$K_{R(F6P)} = 0.08$ mM	$K_{R(ATP)} = 0.005$ mM
	$K_{T(F6P)} = 15.00$ mM	$K_{T(ATP)} = 0.500$ mM
And for the effectors:	$K_{R(FBP)} = 0.03$ mM	$K_{R(ATP)} = 4.000$ mM
	$K_{T(FBP)} = 6.00$ mM	$K_{T(ATP)} = 0.600$ mM

The input rate $v_{in(F6P)}$ and the rate $v_{out(FBP)}$ for the removal of the product were varied in the different computer runs.

In the R state the binding of one ligand has almost no effect on the binding of the other ($g_R = 0.98 \approx 1$); in the T state the affinity for the second ligand is decreased by the binding of the first one ($g_T = 36.97 > 1$). From the dissociation constants $K^d_{R(F6P)} = 0.08$ mM and $K^d_{T(F6P)} = 15$ mM the association constants $K'_{R(F6P)} = 12.76\ \mathrm{mM}^{-1}$ and $K'_{T(F6P)} = 0.002\ \mathrm{mM}^{-1}$ are obtained. Therefore, in the R state the association to the ternary complex is significantly favoured. The maximum turnover rate $V_{R,max}$ is 6.9 times as high as $V_{T,max}$ ($q = 0.145$).

The main characteristics of PFK, such as cooperative substrate saturation and activation or inhibition by allosteric effectors can account for oscillatory changes in glycolytic flux and ATP concentration. However, spontaneous glycolytic oscillations appear only within the oscillatory domain, i.e., at definite F6P input/FBP output rates (Fig. 24). Period durations range from 35 s up to 140 s and concentration amplitudes up to 0.3 mmol/kg wet wt. The wave-like lines illustrate the time course of ATP. One sees that via the glycolytic turnover rate, the frequency, amplitude and form of oscillations in metabolite and effector concentrations can be altered and regulated within relatively wide boundaries. Furthermore, the PFK input and output rates can be modified by the concentration of many extracellular regulatory substances, e.g., catecholamines, thyroid hormones, endothelins, histamine, kinins and thrombin. These mediators frequently change arterial pressure, thus stimulating another feedback cycle, namely between pressure-induced vasoconstriction and flow-induced vasodilatation. Finally, allosteric activators (e.g., FBP, Fru-2,6-P_2) and inhibitors (e.g., ATP) directly influence the regulatory properties of PFK. Under the influence of Fru-2,6-P_2, PFK can aggregate up to the octamer form which can easily attain the frequency range

Table 2
Ratios of enzyme activities in vascular smooth muscle and cardiac muscle (from [202,210]).

	Vascular smooth muscle	Cardiac muscle		
	Carotid artery	Sinus node	Atrium	Ventricle
Triosephosphate dehydrogenase	14.04	11.05	7.22	4.76
β-hydroxyacyl-CoA dehydrogenase Hexokinase	$1.21\cdot 10^{-2}$	$2.19\cdot 10^{-2}$	$0.38\cdot 10^{-2}$	$0.36\cdot 10^{-2}$
Triosephosphate dehydrogenase Phosphorylase	1.10	0.21	1.61	5.67
Hexokinase m-Glycerophosphate dehydrogenase	$5.1\cdot 10^{-3}$	$15.7\cdot 10^{-3}$	$6.0\cdot 10^{-3}$	$3.0\cdot 10^{-3}$
Triosephosphate dehydrogenase				

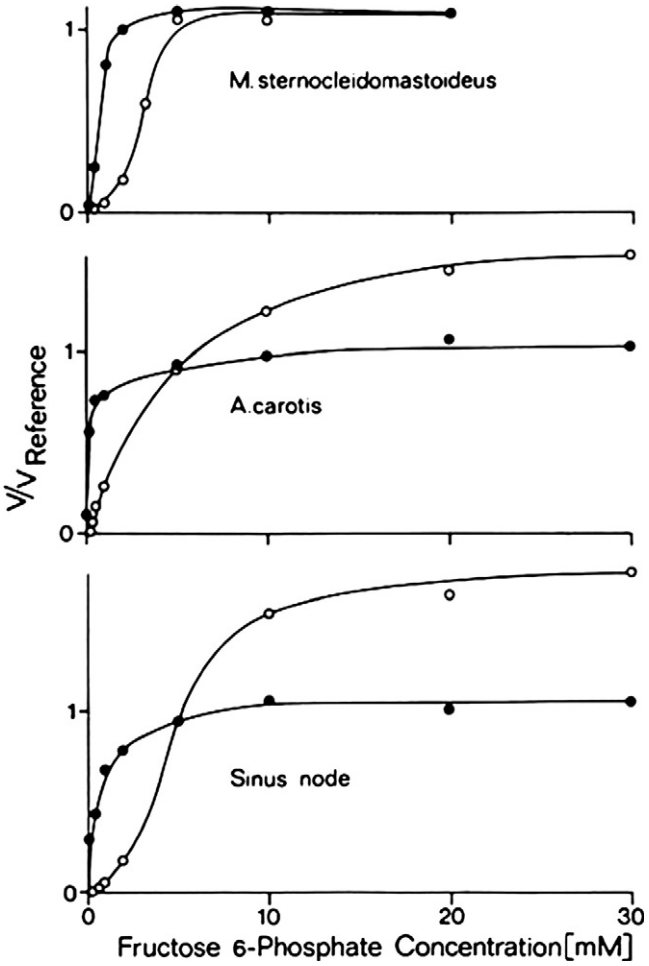

Fig. 23. Substrate saturation curves of PFK from different muscles of the dog for F6P in the absence (○) and presence (●) of effector FBP. The PFK activity was determined using an optical assay system as follows: Imidazole-HCl 0.1 mol/L, F6P 0.5 mmol/L, ATP 5 mmol/L, $MgCl_2$ 5 mmol/L, NADH 0.25 mmol/L, FBP aldolase 10 μg/mL, triosephosphate isomerase 4 μg/mL, glycerol-3-phosphate dehydrogenase 8 μg/mL (pH 6.9, temp. = 25 °C). The reaction rates V were relative to a reference activity ($V_{Reference}$) determined at pH 7.6 in the presence of 3 mmol/L F6P and 1.5 mmol/L ATP. The extracts were extensively dialysed against the extraction medium and diluted to about the same reference activity previous to the experiment. The coefficients g_R and the ratio q in the absence of FBP were evaluated by a computer fit. A. carotis: $g_R = 1.36$, $g_T = 58.49$, $q = 0.083$; sinus node: $g_R = 2.21$, $g_T = 56.37$, $q = 0$ (from [210]).

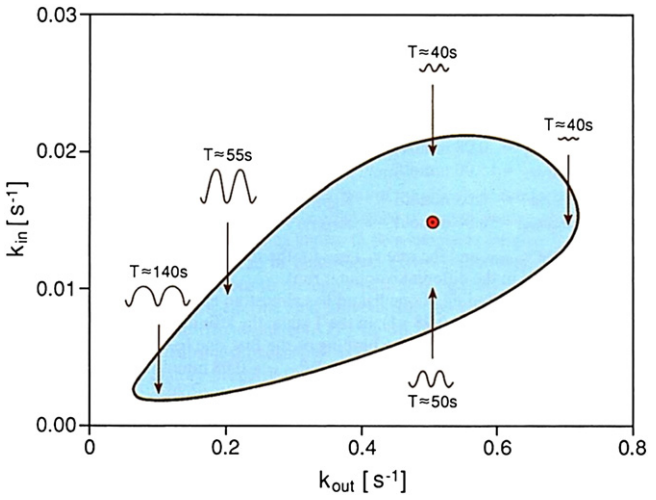

Fig. 24. Oscillatory domain (blue area) of spontaneous glycolytic oscillations for the system shown in Fig. 22. The wavelike lines illustrate the time course of the ATP concentration at the points indicated by the arrows. The period duration (T) of the oscillations is also given. The red point within the limit cycle represents the $k_{in(F6P)}/k_{out(FBP)}$ constellation used for Fig. 23 (from [222]).

0.001–0.004 Hz of sinus node cells. This could possibly answer the seemingly simple question why the heart beats.

5.2.2.2. Adenosine triphosphate concentration changes. A periodically changing ATP concentration is converted into the operation of the electrogenic ion pump by the Na^+/K^+-ATPase. This enzyme is also an oscillator [216]. Its reaction sequence consists in a single cycle that includes at least two reactive states, the Na^+ (E_1) and K^+ (E_2) conformations [217]. Na^+/K^+-ATPase transports three Na^+ ions outward per two K^+ inward per cycle and thus generates a net movement of one positive charge per cycle, a small electric current. When the electrogenic pump acts rhythmically, the membrane becomes hyperpolarized in phases of increased activity and depolarized in phases of decreased activity. The electrogenic pump current can generate the observed potential waves of up to ±5 mV. The oscillation in membrane potential is transformed into rhythmic tension changes via the voltage-sensitive Ca^{2+} channels [205]. It is the export of Na^+ by the Na^+/K^+-ATPase cycle that moves the charge. Indeed, in vessels with slow wave activity distinct oscillations were detected in the $^{24}Na^+$ efflux [202]. Due to the electrogenicity of the pump, the E_1/E_2-conformational transition is also voltage dependent. The E_1 conformation is stabilized by a more positive membrane potential, and the E_2 conformation by a more negative membrane potential [216]. This means that the orientation of a dipole in the enzyme is dependent on the transmembrane field gradient.

In simultaneous $^{24}Na^+$-$^{42}K^+$ efflux experiments we could confirm with a sophisticated mathematical procedure that preferably the active Na^+ outward transport oscillates (Fig. 25). Assuming that a random process X_t is composed of an exponential component and a stationary process like in an efflux curve, then the original data can be transformed to an approximately stationary random signal. Given a sample of equally spaced data from this approximately stationary random signal, the power density spectrum was computed [218,219]. The sample time interval is supposed for the following calculation to be unity. In computing the power spectrum, it is necessary to reduce the noise. Thus, it is advantageous to prewhiten the data X_t, $0 \le t \le n$ (t = sample time, n = total length of record):

$$X_t' = X_t - p \cdot X_{t-1}, \quad 1 \le t \le n. \tag{5}$$

If $0.2 \le p \le 2.0$ was chosen, a good prewhitening was obtained [218]. Even if the data was not prewhitened a distinct periodicity in the autocovariance function was evident. As a result of this intentional modification of the data the power density spectrum was multiplied by

$$g_r = 1 + p^2 - 2 \cdot p \cdot \cos\frac{r\pi}{m}. \tag{6}$$

Next we calculated the mean lagged products (autocovariance)

$$C_r = \frac{1}{n-r}\sum_{t=1}^{n-r} X_t' \cdot X_{t+r}', \quad 0 \le r \le m \le n, \tag{7}$$

whereby r is the lag time, m is the maximum lag interval and thus the reciprocal of the bandwidth. The maximum lag interval in our calculations covered ¼ to ⅓ of the total number of experimental points.

Before calculating the power density spectrum, adjustments can be made. Here we shall consider only one adjustment for the mean. For this purpose and in order to estimate the power noise, the function

$$N_r = \mu + \sigma \cdot e^{-\omega \cdot r}, \quad 0 \le r \le m \tag{8}$$

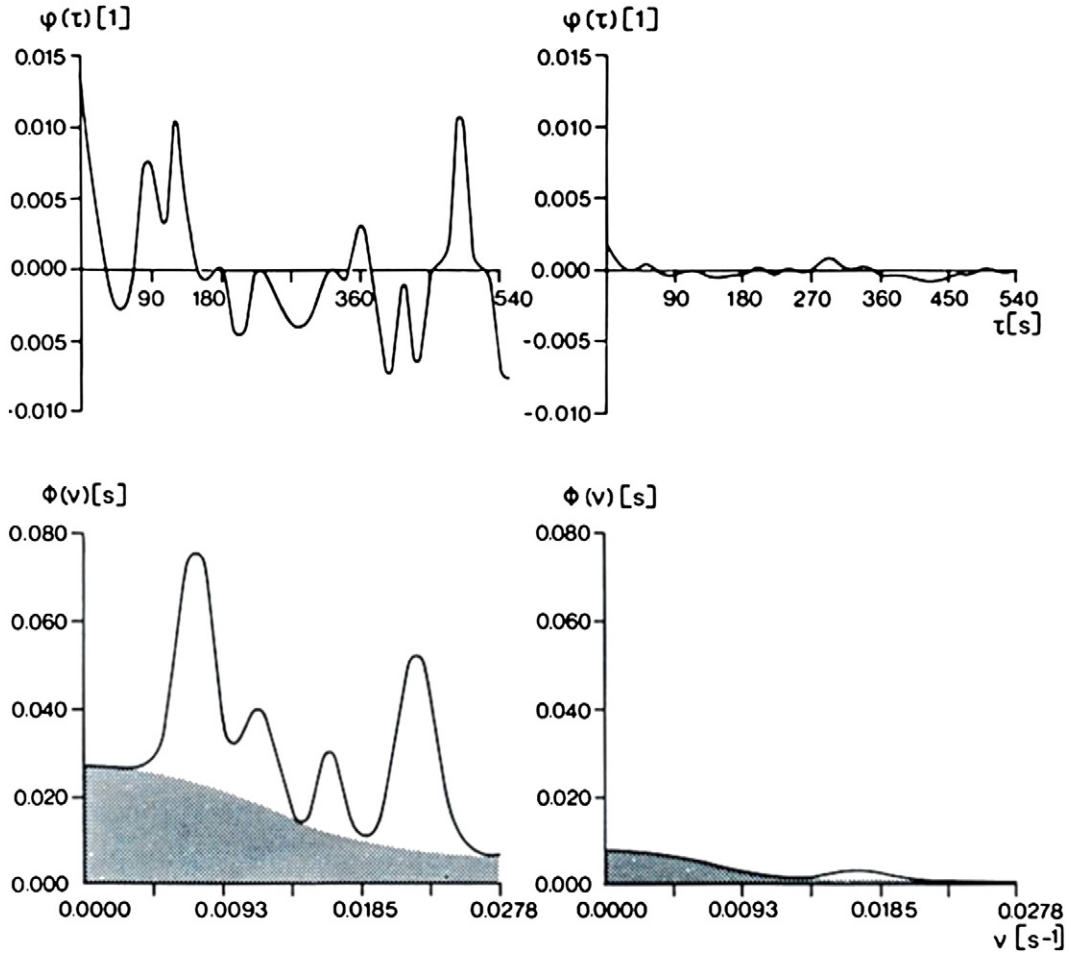

Fig. 25. Autocovariance functions and power spectra of a simultaneous $^{24}Na^{+}$–$^{42}K^{+}$ efflux experiment in the canine carotid artery. The left half of the figure is derived from the Na^{+} efflux, the right half from the K^{+} efflux. Oscillations with period durations of 45, 62, 87 and 134 s can be seen in the Na^{+} efflux (from [210]).

was fitted to the data C_r according to the Gaussian least square method [215]. As a result one finds the three parameters: mean μ, variance σ and cut-off frequency ω. Estimating the first addend in Eq. (8) by

$$\mu = \frac{1}{n}\sum_{t=1}^{n} X_t' \tag{9}$$

there resulted a re-adjustment of the zero line in the autocovariance function:

$$C_r' = C_r - \mu^2, \quad 0 \le r \le m. \tag{10}$$

The second addend in Eq. (8) expresses the autocovariance of the noise. This corresponds to the power density spectrum according to the Wiener–Khinchin relation

$$R_r = 2 \cdot \frac{m \cdot \sigma}{\pi} \cdot \frac{\frac{m \cdot \omega}{\pi}}{\left(\frac{m \cdot \omega}{\pi}\right)^2 + r^2}, \quad 0 \le r \le m. \tag{11}$$

This function makes possible an estimate of the amount of noise in the power density spectrum of the random signal. Next we calculated the raw spectral density function as the Fourier transform of the autocovariance function C_r' (Wiener–Khinchin relation)

$$U_r = C_0' + 2\sum_{q=1}^{m-1} C_q' \cos\left(\frac{\pi r q}{m}\right) + (-1)^r C_m', \quad 0 \le r \le m. \tag{12}$$

These values of the power density spectrum were then smoothed according to the Hanning method as follows

$$\begin{aligned} V_0 &= \frac{1}{2}U_0 + \frac{1}{2}U_1; \\ V_r &= \frac{1}{4}U_{r-1} + \frac{1}{2}U_r + \frac{1}{4}U_{r+1}, \quad 1 \le r \le m-1; \\ V_m &= \frac{1}{2}U_{m-1} + \frac{1}{2}U_m. \end{aligned} \tag{13}$$

These can then be corrected both for prewhitening and for the corrected mean by forming

$$\begin{aligned} W_0 &= \frac{V_0}{g_{1/3}} \cdot \frac{r}{n-m}, \\ W_r &= \frac{V_r}{g_r}, \quad 1 \le r \le m-1, \\ W_m &= \frac{V_m}{g_{2m-1/3}}, \end{aligned} \tag{14}$$

as smoothed estimates of the power density. The smoothing by Eqs. (13) and (14) was also performed on the function R_r. Fig. 25 is a

good example for applying this computation to calculate autocovariance functions and power spectra.

Since the connection between the periodically changing ATP concentration and the oscillation of metabolism-dependent, electrogenic ion pumps is still uncovered, a physicochemical membrane model involving active pump processes was applied [220]. In this model, the mean stationary activation energies of an ion species *i* are given by

$$A_{s,i}^{'(")}(V) = \frac{A_{m,i}^{'(")}}{1 + \left[\frac{\sigma F}{RT}(V - V_b)\right]^2}, \tag{15}$$

with $\sigma = \sigma_i$ and $V_b = V_{b,i}$ for all i, where V is the membrane potential, V_b the potential, for which all supposed "membrane channels" are open, and σF/RT a proportionality factor including the Faraday constant F, the gas constant R and the absolute temperature T. $A_m^{'(")}$ are the maximum activation energies, which are independent of the membrane potential. In the case of a metabolism, which renders energy periodically, the active outward transport of Na^+ ions and the active inward transport of K^+ ions are directly subject to these oscillations by means of the Na^+/K^+-ATPase. Therefore, the stationary activation energies had to be formulated as functions of the rhythmic changes in ATP concentration ATP(t)

$$\widetilde{A}_{s,i}^{'(")}(V, ATP(t)) = \frac{\widetilde{A}_{m,i}^{'(")}(ATP(t))}{1 + \left[\frac{\sigma F}{RT}(V - V_b)\right]^2} \tag{16a}$$

for the energy used for outward or inward transport, respectively, and

$$A_{s,i}^{"(')}(V) = \frac{A_{m,i}^{"(')}}{1 + \left[\frac{\sigma F}{RT}(V - V_b)\right]^2} \tag{16b}$$

for the ATP independent diffusion into the intracellular or extracellular space with

$$\widetilde{A}_{m,i}^{'(")}(ATP(t)) = A_{m,i}^{'(")} + a_0 \cdot ATP(t), \quad a_0 = const. \tag{16c}$$

If the active, electrogenic ion pumps are driven by oscillating ATP(t), one observes a corresponding rhythm in ionic currents and membrane potential, which was similar to the experimental findings. Fig. 26A shows that membrane hyperpolarization is due to a net outward current of positive charge carriers (I_t). Initially, the outward current is caused by a strong decrease of the inwardly directed I_{Na}, later by the reversal of the Na^+ current in an outward direction. Positive Na^+ current means a predominance of the active Na^+ outward transport over the passive Na^+ inward diffusion. Thus, the time course of the Na^+ pump current is decisive for the hyperpolarizing phase of the membrane potential oscillation (Fig. 26B), as is also evident from the flux measurements.

5.2.2.3. Oscillatory control point: flow sensor conformation. Reportedly, we were successful in investigating the effects of electrolytes on the interfacial behaviour of the flow sensor by ellipsometric techniques [186,221]. Upon application of a 1.25 mmol/L $[Ca^{2+}]_o$ solution, measuring of HS-PG yielded a shortening of the macromolecule by 8.9 nm (−23%), whereas Na^+ ions effected a molecular elongation by 13.7 nm (+35%) (Fig. 27). The Ca^{2+}-induced contraction leads to a decrease in Na^+ binding, and the Na^+-induced extension to a promotion of Na^+ binding. This means that Na^+ ions amplify the sensitivity of the flow sensor for Na^+ in an autocatalytic process. On the other hand, Ca^{2+} ions impair the sensitivity of the sensor to bind Na^+ [75].

Since both the voltage-gated Na^+ channel and the Na^+/K^+-ATPase are roofed over as by an umbrella through heparan sulfate proteoglycan [76,189], the Na^+ concentration close to the macromolecule may be changed by an increased activity of the electrogenic ion pump. Such a 'Na^+ jump' (+135.4 mmol/L) extends the 110.7 nm long flow sensor effectively by 10.4 nm (transient change 56.5 nm = 51% of total length), whereby the viscoelastic helical spring resets itself to the new length via strongly damped oscillations with a period duration of 47.4 ± 5.7 s (n = 3) (Fig. 28B). When the system is strained through a further Na^+ jump, the period duration of the reactive fluctuations in flow sensor length decreases to 27.9 ± 1.6 s (n = 3). Thus, ongoing rhythmic activity of the Na^+/K^+-ATPase can generate undamped oscillations in sensor length dependent on Na^+ binding, which themselves may mutually interact with the self-oscillations of the flow sensor and could transmit rhythmic fluctuations to the vascular tone via a

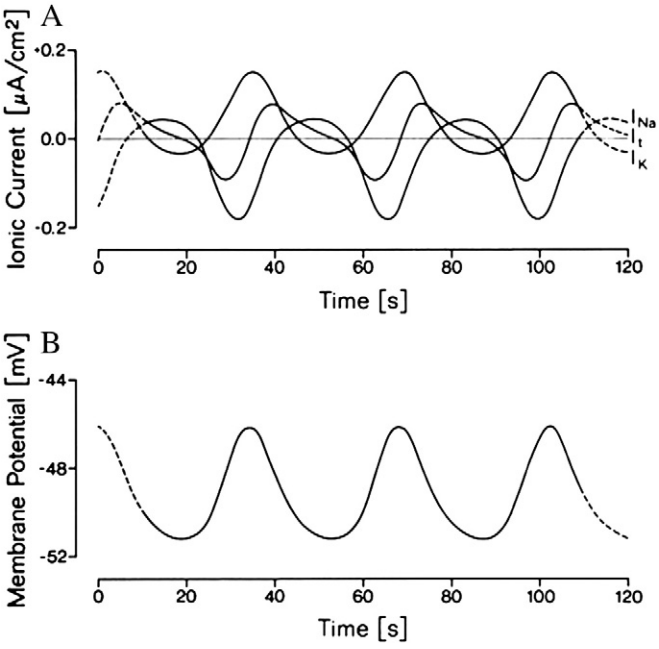

Fig. 26. (A) Oscillation of Na^+, K^+ and total ion current in vascular smooth muscle cells induced by driving the active, electrogenic ion pumps by oscillating ATP(t). The computations are based on the physicochemical membrane model described above [220]. (B) Corresponding membrane potential oscillation with a period duration of 34 s and an amplitude of ±2.5 mV (from [210]).

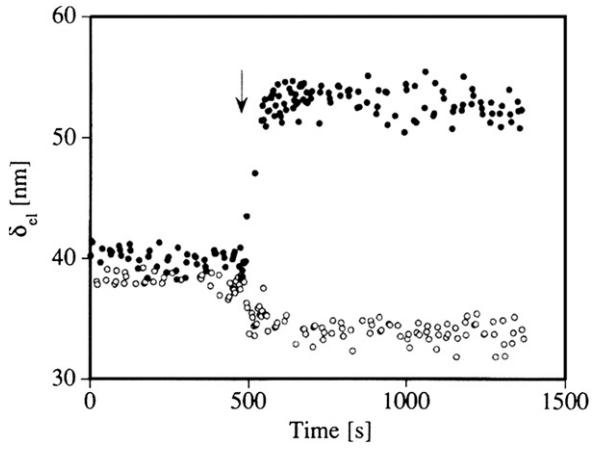

Fig. 27. Adsorbed layer thickness for proteoheparan sulfate (0.1 mg/mL) at methylated silica from a Na^+-, Ca^{2+}- and Mg^{2+}-free K^+-Krebs solution (pH 7.25). At the time point identified by the arrow, Na^+ in a physiological concentration of 135.40 mmol/L (●) or Ca^{2+} in a physiological concentration of 1.25 mmol/L (○), respectively, was added (from [222]).

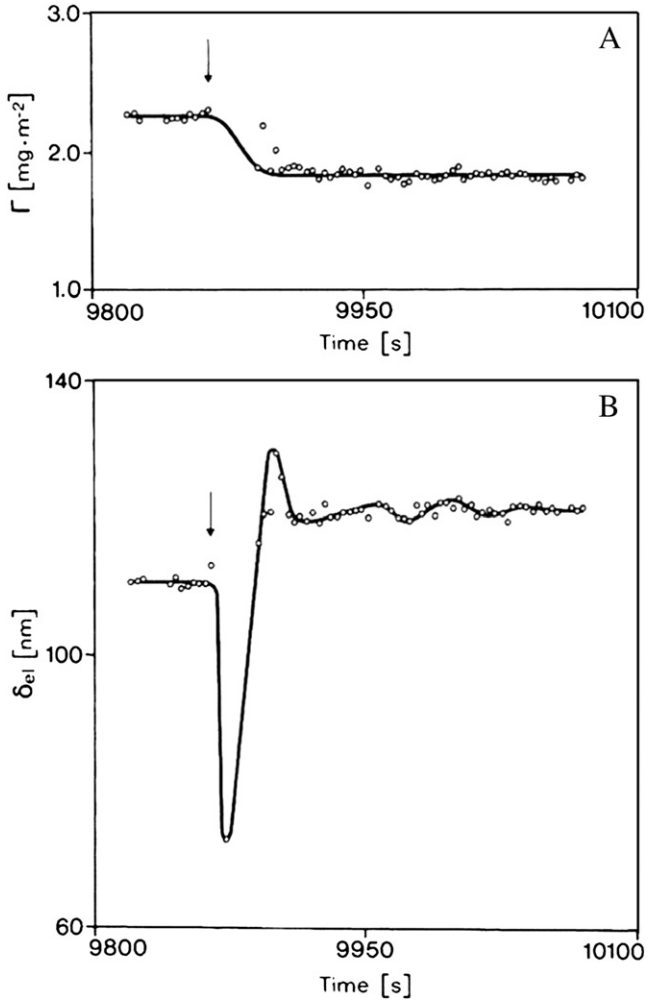

Fig. 28. Adsorption (A) and adsorbed layer thickness (B) of proteoheparan sulfate (0.1 mg/mL) from Na^+-deficient K^+-Krebs solution at methylated silica (pH 7.25). The arrows indicate addition of Na^+ to a final concentration of 135.40 mmol/L, corresponding to a $c_{s,tot}$ (1:1) of 155.85 mmol/L. $c_{s,tot}$ (2:1) was 3.62 mmol/L (from [222]).

membrane hyper- or depolarization and an oscillatory stimulation of nitric oxide synthase [222].

Our ellipsometric, surface force and $^{23}Na^+$ nuclear magnetic resonance measurements confirmed that the integral membrane, hybrid HS/CS proteoglycan syndecan of functioning endothelial cells and/or the basement membrane and matrix HS-PG perlecan of vessel walls represent the mechanochemical and mechanoelectrical transducer in shear-stress-dependent vascular regulation (Fig. 15) [18,76]. HS-PG is able to change its conformation both through intervening shear forces and through the action of cations. The former configurational transition is based upon the viscoelastic properties of these macromolecules, the latter upon the anionic polyelectrolyte characteristics. Therefore, the coil – helix and helix – coil phase conversions seem to be tightly linked to the protein moiety, while the fine adjustment of the flow sensor could additionally be determined by the cation composition of its microenvironment.

The viscoelastic properties of the syndecan/perlecan proteoglycans and their rapid reaction by a conformational change of their polyelectrolyte moiety to alterations of the microenvironmental Na^+ concentration are prerequisites for negatively feedback-coupled intramolecular configurational transitions, which control the flow-sensitive vascular adjustment (Fig. 28). Obviously, this system is also capable of eigenoscillations. When considering the interference of the feedback-coupled systems 'Na^+/K^+-ATPase' of the vascular smooth muscle cell and 'flow sensor' of the endothelial cell, rhythmic Na^+ outward pumping causes local Na^+ concentration changes in the immediate vicinity of the sensor macromolecules, which react with more or less Na^+ binding. Dependent on the amount of Na^+ ions bound, the molecular helical spring of the GAG side chains is more or less stretched. The greater the extension, the higher the oscillation frequency in sensor length. An intensified Na^+ outward pumping induces a hyperpolarization of the vascular smooth muscle cell membrane [210]. The augmented Na^+ binding to the flow sensor, with subsequent counterion migration and passage of the voltage-dependent Na^+ channel, effects a depolarization of the endothelial cell membrane, with an increase in Ca^{2+} open probability [76,223]. This increase in Ca^{2+} permeability elicits a Ca^{2+} inward current into the endothelial cell, stimulation of the NO-synthase and an augmented nitric oxide formation [224]. The hyperpolarization of the smooth muscle cell membrane effected by the pump current, in association with the increased NO release from the endothelial cells, initiates relaxation of the vascular smooth muscle cells. As may be easily realized, the time constants and the phase shift between the individual processes are of decisive importance for the resulting oscillation. Finally, the rise or fall in the intracellular ion concentrations (Na^+, Ca^{2+}) of endothelial and vascular smooth muscle cells interacts with the enzymatic activity of PFK. This multiply feedback-coupled network of rhythmic capable systems can create the periodic events in the cardiovascular system (slow waves, pacemaker potential) and, furthermore, provides a plausible explanation for their causal origin.

5.2.3. Synchronization, conduction, and functional significance of oscillatory activity

The detection of electromechanical slow waves and vasomotion presupposes synchronization in cellular and subcellular events. Even if the PFK and Na^+/K^+-ATPase molecules all oscillate at the same frequency, their mutual phase relationship has to be synchronous to be able to collect a uniform signal. Frequency entrainment and phase synchronization ensue by varying a force, such as pressure or an electric field [216]. A prerequisite is that both the conformational states of the enzyme differ in a displacement such as volume or dipole moment. Even the secondary structure of the oscillator molecules in question can have a dipole moment.

Dealing with a population of closely interconnected cells, each one of which is capable of sustained oscillations in membrane potential, the next question to ask is whether synchronization among the single elements takes place and what role it plays in intercellular communication. Using the technique of harmonic balance [225] in the analysis of a set of mutually coupled, nearly sinusoidal Van der Pol oscillators [226]

$$\ddot{x} - c\left(a^2 - x^2\right)\cdot\dot{x} + \omega_n^2\cdot x = 0 \tag{17}$$

with a small non-linearity parameter c, Linkens [227] presented the analytical solution. Dealing with a chain of n mutually coupled oscillators, it is assumed that the kth oscillator in the chain is coupled to the preceding and succeeding element by a coupling factor λ_k. Then the kth oscillator is represented by

$$\ddot{x}_k + \lambda_k\cdot\dot{x}_{k+1} + \lambda_{k-1}\cdot\dot{x}_{k-1} - c_k\left(1 - x_k^2\right)\cdot\left(\dot{x}_k + \lambda_k\cdot x_{k+1} + \lambda_{k-1}\cdot x_{k-1}\right) + \omega_k^2\cdot x_k = 0 \tag{18}$$

To answer the question of frequency entrainment, Rosenbrock's hill-climbing routine [228] was applied to the minimizing procedure suggested by Linkens [227]. Drawing the starting values of amplitudes and frequencies from a normal distribution with means and variances of physiological significance by a random procedure and dealing with phase shifts, which are equally distributed, in all cases synchronization was observed. Table 3 shows the frequency entrainment in a 6-oscillator chain, where the results for frequency, amplitude and

Table 3
Entrainment in a 6-oscillator chain using hill-climbing routine (from [210]).

Step number	675 (Minimum)					
Hill value	0.3712					
Entrained frequency	0.155 rad/s					
Oscillator number	Frequency [rad/s]		Amplitude [mV]		Phase angle [rad]	
	Step no. 370	Step no. 675	Step no. 370	Step no. 675	Step no. 370	Step no. 675
1	0.201	0.155	4.415	4.335	0.030	0.021
2	0.127	0.154	4.951	4.835	0.012	0.007
3	0.178	0.155	2.709	2.623	−0.019	−0.015
4	0.118	0.154	5.920	4.627	0.012	0.011
5	0.212	0.156	4.314	4.548	−0.028	−0.022
6	0.160	0.155	2.913	2.835	−0.015	−0.008

phase angle are summarized in an intermediate step (step no. 370), as well as in the minimum. The frequency synchronization is excellent, the phase angle is in the scope of $\pm 1.3°$. Generally, the entrained frequency was found to be in the range of the oscillator with a medium period duration in the chain before coupling. In the present case the period duration after synchronization is 41 s, in agreement with the flux and potential oscillations in vascular smooth muscle. It remains for future experimental and theoretical studies to obtain a physiological interpretation of coupling parameter λ in terms of both time and space constant, and cytoplasm and membrane resistance. Only then a complete description of the dynamic membrane properties of obligate spontaneously rhythmic organs of the cardiovascular system (vascular smooth muscle, cardiac sinus node) is possible.

Synchronized potential waves spread from one cell to the next via the gap junctions. If the vascular smooth muscle cells contract synchronously, the blood vessel experiences periodic variations in diameter. Slow waves or vasomotion are created from a peripheral, functioning vascular system. What is the significance of this vasomotion? Is it an epiphenomenon or a crucial point in coordination? The significance of the oscillatory events in the cardiovascular system is found in the spatial and temporal synchronization of the cells, in metabolic energy saving, and in the constant readiness of the vessels to adapt to changing circulation requirements. The precise control of the resistance vessels to permit minute changes in flow requires contraction in concert with adjacent cells. An essential property of vascular smooth muscle cells is a marked ability to cooperate. Intercellular communication is reflected by the coordinated, periodic contraction of arterioles, a central aspect of their behaviour. Cell–cell coupling is the crucial point in this coordination and perhaps in the adjustment of vascular resistance. Moreover, periodic vasomotion in terminal arterioles is decrementally conducted upstream to larger vessels, which integrate input from many branches [165].

This intervention of vascular rhythmicity in the circulatory regulation through synchronization and conduction is supplemented by the phase dependence of effector actions, e.g., of an autonomic nervous impulse (Fig. 29). The result of sympathetic or any effector interference depends on the phase of the spontaneous contraction–dilatation cycle. This rhythmicity guarantees a particularly fast vascular reaction within a few seconds [204] to satisfy both general and local demands in most situations, predominantly in states of emergency. Adaptation to changed circulatory requirements can be performed more rapidly from an oscillating than from a stationary system. Moreover, it has advantages in terms of metabolic energy cost. From the clinical point of view, a changed vasomotion might present an additional pathogenetic

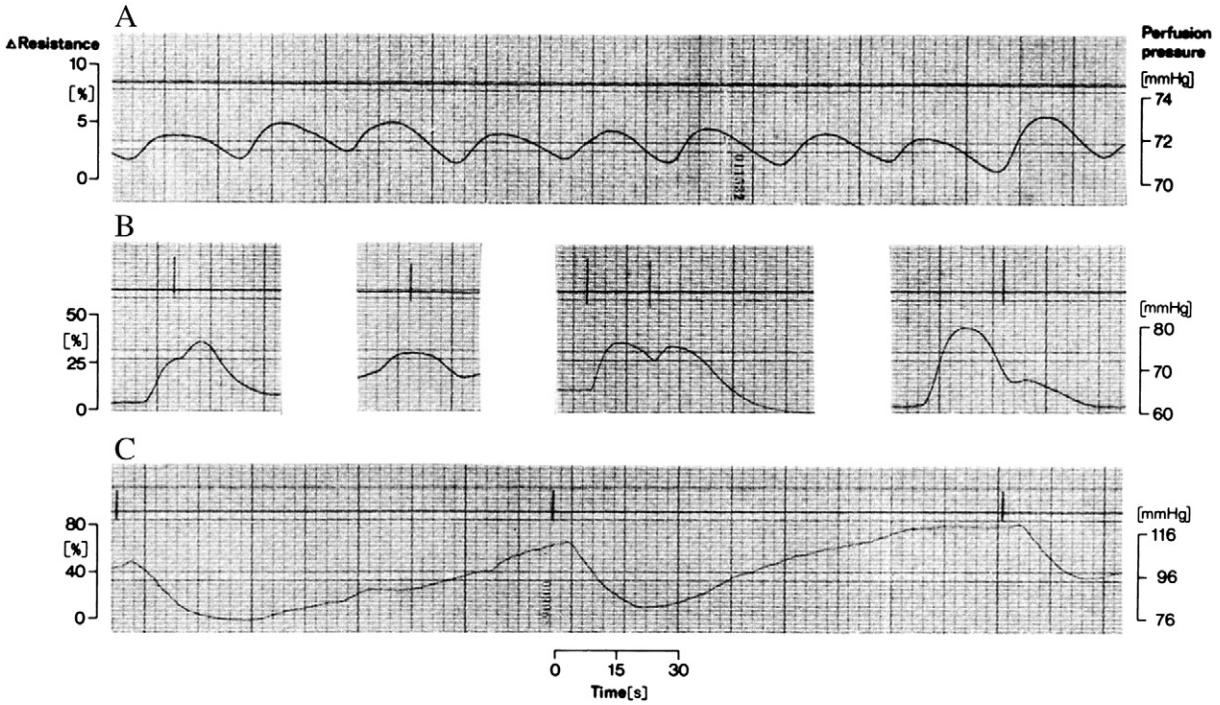

Fig. 29. Oscillations of resistance in an isolated perfused skin area of a dog. (A) Spontaneous fluctuations. (B) During single stimulation of the vasoconstrictor nerve at various phases of resistance increase. (C) During a short impulse series to the vasoconstrictor nerve of a spontaneously rhythmic vessel (from [204]).

factor, e.g., in diabetic microangiopathy and arterial hypertension. Large and small flow motion waves were found in patients with arterial occlusive disease. The prevalence of small waves increases with more severe ischemia. Thus, the analysis of oscillatory activity may gain diagnostic and prognostic significance.

In conclusion, it should be emphasized that under normal conditions the various vascular-regulatory effector influences are interwoven in a dynamic, and not a static circulatory system. The reaction of a smooth muscle cell is thus reflected only incompletely by the stationary activation curve "developed tension versus membrane potential". The missing time domain is a reflection of our as yet limited understanding of the system's behaviour in space and time.

6. Scaffolding basal laminae, an intricate network of the extracellular matrix

The preceding sections and paragraph 3.3 have shown that proteoglycans are biopolymers which participate in the organization of the extracellular connective tissue matrix and influence the structure and function of the cell membrane [7,169]. The physicochemical and functional properties of the proteoglycans are mainly due to their amphiphilicity and anionic polyelectrolyte character. Proteoglycans and HA are highly viscoelastic in solution [189], and they have a large hydrodynamic radius [8]. Furthermore, they interact with cations, albeit in a rather complex manner. From a physicochemical standpoint, this interplay is highly complicated and influences fundamental cell and organ functions.

6.1. Ionic microenvironment of cells

For example, in the vascular wall about 65% of the cations are structurally bound mainly to these biopolyelectrolytes, which comprise only 1% of the connective tissue. The basic significance of this large, extracellular cation pool becomes clear not only with respect to tissue hydration, but also upon consideration of ion activities close to the cell membrane. These depend on the ion-binding properties of proteoglycan and free GAG chain polyelectrolytes in the extracellular matrices and basement membranes that form a tight-fitting sheath around the plasma membrane of muscle and Schwann cells and underlie epithelial and endothelial cell sheets and tubes. Under nonstationary conditions, a release of cations from or an adsorption to the polyanionic macromolecules can transiently lead to fast and drastic activity changes in these tiny extracellular tissue compartments between cell membrane, basement membrane, and the connective tissue fibres. In the discussion of the time courses, we shall see that in this situation with an unstirred layer there is no a priori reason for expecting the extracellular cleft K^+ concentration $[K^+]_c$ to be equal to the bulk phase K^+ concentration $[K^+]_o$ [229]. Ion activity changes in the microenvironment of cells influence transmembrane ionic currents and membrane potential of these cells and/or sympathetic nerve endings located in the extracellular matrices.

6.1.1. Mechanisms of cation binding

The fixed ionized groups of connective tissue structures bind counterions to maintain electroneutrality [230]. Thermodynamic parameters such as exchange rates and osmotic, activity, or diffusion coefficients are differently influenced depending on the binding type:

- "Diffuse" or "statistical" binding [231],
- Electrostatic counterion binding [232,233],
- "Specific" ion binding [231].

Diffuse or statistical binding originates from the electrostatic interaction of fixed and mobile charges. Polyelectrolytes whose analytical charge density exceeds a critical value display unique electrostatic binding phenomena ("free", "uncondensed", "condensed" counterions) [232,233]. The quantitative determination of this polyelectrolyte effect in statistical–mechanical models is possible for simple systems. Basically, they allow neither "specific binding" to discrete sites with spatiotemporal allocation of the bound cations nor ion selectivity [181,230,234]. Finally, counterions can enter into a complex bond with discrete sites of polyelectrolytes [231]. Thus, the stereochemical alignment of polar and ionized groups close to the sites, their concordance with the coordination geometry favoured by the counterions, and changes in hydration during binding play a role, as do charge density, distribution of the polyelectrolytes, and the charge of the counterions. Even distinct neutral sugars can form complexes of considerable stability with mono- and divalent inorganic cations when the arrangement of several hydroxyl groups upon displacement of water molecules from the hydrational shell of the cation corresponds to the coordination domain of the cation [235]. This concordance is known for the alignment axial – equatorial – axial in the pyranose ring and ions with a Pauling crystal radius close to 0.1 nm (Na^+, 0.095 nm; Ca^{2+}, 0.065 nm) [236].

6.1.2. $^{23}Na^+$ and $^{39}K^+$ NMR theory in ion binding

The quadrupole relaxation method for $^{23}Na^+$ and $^{39}K^+$ under extreme narrowing and non-extreme narrowing conditions can constitute a very general experimental approach to the problem of ion binding in biological systems [2]. $^{23}Na^+$ and $^{39}K^+$ have a spin quantum number $I = 3/2$. In aqueous solution its nuclear magnetic relaxation is dominated by quadrupole effects. Under extreme narrowing conditions ($\omega\tau_c \ll 1$), $^{23}Na^+$ and $^{39}K^+$ rates of relaxation may be written [2]:

$$R_1 = R_2 = \frac{2\pi^2}{5} \cdot \chi^2 \cdot \tau_c \tag{19}$$

Here R_1 and R_2 are the longitudinal and transverse relaxation rates, respectively, χ ($=e^2qQ/h$) the quadrupolar coupling constant, and τ_c the correlation time for the fluctuation of the electric field gradient at the position of the nucleus.

Normally, the sodium and potassium ions exchange rapidly (compared to relaxation) between different states in a solution [177]. If only two states are considered, namely free (F) and bound (B) ions, the observed relaxation rate, R_{obsd}, is

$$R_{obsd} = p_F R_F + p_B R_B \tag{20}$$

where p_F and p_B are the fraction of free and bound ions, respectively. Under certain conditions (for example where $p_F \simeq 1$ or the same molecular motion contributes equally to relaxation in the free and bound state) $p_F \cdot R_F$ may be replaced by R_0, i.e., the relaxation rate in dilute aqueous solution of a simple electrolyte. In such a case it is useful to define the excess relaxation as $R_{ex} = R_{obsd} - R_0$, and with this notation, Eq. (20) becomes

$$R_{ex} = p_B R_B \tag{21}$$

In polyelectrolyte systems it has been found that the extreme narrowing conditions are not always fulfilled. It has been demonstrated by Hubbard [237] that the time dependence of the magnetization – both longitudinal and transverse – cannot be described by a single exponential for nuclei with $I > 1$. In the case of spin $I = 3/2$, each magnetization will decay with two exponentials, for a spin 5/2 with three exponentials and for a nucleus with spin 7/2 with 4 exponentials [237].

The relaxation equations for non-extreme narrowing conditions for sodium and potassium ($I = 3/2$) involved in chemical exchange, have been worked out by Bull [238]. The general expressions are rather complex and we shall in the following consider only the case where the chemical exchange is rapid in comparison with the fastest decaying component of magnetization. Then, in a two state situation the longitudinal magnetization will follow the equation

$$M_L(t) - M_{L,0} = \left(M_L(0) - M_{L,0}\right) \cdot \left(0.2e^{-a_1 t} + 0.8e^{-a_2 t}\right) \tag{22}$$

and the transverse magnetization in a coordinate system rotating at the resonance frequency follows the equation

$$M_T(t) = M_T(0) \cdot \left(0.6e^{-b_1 t} + 0.4e^{-b_2 t}\right) \tag{23}$$

where

$$a_1 = p_F \cdot R_F + p_B/T_{1,\text{fast}} \tag{24}$$

$$a_2 = p_F \cdot R_F + p_B/T_{1,\text{slow}} \tag{25}$$

$$b_1 = p_F \cdot R_F + p_B/T_{2,\text{fast}} \tag{26}$$

$$b_2 = p_F \cdot R_F + p_B/T_{2,\text{slow}} \tag{27}$$

The symbols p_F, R_F and p_B have been defined above and the *T*'s are given by

$$1/T_{1,\text{fast}} = \frac{2\pi^2}{5} \cdot \chi^2 \cdot \tau_c / \left(1 + \omega^2\tau_c^2\right) \tag{28}$$

$$1/T_{1,\text{slow}} = \frac{2\pi^2}{5} \cdot \chi^2 \cdot \tau_c / \left(1 + 4\omega^2\tau_c^2\right) \tag{29}$$

$$1/T_{2,\text{fast}} = \frac{\pi^2}{5} \cdot \chi^2 \cdot \tau_c \cdot \left(1 + 1/\left(1 + \omega^2\tau_c^2\right)\right) \tag{30}$$

$$1/T_{2,\text{slow}} = \frac{\pi^2}{5} \cdot \chi^2 \cdot \tau_c \cdot \left(1/\left(1 + 4\omega^2\tau_c^2\right) + 1/\left(1 + \omega^2\tau_c^2\right)\right) \tag{31}$$

If $\omega\tau_c$ is not much greater than unity (in practice ≤ 1.5), then Eqs. (22) and (23) can, through a logarithmic linearization, be approximated as single exponentials with time constants given by

$$R_1 = p_F R_F + p_B\left(\frac{0.2}{T_{1,\text{fast}}} + \frac{0.8}{T_{1,\text{slow}}}\right) \tag{32}$$

$$R_2 = p_F R_F + p_B\left(\frac{0.6}{T_{2,\text{fast}}} + \frac{0.4}{T_{2,\text{slow}}}\right) \tag{33}$$

where $R_1(=1/T_1)$ and $R_2(=1/T_2)$ are the longitudinal and transverse relaxation rates, respectively. The appearance of the high resolution NMR spectrum under non-extreme narrowing conditions can be obtained by taking the Fourier transform of Eq. (23). The signal is a superposition of two Lorentzians with the same resonance frequency but with the line-widths corresponding to the two relaxation rates b_1 and b_2.

6.1.2.1. Determination of correlation times. When extreme narrowing conditions are prevalent ($\omega\tau_c \ll 1$) it is not possible to determine the correlation time from observed relaxation rates of quadrupolar ions unless the value of the product $p_B\chi^2$ is known. When, however, $\omega\tau_c$, or rather $(\omega\tau_c)^2$, is non-negligible in comparison with unity it becomes possible to determine τ_c without knowledge of $p_B\chi^2$. At least three ways for doing this are practicable. Through an analysis of the decay of the non-exponential transverse magnetization, or by fitting the high resolution spectrum to two Lorentzians, the two rate constants b_1 and b_2 of Eq. (23) may be obtained. Subtracting R_0 (or in some cases $p_F R_F$) from each of the rate constants, we can calculate [239]:

$$\Delta R_2 = \frac{R_{2,\text{fast}}}{R_{2,\text{slow}}} = \frac{b_1 - R_0}{b_2 - R_0} = \frac{1 + 1/\left(1 + \omega^2\tau_c^2\right)}{1/(1 + \omega^2\tau_c^2) + 1/(1 + 4\omega^2\tau_c^2)} \tag{34}$$

where ΔR_2 is a function of only τ_c.

If we are in the region where the decay of magnetization is virtually exponential but the relaxation rates R_1 and R_2 are unequal (i.e., $0.2 \leq \omega\tau_c \leq 1.5$) we can use the linearized expressions of Eqs. (32) and (33) to calculate [2]:

$$\Delta\left(\frac{T_2}{T_1}\right) = \frac{R_1 - R_0}{R_2 - R_0} = \frac{\dfrac{1.6}{1 + 4\omega^2\tau_c^2} + \dfrac{0.4}{1 + \omega^2\tau_c^2}}{0.6 + \dfrac{0.4}{1 + 4\omega^2\tau_c^2} + \dfrac{1}{1 + \omega^2\tau_c^2}} \tag{35}$$

which also is a function only of $\omega\tau_c$. After some transformations we obtain [7,9,169,240]:

$$R_1 = \frac{1}{T_1} = p_F R_F + p_B \frac{2\pi^2}{5} \cdot \chi^2 \cdot \tau_c \left(\frac{0.8}{1 + 4\omega^2\tau_c^2} + \frac{0.2}{1 + \omega^2\tau_c^2}\right) \tag{36}$$

$$R_2 = \frac{1}{T_2} = p_F R_F + p_B \frac{\pi^2}{5} \cdot \chi^2 \cdot \tau_c \left(0.6 + \frac{1}{1 + \omega^2\tau_c^2} + \frac{0.4}{1 + 4\omega^2\tau_c^2}\right) \tag{37}$$

As the relaxation rates can be measured directly, $R_{1,2_{ex}}$ can be determined by means of Eq. (21), and thus the term $p_F R_F$ can be eliminated from Eqs. (36) and (37). Now, two equations with only two unknown quantities, $p_B\chi^2$ and τ_c, result, which can easily be resolved for τ_c. When τ_c is known, $p_B\chi^2$ can be calculated by renewed insertion in Eqs. (36) or (37). For a separation of p_B and χ, further considerations are needed.

6.1.2.2. Affinity and dissociation constants. With continuing dilution, equal for CS-P and Na^+, the $^{23}Na^+$ relaxation rate decreases until it reaches the value for free Na^+ ions (Fig. 30). The purpose of such a dilution experiment is to be able to determine the specific Na^+ affinity constants and relaxation rates [11]. These data are required for a parameter reduction in the calculation of affinity constants, e.g., for K^+ and Ca^{2+}, in much more complicated competition experiments. The observed $^{23}Na^+$ relaxation rate, R_{obsd}, depends on the relaxation at the various binding sites which the ligand Na^+ can occupy. With a fast exchange between

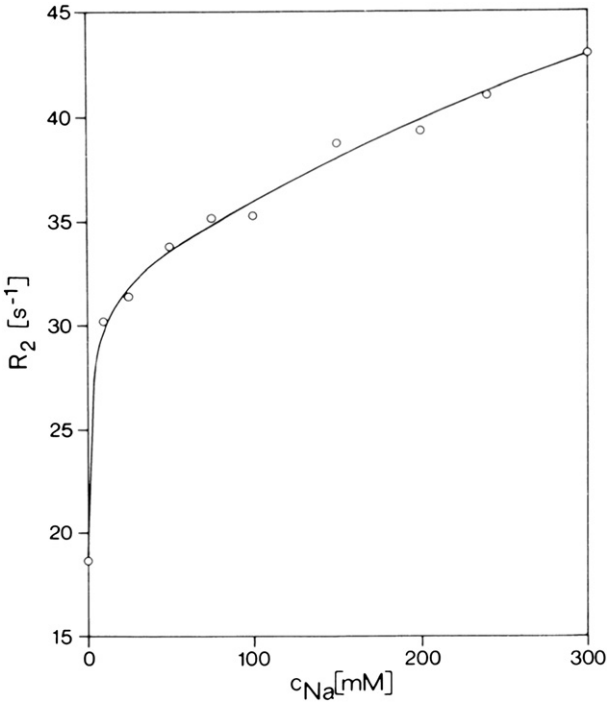

Fig. 30. The $^{23}Na^+$ relaxation rate, R_2 [s^{-1}], as function of the Na^+ concentration in aqueous solutions of CS-P during a dilution experiment (from [11]).

the binding sites, R_{obsd} is the weighted average of the individual relaxation rates; the weighting factors are the fractional concentrations

$$R_{obsd} = p_F R_F + \sum_i p_i R_i, \tag{38}$$

where R_F = relaxation rate of the free ligand; R_i = relaxation rate for binding at site i; p_F = fractional concentration of free ligands; p_i = fractional concentration of ligand bound to site i. If one takes a monomeric unit of CS, then the ligand can associate with the substrate at two binding sites (carboxylate and sulfate groups) with relaxation rates R_1 and R_2.

$$R_{obsd} = \frac{[L]}{c_L}\cdot R_F + \frac{[LS_1]}{c_L}\cdot R_1 + \frac{[LS_2]}{c_L}\cdot R_2, \tag{39}$$

where [L] = concentration of the free ligand; [LS_1], [LS_2] = concentrations of the ligands bound to sites 1 and 2; c_L = total concentration of the ligand. The concentrations of the free and bound ligands are connected through their dissociation equilibria

$$K_1 = \frac{[L][S_1]}{[LS_1]}; \quad K_2 = \frac{[L][S_2]}{[LS_2]} \tag{40}$$

and

$$c_L = [L] + [LS_1] + [LS_2] \tag{41}$$

$$c_S = [S_1] + [LS_1] \tag{42}$$

These relations can be utilized to find [LS_1] and [LS_2] as functions of [L] and the dissociation constants. From these equations one gets an equation of the third order in [L]

$$[L]^3 + [L]^2\{c_S + (c_S - c_L) + (K_1 + K_2)\} + [L] \{(c_S - c_L)(K_1 + K_2) + K_1K_2\} - c_L K_1 K_2 = 0 \tag{43}$$

Writing the solution to this equation as [L] = f(c_L,K_1,K_2) and considering also that during a dilution experiment the concentration ratio $\frac{c_S}{c_L} = A$ remains constant, we arrive at the relaxation rate R_{obsd} (c_L)

$$R_{obsd} = \frac{f(c_L,K_1,K_2)}{c_L}R_F + \frac{f(c_L,K_1,K_2)\cdot A}{f(c_L,K_1,K_2)+K_1}R_1 + \frac{f(c_L,K_1,K_2)\cdot A}{f(c_L,K_1,K_2)+K_2}R_2 \tag{44}$$

After making a nonlinear least square fit to the curve $R_{obsd}(c_L)$ in Fig. 30, the ratio of the dissociation constants results as K_1: K_2 = 1:1000. These dissociation constants will be required for the calculation of K^+ and Ca^{2+} dissociation constants in competition experiments.

6.1.2.3. Models for counterion binding to polyelectrolytes. The Debye–Hückel theory provides an adequate description of ionic interactions only if each charge is surrounded by charges in spherical symmetry and if the electrostatic energy of interaction with a test charge is much smaller than kT. None of these conditions apply for extended polyelectrolytes. Several models for counterion binding to polyelectrolytes have been advanced. Fundamentally, they are all, with varying degree of sophistication, based on the Poisson–Boltzmann equation, which provides the means for obtaining the electrostatic contribution to the total free energy of the interaction.

In the Manning model [190,232,233], a linear (rodlike) polyelectrolyte is approximated by a uniform and continuous line-charge. The key parameter in the model is the dimensionless linear charge parameter, defined as

$$\xi = \frac{e^2}{\varepsilon\varepsilon_0 kTb} \tag{45}$$

where $e^2/(\varepsilon\varepsilon_0 kT)$ is equal to the classical "Bjerrum length", and b is the average spacing of the projection of the charged groups on the polyion onto the axis of the fully extended polyion. The Manning theory states that for values of ξ less than $\xi_{crit} = |Z|^{-1}$, where $|Z|$ is the valency of the counterions (corresponding to a $b > 0.7135$ nm for monovalent charges in aqueous solution at room temperature), the interaction of the counterions with the polyion may be treated in the Debye–Hückel approximation for dilute solutions. When, however, ξ exceeds ξ_{crit} the polyion–counterion interaction will become so strong that counterions will "condense" on the polyion so as to effectively reduce the value of ξ down to ξ_{crit}. The uncondensed counterions may again be treated in the Debye–Hückel approximation. The concept of "counterion condensation" was originally introduced by Imai, Ohnishi and Oosawa [241,242]. The predictions from the Manning theory in the case of a polyelectrolyte solution with no added electrolytes are that the fraction of "condensed" counterions p_c ($=p_B$) should be given by

$$p_c = 1 - 1/|Z|\xi \tag{46}$$

and the fraction of "free" counterions, p_F, correspondingly by

$$p_F = 1 - p_c = (|Z|\xi)^{-1} \tag{47}$$

In the Oosawa model [243], the electrical potential around a polyelectrolyte is approximated as a step function, with a high potential (Ψ_1) close to the polyion and an outer region where the electrical potential (Ψ_2) is lowered by a certain amount $\Delta\Psi$ (see Fig. 31B). The distribution of counterions between the two regions is assumed to be determined by the Boltzmann equation with the exponent $-e\Delta\Psi/kT$.

In the approach by Katchalsky et al. [244,245], the polyion is treated as an infinitely long cylinder with a radius, a, and with the polyion charges smeared out as a continuous charge density, σ, over the surface of the cylinder (Fig. 31A). The distribution (in cylindrical symmetry) of counterions outside the polyion is obtained from the Poisson–Boltzmann equation. This model allows the calculation of the fraction of counterions inside any cylindrical shell around the cylinder. As treated by Wennerström et al. [246], this model may take into account differences in polyion structure (variation of a and σ), differentiate between different counterions (variation of the closest approach to the cylinder), and, finally, this model may, without any further assumptions, be extended to include the effect of added simple electrolytes to the polyelectrolyte solution.

Much research in the polyelectrolyte field was devoted to the distribution of counterions around a polyion and the testing of theoretical models like those briefly outlined above. Other problems in the field concern the type of binding of the "condensed" ions. Here such models are used simply to demonstrate qualitatively the principal behaviour of counterion binding to polyelectrolytes in order to aid in the evaluation of p_B and χ from NMR results.

6.1.3. Specific ion binding to extracellular matrices

Specific cation binding to anionic GAGs and proteoglycans has been demonstrated by spectroscopic methods [231]. Sites with high affinity and selectivity of cation binding were identified apart from diffuse binding [221,247]. Fig. 32 shows $^{23}Na^+$ NMR relaxation rates obtained as a function of the ionization degree of the polyanions DS, CS, and HA [9]. The investigations indicate the feasibility of the method to establish changes in counterion binding occurring as a result of both changed degree of ionization and changed chemical structure of the GAGs. Since in this pH titration experiment the correlation time and quadrupole

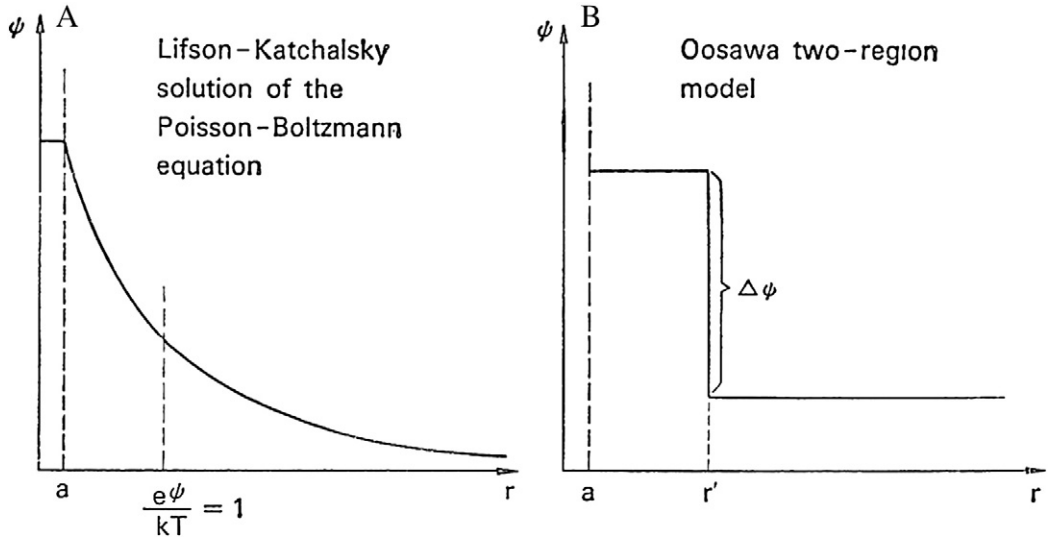

Fig. 31. Illustration of two approaches to the description of the electrostatic potential, Ψ, outside a polyion. (A) The solution of the Poisson–Boltzmann equation for the case where the polyion is treated as an infinite cylinder of radius *a*. (B) The variation of the potential in the simplified Oosawa model. *r* is the distance from the centre of the polyion (from [177]).

coupling constant did not vary markedly between the different GAGs, the changes in the $^{23}Na^+$ relaxation rate for the three polyelectrolytes reflect an increase (decrease) in Na^+ binding as the rate rises (falls). These findings were already raised by Lindman et al. [10] in preliminary joint $^{23}Na^+$ NMR experiments with a CS-P peptidoglycan. Fig. 33 shows the relations between the pH, the degree of neutralization and the $^{23}Na^+$ relaxation rate. It is not possible to discuss these results in full but some interesting observations can be made: i) with the usual fast exchange assumption it is suggested from comparisons of the R_1 and R_2 results that the change in R_2 at high α (and pH) values is dependent on a correlation time change and thus some conformational alteration. The change in R_2 at neutral pH and below is at least partly due to a release of Na^+ ions with decreasing pH. ii) Comparisons with corresponding data for the pure CS and DS show that the results of Fig. 33 do not constitute a simple sum of the results of the separated components. For the purified CS and DS simple sigmoid titration curves were obtained in studies of R_2 as a function of α. Apparently, the protein content has a marked effect on the ionic interactions and probably cooperative effects have to be invoked to explain the differences. It should be noted that in all cases studied marked variations were observed around physiological pH values (cf. dashed lines in Fig. 33).

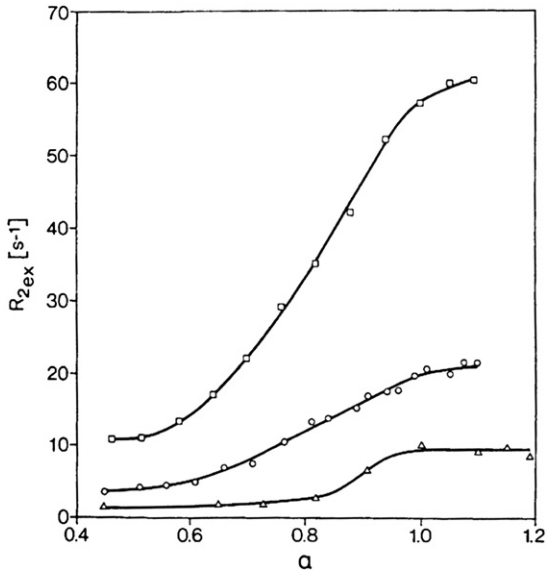

Fig. 32. $^{23}Na^+$ excess relaxation rates, R_{2ex}, as a function of the 'stoichiometric' degree of neutralization, α, for aqueous solutions of dermatan 4-sulfate (□), chondroitin 4-sulfate (○) and hyaluronate (Δ). The concentrations are in monomeric units 0.2, 0.2 and 0.05 mol/L, respectively. The Na^+ concentrations are for the first two substances 0.3 mol/L and for the hyaluronate 0.075 mol/L (from [5,180]).

It may be mentioned in connection with these results that only the carboxylate groups were titrated while the sulfate groups stay ionized and also that as a result of polarity variations and other factors there may be a considerable spread in the pK values of the carboxylate groups. Although these $^{23}Na^+$ relaxation studies were far from complete they demonstrated a novel, specific way of probing into ionic interactions in ion binding compounds from connective tissues. A determination of the effects of Ca^{2+} and Mg^{2+} ions on the conformation and the Na^+ binding is of particular interest.

Also, the speculations about medical significance are valid still today. Supposing that the Ca^{2+} binding and releasing properties of in vivo proteoglycans are similar to those described for Na^+ in CS-P with changing pH, then an autoregulatory mechanism can be suggested for local blood perfusion of a tissue area. Changing the pH to tissue acidosis leads to a release of a certain amount of Ca^{2+} ions from the connective tissue, especially from the basal lamina of vascular smooth muscle and endothelial cells. The released Ca^{2+} increases the Ca^{2+} concentration in the small cleft spaces between cell membrane and basal lamina thus possibly effecting a membrane stabilization. The result is a decrease in P_{Na} and a relative increase in P_K, leading to membrane hyperpolarization. The hyperpolarization causes relaxation of the vascular smooth muscle cells via electromechanical coupling [10]. The final step is an increase in tissue perfusion and local blood supply, changing the pH value of the tissue to normal. Ca^{2+} ions will be bound again to the high affinity binding sites. The inverse argumentation can be applied to alkalosis. Alternatively, Na^+ ions released under changes to acidic pH (Fig. 33C) can pass the endothelial cell membrane, thus mediating a depolarization [199]. The depolarization increases P_{Ca}, an augmented Ca^{2+} influx via nonselective cation channels results and stimulates NO synthase [161]. NO and coreleased PGI_2 diffuse to the subjacent vascular smooth muscle cells and elicit here the cascade of cG-PK- and cA-PK-dependent reactions, including membrane hyperpolarization of the muscle cells. The resulting flow dilatation reverses the pH to normal. Both these fundamental interpretations may be coupled under in vivo conditions.

6.1.3.1. Monovalent ion binding to vascular connective tissue. Since a tight electromechanical coupling exists in arterial smooth muscle, even small shifts of the membrane potential are sufficient to change the vascular

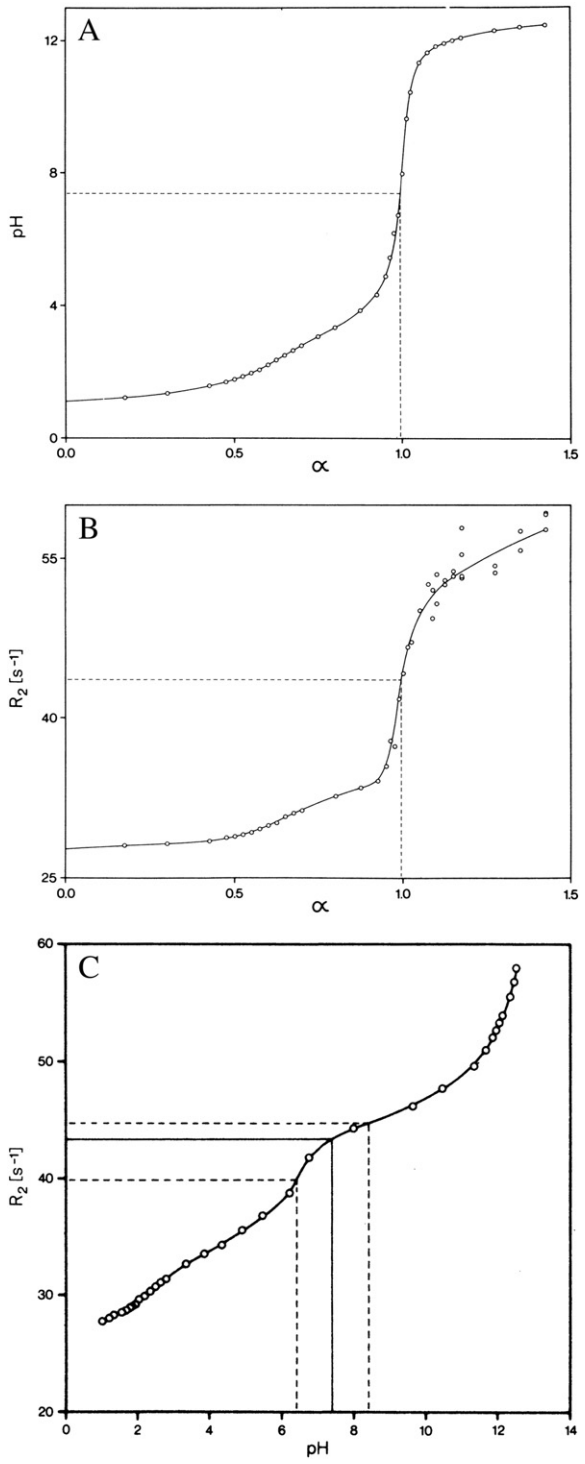

Fig. 33. The pH (A) and $^{23}Na^+$ relaxation rate, R_2 (B), as function of the degree of neutralization, α, for aqueous solutions of CS-P at 0.1 mol/L concentration calculated on carboxylic acid content. The total Na^+ ion concentration is 0.3 mol/L. (C) Relaxation rate, R_2, as a function of pH in the presence of CS-P. Dashed lines indicate characteristic physiological pH values (from [10]).

lumen. The extracellular H^+, Na^+, K^+, Mg^{2+} and Ca^{2+} concentrations are important effectors for the adjustment of the membrane potential. The ion concentrations in the immediate neighbourhood of the cell membrane can be influenced by the microdynamic binding properties of the basal lamina and the surrounding extracellular connective tissue matrices, which are separated from the vascular smooth muscle cell membranes by tiny cleft spaces. These structures display a high binding capacity for small cations which has been ascribed to the presence of polyanionic proteoglycans [248]. Fig. 34A shows K^+ binding curves for normal and Ca^{2+}-free Krebs solutions as well as for a 4.7 mmol/L KCl solution. In a normal Krebs solution, the K^+ binding increases with increasing pH and attains a maximum at pH = 6.8. Surprisingly, it decreases in the basic pH range, which is a most remarkable fact for a pH-dependent cation binding curve [11,248]. Before an explanation for this behaviour is given, the significance of the K^+ binding curve shall be discussed. Following transition from pH 7.3 to 6.8, 0.64 mmol K^+/kg fibre wt. are bound to connective tissue structures, while 1.52 mmol K^+/kg fibre wt. are released upon transition from pH 7.3 to 7.8. Application of a simple geometric model, which considers the narrow cleft spaces between cell membrane, basal lamina and connective tissue fibres, can lead to a reduction of the K^+ concentration in the cleft spaces to ⅔ to ½ in the first case, in the latter case to an increase to the double to triple of its normal value. Extracellular accumulation of K^+ would lead to membrane depolarization of smooth muscle cells and sympathetic nerve fibres located at the adventitia–media boundary, and thus to contraction, depletion of K^+ to hyperpolarization with vasodilatation.

The K^+ binding characteristic in a Ca^{2+}-free Krebs solution explains the unusual course of the K^+ binding curve under normal conditions. Comparing both curves, one can immediately conclude that the decrease of K^+ binding in the basic pH range for normal Krebs solution must be attributed to Ca^{2+} competition. The Ca^{2+} competition is least pronounced between pH 6 and 7. Therefore, the result of a Ca^{2+}-free Krebs solution is a simple sigmoid K^+ titration curve. Furthermore, the regulating role of K^+ ions on the membrane potential is abolished by flattening its binding characteristic, since the K^+ binding at pH = 7.4 has reached a steady state value.

Incubating vascular connective tissue in a 4.7 mmol/L KCl solution, we found a pH-dependent K^+ binding characteristic similar in principle to the K^+ binding curve in Ca^{2+}-free Krebs solution. Also in this KCl solution, which contains KCl in physiological concentration but is free of Ca^{2+} and has a considerably diminished ionic strength in comparison to blood, a sigmoid K^+ titration curve was determined. Although there is no competition by other counterions, the binding curve lies distinctly below that in Ca^{2+}-free Krebs solution. Physicochemically, there is the possibility of an 'occlusion' of unspecific and specific sites by their steric arrangement within a polyelectrolyte system [181]. Thus, the site-bearing proteoglycans embedded in a fine collagen and laminin mesh-work could be excluded from the fast cation exchange with increasing 'felting' by aggregation of collagen and laminin molecules with each other and with the proteoglycans. Increasing macromolecular interactions with decreasing ionic strength of the incubation medium are well-known [231,249–251].

Fig. 35 illustrates $^{42}K^+$ washout curves for 0.47 mmol/L and 4.7 mmol/L KCl solutions, respectively. Under the assumption of three compartments (K^+ efflux from tissue water and from two binding sites) a triple-exponential decay curve has been fitted iteratively to the measured values with the aid of a nonlinear least square fit (thin-traced lines) [215]. The three amplitudes and rate constants of the e-functions were calculated. The same procedure was applied for calculation of the affinity constants of Na^+ and Mg^{2+} ions. For example, $^{28}Mg^{2+}$ washout curves in a 1.1 mmol/L and 11 mmol/L $MgCl_2$ solution show that the Mg^{2+} exchange runs slower than the K^+ exchange, the curves are flatter. Amplitudes and rate constants were computed. In a compartment model, in which the binding sites S_1 and S_2 exchange via tissue water and also directly with the washout fluid, the quantity of the compartments as well as the kinetic coefficients can be calculated utilizing the amplitudes and rate constants. With the knowledge of the compartments and kinetic coefficients the affinity constants for S_1 and S_2 were computed after having solved a set of reaction kinetic equations which describe the binding of the ligand to these sites. The numerical results of the $^{24}Na^+$, $^{42}K^+$ and $^{28}Mg^{2+}$ flux experiments are summarized in Table 4 [198,252]. One notices that the log K_A values for S_1 and S_2, respectively, are nearly equal for both the ion species K^+ and

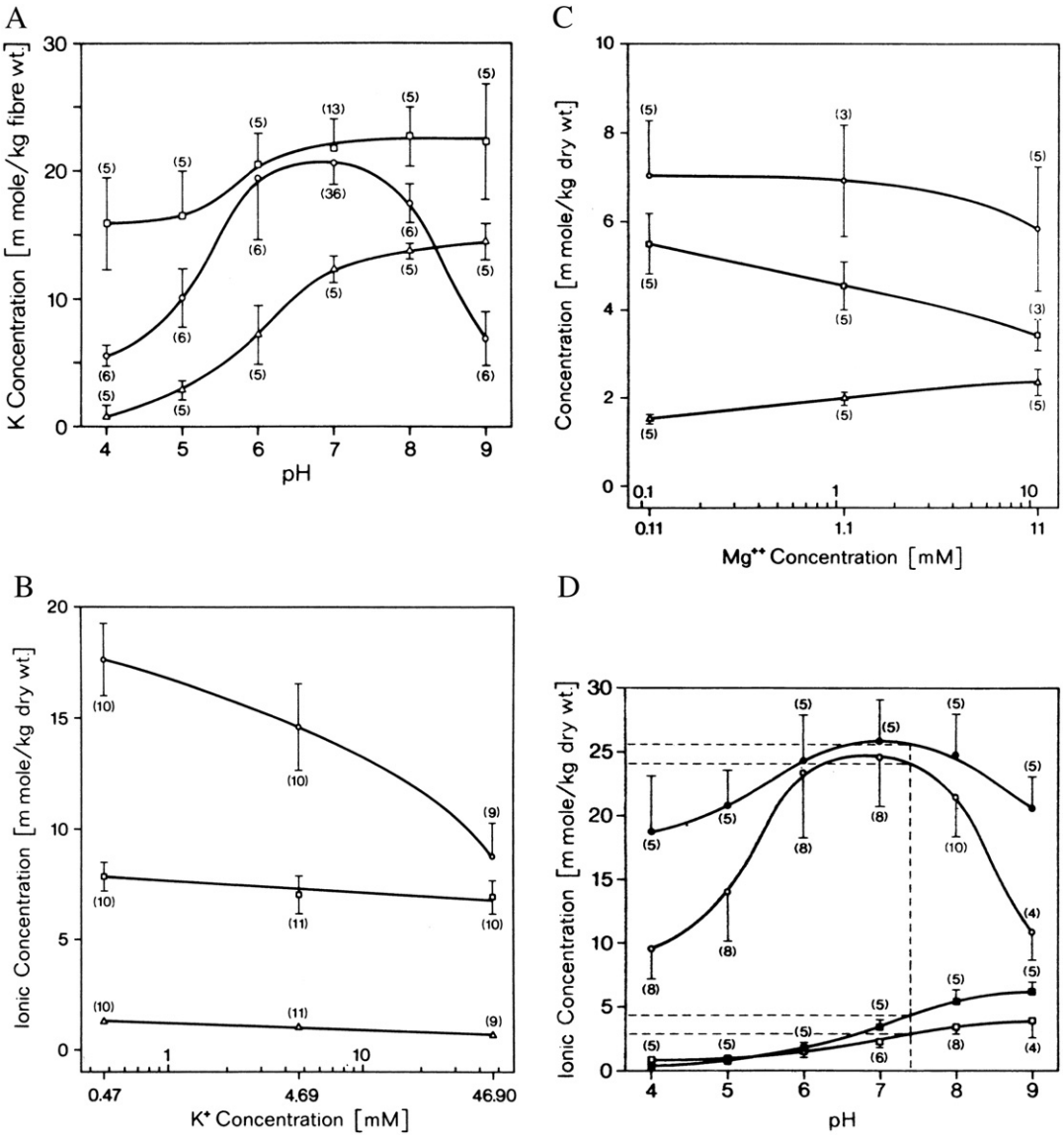

Fig. 34. (A) K^+ binding of isolated adventitial connective tissue from the canine carotid artery as a function of the pH of a normal (○) and a Ca^{2+}-free Krebs solution (□) as well as of a 4.7 mmol/L KCl solution (Δ). (B) Na^+ (○), Mg^{2+} (Δ) and Ca^{2+} binding (□) as a function of the K^+ concentration in aqueous solutions. (C) Na^+ (○), K^+ (Δ) and Ca^{2+} binding (□) as a function of the $MgCl_2$ concentration in aqueous solutions. (D) K^+ (○; ●) and Mg^{2+} binding (□; ■) as a function of the pH of Krebs solutions with 0.11 mmol/L (○; □) or 1.1 mmol/L Mg^{2+} concentration (●; ■) (from [248,252]).

Mg^{2+}, where S_2 binds stronger than S_1. Thus, these data are in excellent agreement with competition experiments from NMR investigations on CS-P.

The competitive effect of K^+ ions can be demonstrated as clearly in the $^{42}K^+$ flux experiments, in which the vascular connective tissue was incubated in pure KCl solutions for hours, and after which the ionic concentrations were determined by atomic absorption spectroscopy. Fig. 34B illustrates the competitive effect of bound K^+ on the remainder ions in the tissue. The Na^+ binding is reduced strongest with increasing K^+ concentration. But Mg^{2+} and Ca^{2+} binding decrease clearly as well. The competitive effect of increasing the Mg^{2+} concentration on Na^+ and Ca^{2+} binding is easily recognizable from Fig. 34C. Na^+ and Ca^{2+} binding curves decrease steadily. After having seen that K^+ and Mg^{2+} ions compete for the same binding sites, the significant *increase* in K^+ binding in correspondence to the increase of Mg^{2+} is at first a surprising finding. A cooperative binding of K^+ ions with an increase in Mg^{2+} binding can be offered as an explanation. Before one enters into a possible cooperative interaction between Mg^{2+} and K^+ binding, the effect of a normal Mg^{2+} concentration on the pH-dependent K^+ binding had to be investigated. As already mentioned, we measured the binding of various cations in Krebs solutions with Mg^{2+} concentrations of 0.11 and 1.1 mmol/L, respectively. In Fig. 34D, the Mg^{2+} and K^+ binding is represented. An elevation from 0.11 to 1.1 mmol/L of the Mg^{2+} concentration of the Krebs solution causes an increase of bound Mg^{2+} as well. Correlated to this, both an increase of bound K^+ over the entire pH range and a flattening of the K^+ binding characteristic were found. This means physiologically that Mg^{2+} ions amplify K^+ binding to the proteoglycans and thereby accelerate the decrease of the K^+ concentration in extracellular cleft spaces. This leads to hyperpolarization of the smooth muscle cell membrane and thus to vasodilatation. When we remember the experiments in a Ca^{2+}-free Krebs solution (Fig. 34A), we can finally conclude that a rise in K^+ binding as well as a flattening of the pH-dependent K^+ binding characteristic can be effected by a decrease of the extracellular Ca^{2+} concentration and/or by an increase of the external Mg^{2+} concentration. Apparently, in this way the extracellular K^+ concentration in the narrow tissue clefts between cell and basement membranes is carefully controlled by nature.

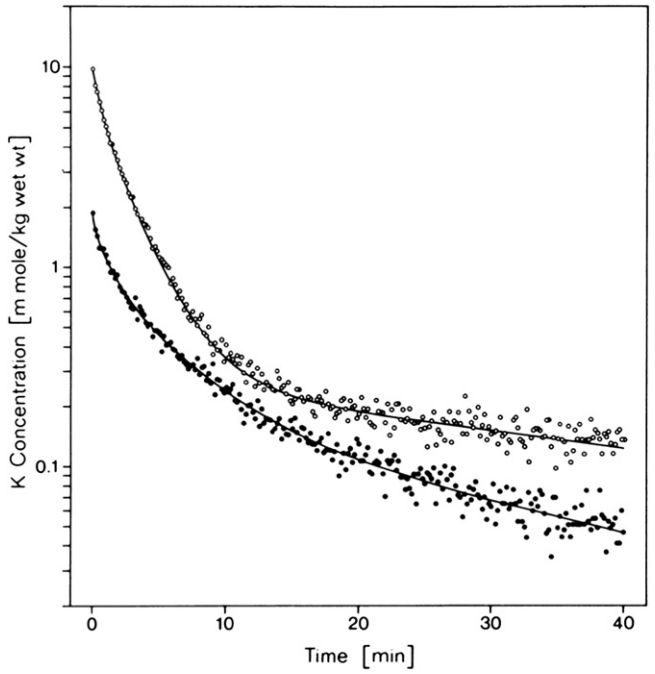

Fig. 35. $^{42}K^+$ efflux of isolated adventitial connective tissue from canine carotid artery according to the direct method. The graph shows the time course of radioactive K^+ decrease within the preparation at intervals of 10 s in single experiments for 0.469 mmol/L (●) and 4.69 mmol/L (○) K^+ solutions, respectively. The thicker-traced lines represent the optimal triple-exponential functions found by computer fitting (from [248]).

6.1.3.2. Affinity constants of vascular connective tissue. As already outlined, in order to determine global affinity constants for in vivo vascular connective tissue, tracer efflux experiments were designed, which would supply us with the amplitudes and rate constants for calculating affinity constants (cf. Fig. 35). Isolated adventitial connective tissue was used as a polyelectrolyte, and $^{24}Na^+$, $^{42}K^+$ or $^{28}Mg^{2+}$ as counterions in three different concentrations [248]. Each series of flux experiments with one cation species resulted in equal and mutually uniform kinetic coefficients for the slower exchange fractions. The kinetic coefficients are an expression of the exchange deceleration by chemical binding and the affinity of binding sites. The homogeneity of the kinetic coefficients under the various experimental conditions shows that the negatively charged groups in the preparations after Na^+, K^+ or Mg^{2+} accumulation can be subdivided into few classes of binding sites with uniform intrinsic affinity constants. The result of these flux experiments is summarized in Table 4. One notices that the log K_A values for $S_{i,1}$ and $S_{i,2}$, respectively, are nearly equal for both the ion species K^+ and Mg^{2+}, where $S_{i,2}$ binds more strongly than $S_{i,1}$. Also the total number of binding sites for K^+ and Mg^{2+} ions is nearly identical. This means that K^+ and Mg^{2+} ions with equal affinities strongly compete for the same molecular sites. In general, the log K_A values are between 1.8 and 3.7 indicating binding sites with high affinity and selectivity for cation binding. Computer models for chain association in proteoglycans [253] define binding sites formed by several ionized and hydroxyl groups, with a striking structural analogy to crown ethers [231]. These are strong and selective complexing agents whose affinity constant for K^+ is typically between log K_A 0.6 and 2.2 [254].

Affinity constants of logK_A 1.5–2 L/mol were found for Ca^{2+} complexes of uronic acid monomers, whereby the galacturonate complexes are more stable than the glucuronate complexes [255,256]. The behaviour of these proteoglycan units can be observed again in isolated anionic polysaccharides in aqueous solutions. Alginates, polymeric compounds of D-mannuronic and L-guluronic acid, have a high binding affinity and selectivity for alkali metal and alkaline earth metal ions [235]. The content of L-guluronic acid that contains an *ax-eq-ax* configuration of hydroxyl groups is decisive for cation binding favouring Na^+ and Ca^{2+}. The analogy to the cation binding being stronger in DS than in CS is striking (see Fig. 32), the C-5 epimeric uronic acid moieties (L-iduronic acid versus D-glucuronic acid) of which correspond to the C-2 epimers of L-guluronic acid versus D-mannuronic acid [247,249]. Since DS and CS have different cylinder radii due to the axial and equatorial carboxylates, respectively, the Katchalsky approach confirms the different counterion binding in the two substances [245]. It may be recalled that both DS and CS have one ionizable group on each monosaccharide unit and that these are alternatively sulfate and carboxylate groups in different positions. HA, which has much longer chains than the others, has a carboxylate group on every second monosaccharide unit and no sulfate group.

Ion binding with high affinity and specificity to the extracellular matrix polyanions is intricately dependent on secondary and tertiary structure [253,257,258]. An electrostatic interaction according to statistical binding with or without polyelectrolyte effect (counterion condensation) between the cations and the anionic moieties fixed on

Table 4
Binding site $S_{i,j}$, affinity constant K_A and concentration of sites $[S_{i,j}]$ of canine arterial vascular connective tissue for the cation species Na^+, K^+ and Mg^{2+} (from [252]).

$S_{i,j}$	K_A [L/mol]	logK_A	$[S_{i,j}]$ [mmol/kg fibre wt.]	$\Sigma[S_i]$ [meq/kg fibre wt.]
$S_{Na,1}$	4522	3.66	0.850	2.176
$S_{Na,2}$	58	1.76	1.326	
$S_{K,1}$	365	2.56	13.940	16.068
$S_{K,2}$	1009	3.00	2.128	
$S_{Mg,1}$	559	2.75	6.407	15.672
$S_{Mg,2}$	3177	3.50	1.429	

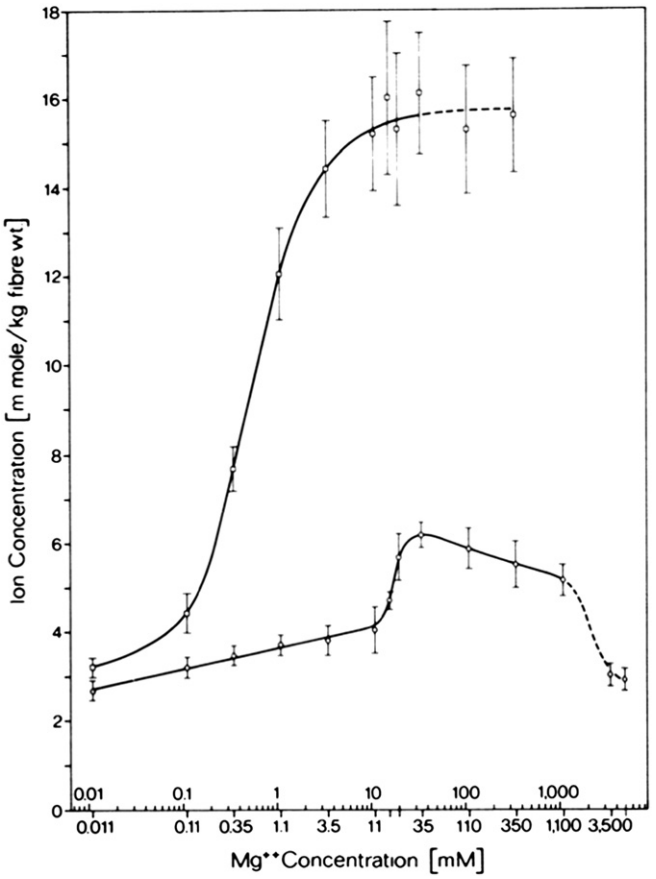

Fig. 36. K^+ (○) [n = 8] and Mg^{2+} (□) [n = 9] of isolated adventitial connective tissue of the canine carotid artery after a 3 h incubation in pure aqueous $MgCl_2$ solution at pH 7.0 (from [252]).

connective tissue structures cannot completely account for the high affinity. Unlike collagen and elastin, the proteoglycans are available for complexation with small cations. Ionized and polar groups of several GAG chains can participate in the formation of single sites when mobile cations shield the negative fixed charges and thus allow their chains to be approached [259,260]. Thus, chain association in proteoglycans can form binding sites of distinctive structural analogy to crown ethers bounded by several hydroxyl and ionized groups [231,258]. These macrocyclic polyethers are strong and selective complexing agents.

6.1.3.3. Divalent ion binding to vascular connective tissue. Investigating the mode of interaction of various counterions (Na^+, K^+, Mg^{2+}, Ca^{2+}) with native polyanionic vascular connective tissue in dependence on the concentration of a single cation species, competition is found in all cases but two: a rise of the external Mg^{2+} (Ca^{2+}) concentration leads not only to an enhanced Mg^{2+} (Ca^{2+}), but also to an increased K^+ (Na^+) binding. Consequently, the K^+ binding was inspected more closely for a wide range of Mg^{2+} concentrations (Fig. 36). In pure $MgCl_2$ solutions the K^+ binding increases continuously in a low Mg^{2+} concentration range [248], then increases steeply between 15 and 20 mmol/L, and finally decreases gradually after saturation. The initial rise of K^+ adsorption can be explained by a steady augmentation of K^+ binding sites with increasing ionic strength, and thus a more effective shielding by mobile cations of the high charge density of fixed anionic groups of GAG chains. This effect promotes an association of GAG chains whose share in the generation of specific sites of high affinity was suggested [231,249,253]. However, the steep increment of K^+ binding can be attributed only to an allosteric interaction due to further increasing Mg^{2+} concentrations, the following graded fall probably to a gradual configurational transition of the macromolecules with unphysiologic high Mg^{2+} concentrations and ionic strength. Fitting the measured values to the function

$$Y = \frac{a[S]^n \cdot C_{max}}{(1 + a[S]^n)(1 + b[S]^m)} + c \ln[S] + d \quad (48)$$

results in the following parameters: $a = 2.7 \cdot 10^{-9}$ (mmol/L)$^{-n}$; $b = 4.5 \cdot 10^{-3}$ (mmol/L)$^{-m}$; $c = 0.19$ mmol/L; $d = 3.61$ mmol/L; $n = 6.77$; $m = 1.07$; $C_{max} = 2.33$ mmol/kg. Thus, the HILL coefficient of cooperative K^+ binding is 6.8, the $[Mg^{2+}]_o$ concentration at half-maximal velocity $S'[0.5] = 18.5$ mmol/L ($S''[0.5] = 153.7$ mmol/L). When the curves for K^+ and Mg^{2+} binding are compared, a distinct rise of Mg^{2+} binding is seen already at $[Mg^{2+}]_o = 0.1$ mmol/L as well as a saturation in the same $[Mg^{2+}]_o$ range, in which the K^+ binding increases drastically. This relation permits the conclusion that only saturation of all specific Mg^{2+} binding sites leads to the conformational transitions in the polyanions necessary for a cooperative K^+ binding. Finally, it shall be mentioned that the ionic strength of these pure $MgCl_2$ solutions is by no means physiologic. Studies in Krebs solutions of increasing Mg^{2+} concentration yielded also cooperative K^+ binding for an $[Mg^{2+}]_o$ range between 0.3 and 0.8 mmol/L.

Cooperative binding is possible if a conformational change of the polyelectrolyte takes place via the allosteric effect of a ligand [10]. Monovalent cations are not suitable for such a change of proteoglycan structure, but rather cations like Mg^{2+} and Ca^{2+} with their two valences [176]. Stretched in between the side chains of these polyanions, they can rearrange the whole macromolecular structure. With the help of NMR techniques, the ability of Mg^{2+} ions in a low concentration range has been examined to cause such a change in configuration. In Fig. 37, the $^{23}Na^+$ excess relaxation rates are plotted versus the Mg^{2+} concentration of a physiological Krebs solution at pH 7.38 in the presence of a physiological CS-P concentration. It is highly surprising that $R_{2_{ex}}$ increases for small additions of $MgCl_2$ [cf. 248], and decreases only with higher Mg^{2+} concentrations, that is Na^+ is expelled from its binding sites (normal competition). The additional measurement of the longitudinal relaxation rate, $R_{1_{ex}}$, which exhibits normal competition behaviour,

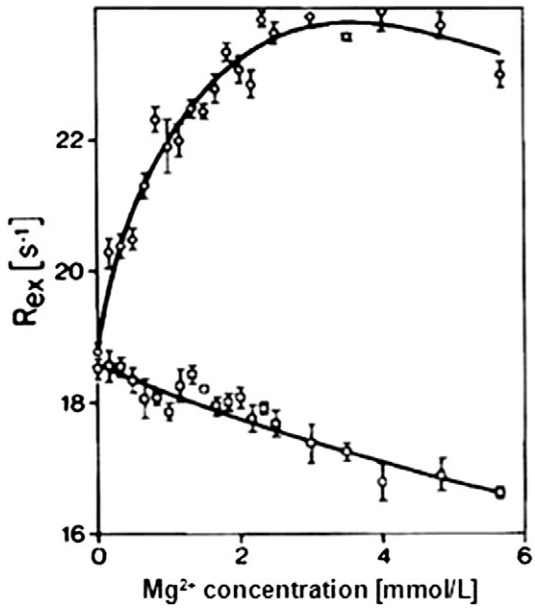

Fig. 37. The $^{23}Na^+$ excess longitudinal (□) and transverse (○) relaxation rates, $R_{1_{ex}}$ and $R_{2_{ex}}$, in dependence on the Mg^{2+} concentration of a Krebs solution containing 0.1 mol/L CS-P at pH 7.38. The initial fall of the longitudinal relaxation rate and the initial rise of the transverse relaxation rate in the range of physiological Mg^{2+} concentrations is indicative of a conformational change of the CS-P macromolecules (from [252]).

gave further evidence for a conformational change of the macromolecules, which is indicated by the $R_{2_{ex}}$ increase.

6.1.4. Competitive and allosteric-cooperative binding

Both static and dynamic aspects of reversible binding of mono- and divalent cations to the polyanions of GAGs, proteoglycans, and connective tissue matrices have supported the idea of variation in the ionic microenvironment of cells [7,203]. Changes in physical state variables, for example, in the pH value, voltage, or osmotic pressure, influence the bound ion fractions interchanging with the ion concentrations in the adjacent extracellular crevices. While monovalent cations exert merely simple competitive behaviour, divalent cations can induce a conformational transition, specifically changing the affinities for other ion species. Mg^{2+} or Ca^{2+} ions cause such a configurational change in the physiological concentration range which promotes allosteric, cooperative binding of K^+ or Na^+ ions, respectively, to the matrix polyanions [7,252]. Thus, ion binding in general has to be considered in terms of concentration, affinity constants, competition, and cooperative effects.

The discussion of mechanisms of cation binding to connective tissue components abundant in the vascular wall has introduced a completely new kind of consideration into the field of membrane physiology of vascular smooth musculature [180]. The ion activities close to the cell membrane depend on the binding properties of anionic biopolyelectrolytes of the basement membrane and connective tissue matrices, which build a tight-fitting sheath around the plasma membrane. Under suitable, non-stationary conditions, a release of cations from or adsorption to the polyanionic macromolecules can lead to transient activity changes in these tiny extracellular tissue compartments between cell membrane, basement membrane and the connective tissue fibres. Such changes may influence transmembrane ionic currents, membrane potential and mechanical tension development [169].

When the GAGs are bound to their natural protein component as they are in native vascular connective tissue, then the ion binding behaviour can be studied under in vivo conditions. $^{23}Na^+$ and $^{39}K^+$ NMR measurements indicate that, while monovalent cations exert merely competitive interaction, divalent cations induce a conformational transition changing specifically the affinities for other ion species

[7,169,176]. Mg^{2+} or Ca^{2+} ions cause such a configurational change in the physiologic concentration range which promotes allosteric, cooperative binding of K^+ or Na^+ ions, respectively, to vascular connective tissue. In Fig. 14A, the $^{23}Na^+$ excess relaxation rates are plotted versus the Ca^{2+} concentration of a Krebs solution at pH 7.3 in the presence of the counteranions of vascular connective tissue. According to normal competition, $R_{2_{ex}}$ at first decreases with low Ca^{2+} concentrations up to 0.5 mmol/L. But then $R_{2_{ex}}$ increases with further small additions of $CaCl_2$ up to 1.5 mmol/L [180]. Above 1.5 mmol/L Ca^{2+}, simple exchange of bound Na^+ with Ca^{2+} was observed. Therefore, as in a CS-P solution, $R_{2_{ex}}$ increases drastically, which indicates a conformational change [176]. The half-maximal conformational transition is observed with 1.15 mmol/L Ca^{2+}, i.e., in the physiologically relevant range, considering that half of the serum Ca^{2+} of 2.5 mmol/L is bound to proteins.

The increased $R_{2_{ex}}$ seen upon Ca^{2+} additions is referred to an increase in the correlation time τ_c for bound Na^+. This is an approximate measure of the mobility of a molecule or an ion. A raised τ_c value means less mobility. In Fig. 14B, the τ_c value for Na^+ increases abruptly in the range 0.5 mmol/L < $[Ca^{2+}]_o$ < 2 mmol/L and then reaches a plateau value. The jump in correlation time cannot be explained by a thermic mobility change of the Na^+–matrix macromolecular complex, because polyanions of the connective tissue should influence the correlation times only insignificantly due to their molecular size and the ensuing relative immobility [250,251]. Therefore, the most probable explanation of the sudden change of τ_c remains the induction of intra- or intermolecular cross-linking leading to conformational transitions of the polyelectrolyte, to molecular associations, or to both [250–252,258].

Besides this conformational transition, the experiment shows an immediate increase of the longitudinal relaxation rate $R_{1_{ex}}$ at the very beginning of Ca^{2+} additions (Fig. 14A). Obviously, Na^+ ions are consecutively bound at an allosteric site. Would there be an expulsion of Na^+ ions by Ca^{2+} ions, then a continuous decrease of $R_{1_{ex}}$ should be discernible as can be seen in comparable Mg^{2+} competition experiments [180]. With the possession of both relaxation rates and correlation times, the static contribution to relaxation, i.e. the Na^+ binding, can be computed.

Indeed, the calculation of $p_B\chi^2$ shows that the Na^+ binding increases at once and reaches a maximum of 1.5 times its value with 1.5 mmol/L Ca^{2+} concentration, and decreases only slightly with further increasing Ca^{2+} concentration (Fig. 14C). Only above values of 1.5 mmol/L Ca^{2+}, bound Na^+ ions exchange for Ca^{2+} ions which means normal, but weak competition. Another explanation of the slight decrease of $p_B\chi^2$ would likewise be conceivable remembering the previously raised finding, that at least two specific binding sites exist for Na^+ ions in the proteoglycan. Considering that the allosteric site binds Na^+ cooperatively due to the Ca^{2+}-induced conformational change, the other site, however, shows normal competition behaviour, it is merely a question of the quantification of both simultaneous processes to enable a simulation of the observed course of the bound fraction. This means that we can state two extraordinary effects of Ca^{2+}: on the one hand a conformational change of the macromolecules of vascular connective tissue with rising Ca^{2+} concentration, on the other hand no Na^+ competition, but on the contrary a Na^+ binding to these polyanions. Therefore, the elevation of the Ca^{2+} concentration in the blood substitute solution does not effect an expulsion of Na^+ ions from their binding sites, but it induces allosteric Na^+ adsorption to the polyanionic macromolecules of vascular connective tissue. The question of whether the elevated Na^+ binding is caused by a conformational change which increases the affinity for Na^+ ions or the number of binding sites requires further investigation.

After the astounding observation of a Ca^{2+}-induced, allosteric Na^+ binding, the question arises as to the dynamic binding properties of K^+ ions. The assumption of an allosteric K^+ binding, the prerequisite of which could be a specific configurational change induced by either Mg^{2+} or Ca^{2+} ions, is substantiated by $^{39}K^+$ NMR competition experiments with native adventitial connective tissue as polyanion. Fig. 14D is a clear demonstration of an immediate increase in $R_{1_{ex}}$ at the very beginning of Mg^{2+} additions [7,180]. Obviously, K^+ ions are consecutively bound at an allosteric site of the matrix macromolecules and not expelled from their binding sites by Mg^{2+} ions. Besides this uncommon effect, the conformational transition appears as reflected by the increase in $R_{2_{ex}}$. Since a K^+ adsorption was not observed in CS-P solution to such an extent as in native connective tissue, the conclusion suggests itself that only the entire connective tissue is capable of this binding after a conformational transition.

The conformational change is again confirmed by calculation of the correlation time. In Fig. 14E, the τ_c value for K^+ increases abruptly in the range 0.55 mmol/L < $[Mg^{2+}]_o$ < 1.1 mmol/L and then reaches a plateau value. Half-maximal conformational transition is reached at 0.9 mmol/L $[Mg^{2+}]_o$, i.e., entirely in the physiological range. Again, the jump in correlation time cannot be explained by a thermic mobility change of the K-matrix macromolecular complex, because polyanions of the connective tissue should influence the correlation times only insignificantly due to their molecular size and the ensuing relative immobility (see above).

With the possession of both relaxation rates and correlation times, the static contribution to relaxation, $p_B\chi^2$, can be calculated. Besides the physical constants of the K nucleus, the quadrupolar coupling constant, χ, depends on the magnitude of the electric field gradient at the nucleus. Hence, χ is partly sensitive to the distance between the small cation and the charges on the polyanion [7]. In this sense χ is a measure of the strength of the interaction between the polyanion charges and the K^+ that reside in the bound state. Values of $p_B\chi^2$ for vascular connective tissue in function of $[Mg^{2+}]_o$ are given in Fig. 14F. The increase of this quantity seen in the region from 0 to 0.3 mmol/L Mg^{2+} primarily corresponds to an increase in the fraction of bound ions [9,232]. Thus, the calculation of $p_B\chi^2$ shows that the K^+ binding increases at once and reaches a maximum with 0.8 mmol/L Mg^{2+} concentration. Thus, an increase of the Mg^{2+}concentration in the blood substitute solution does not cause a displacement of K^+ ions from their binding sites, but, on the contrary, an allosteric K^+ adsorption to the polyanionic macromolecules of vascular connective tissue. The K^+ binding is strongly cooperative as can be inferred from a HILL-coefficient up to $n_H = 6.8$ [252].

We have seen that a rise of the external Mg^{2+} concentration leads not only to an enhanced Mg^{2+}, but also to an increased K^+ binding as could be deduced from the behaviour of the $^{39}K^+$ excess relaxation rates and correlation times with small Mg^{2+} additions. Furthermore, we could demonstrate cooperative K^+ binding to adventitial connective tissue with increasing Mg^{2+} concentration in measurements with atomic absorption spectroscopy [180]. While Mg^{2+} ions were progressively bound with increasing concentration of Mg^{2+}, K^+ ions were not displaced competitively, but bound cooperatively at an allosteric site [7]. Half-maximal effect was attained at 0.8 mmol/L $[Mg^{2+}]_o$.

6.1.4.1. Medical significance of cation binding characteristics. What does the binding of monovalent cations to polyanions of the cell membrane exterior surface and of vascular connective tissue in the immediate vicinity of the cell membrane mean for vasomotor regulations? The geometry of narrow tissue clefts in the interstitial compartment of the vessel wall entails that an increase of extracellular Mg^{2+} (Ca^{2+}) concentration effects a decrease of external K^+ (Na^+) concentration in the vicinity of vascular smooth muscle cell membranes [7]. Thus, the increase of a divalent cation concentration causes a transient hyperpolarization via a fall of the local Na^+ and/or K^+ concentration in the cleft spaces between cell membrane, basement membrane and connective tissue matrices. Inverse effects could be expected after a decrease of the $[Mg^{2+}]_o$ or $[Ca^{2+}]_o$ concentration. The effect on vascular tone of such a hyper- or depolarization of vascular smooth muscle cells can easily be demonstrated in the stationary activation curve tension versus voltage. This curve shows that depolarization is connected with contraction, hyperpolarization with relaxation [7]. Therefore, the indirect action of

divalent effector cations on vascular tone via variations in monovalent cation concentrations of Na^+ and K^+ presents additional knowledge on vasomotor regulations.

We have seen, that an increase in $[Mg^{2+}]_o$ causes a transient hyperpolarization and relaxation of smooth muscle cells via a transient decrease in the local concentration of ionized K^+ in the narrow extracellular cleft spaces between cell membrane, basement membrane, and connective tissue matrices. While interstitial K^+ ions from the unstirred layer spaces are bound cooperatively to matrix proteoglycans that have undergone a Mg^{2+}-induced conformation change, $[K^+]_c$ can be reduced to two thirds to one half of its normal value. This event is temporally limited by K^+ diffusion into the depleted region to restore the free concentration to equilibrium with its surroundings. Inverse effects appear after a decrease in the $[Mg^{2+}]_o$ concentration.

Measurements of pacemaker currents in Purkinje fibres have demonstrated that changes in $[K^+]_c$ of 0.2–0.7 mmol/L have time constants for accumulation and decay of 10–30 s and for $[K^+]_c$ depletion of up to 70 s [261]. There are also indications that extracellular cleft and bulk phase K^+ concentrations are not equal even in a quiescent fibre or in sinus node cells embedded in a prominent matrix and wrapped around by basal laminae [262]. In smooth muscle connective tissues, the extracellular K^+ activity enhanced by Na^+ competition did not return to its initial value until after several minutes (see [7]). Therefore, the indirect action of divalent effector cations on excitable cells via variations in monovalent cation concentrations provides additional knowledge on the fundamental mechanisms of their regulation. This becomes particularly evident in the sinus node cells – rhythm generator of the heart – which each is enveloped in a basement membrane and, furthermore, surrounded by a tight connective tissue matrix. Here, the extracellular cleft space ion concentrations directly contribute to a modification of heart beat via intervention into the action potential of the sinus node. The repolarization phase is carried by a K^+ outward current, which leads to a $[K^+]_c$ increase. The latter has two effects: i) Membrane depolarization of sinus node cells with an increase of permeabilities for Na^+ (P_{Na}) and Ca^{2+} ions (P_{Ca}). ii) Competitive release of Na^+ and Ca^{2+} ions from extracellular connective tissue binding sites (cf. Fig. 34B). Released Na^+ and Ca^{2+} ions are instrumental in pacemaker and action potential through i_f and $i_{Ca(T,L)}$ inward current (cf. chapter 5.2.2.3). In this feedback control system, the time constants for accumulation and decay of cleft space ion concentrations are of special significance.

6.2. Aqueous polyelectrolyte mixtures

The primary constituents of extracellular matrices are aqueous solutions of charged macromolecules, including protein copolymers containing both positively and negatively charged domains, as well as proteoglycans with highly negatively charged GAG side chains. This system also contains an excess of electrolytes, which plays an important role in the modulation of electrostatic interactions.

Due to the presence of positively charged amino acid residues [47,263], notably in proteochondroitin sulfate (e.g., aggrecan) and structural glycoproteins (e.g., vitronectin), as well as the presence of overall negatively charged polyelectrolytes (e.g., HA), three-dimensional network formation is feasible through electrostatically driven transient cross-linkages. Due to the electrostatic nature of the network formation, the gelation is strongly affected by the presence of electrolytes, the concentration of which can be regulated according to functional needs. Hence, the gels formed exhibit considerable physiological versatility.

In addition to the electrostatically driven gelation, other physicochemical processes also affect the behaviour of the polyelectrolyte solutions contributing to the extracellular matrix formation. In particular, polyelectrolytes may display a rich phase behaviour [264]. The latter is affected by a number of factors, including the concentration, the molecular weight, and the charge density of the polyelectrolytes. By changing one of these factors it is possible to switch from a two-phase to a one-phase system, or vice versa, or to change the relative composition of the phases. In the connective tissues, system variations may occur during development, cell proliferation, and differentiation, primarily depending on tissue function. These changes occur during macromolecular expression and post-translational modification.

The phase behaviour of ternary polymer systems is usually displayed in the form of triangular phase diagrams (Fig. 38). Each point in the phase diagram represents a composition of the polymer mixture, while each corner corresponds to one of the pure components. Mixtures lying in the areas marked blue represent two-phase systems. Each phase has a composition corresponding to the intersections of the tie-line (solid line in two-phase region) and the borderline of the two-phase area. For example, a sample corresponding to the black circle (20% polymer 1, 30% polymer 2, 50% water) will separate into two phases with compositions corresponding to the white circles (phase 1, 48% polymer 1, 2% polymer 2, 50% water; phase 2, 2% polymer 1, 48% polymer 2, 50% water).

Fig. 38A illustrates the behaviour of a typically segregating ternary polymer system. Hence, only at low polymer concentrations (high water content) does the system display a one-phase behaviour. At higher polymer concentrations, irrespective of polymer composition, the system phase separates. According to the tie-lines, each phase is enriched in one of the polymers and depleted in the other. Fig. 38B, on the other hand, illustrates a system displaying associative phase separation. For mixtures corresponding to the area marked blue, phase separation occurs, with one phase enriched in both polymers and the other consisting essentially of aqueous solution and no polymer. At sufficiently high polymer concentrations, a one-phase behaviour is encountered.

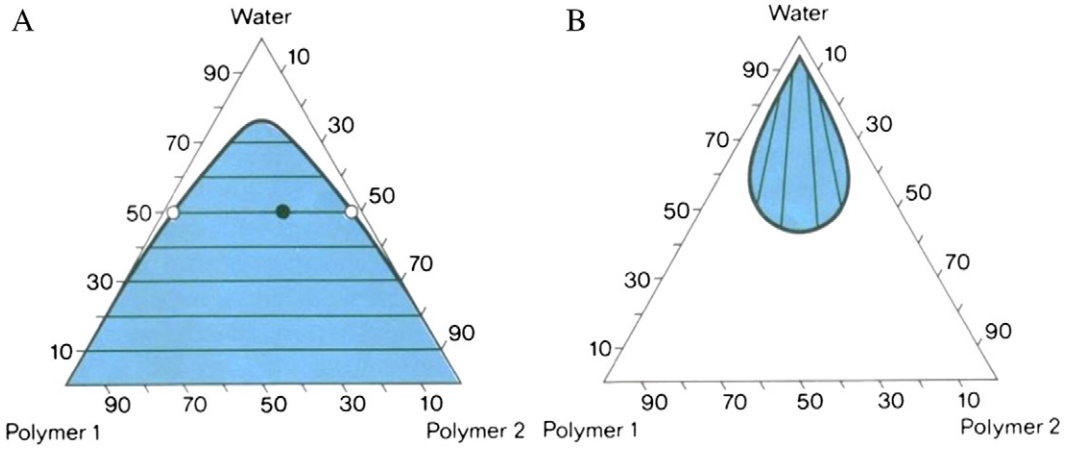

Fig. 38. Phase diagrams for aqueous mixtures of intrinsically segregating, similarly charged (A) and associating, oppositely charged polyelectrolytes (B) (from [5,264]).

The most obvious effect of phase separation is a redistribution of substances present within the system. Thus, an inhomogeneous distribution is generated. Apart from the macromolecules themselves, the inhomogeneity involves substances that may change their distribution within the system on phase separation. In particular, the binding of intermediate and high molecular weight substances such as growth and differentiation factors depends on the phase concentration of these factors. Consequently, phase separation may result in either an increased or a decreased binding to the receptor bearing cells.

Another effect of the phase separation could be a change in the viscosity of the polyelectrolyte solution. On dispersion of the phase containing the more highly viscous polymer in the other phase, aided by the low interfacial tension between the phases, a reduction in the viscosity may be expected in a system with some agitation or flow, e.g., through basement membranes of capillaries in the circulation or the kidney. Since the viscosity of such a solution is governed largely by the viscosity of the continuous phase, and since the latter consists mainly of the less viscous polymer (segregative phase separation), a reduction in the system viscosity will be the result.

6.3. Tumour invasion and metastasis

Proteins, glucoconjugates, and carbohydrate polymers are implicated in extracellular matrix formation and express multifunctionality as well as high versatility in both physiological and pathological processes, as for instance cytokine sequestration, basement membrane scaffolding, and tumour invasion and metastasis. The supramolecular architecture of basement membranes is largely dominated by self-assembly processes and specific heterophilic interactions between type IV collagen, perlecan, laminin, and entactin. These flexible thin mats are the strategic sites at which cells traverse this surface, subbase, and interfacial structure in inflammation and tumour invasion. In inflammatory processes they do so under complete control, and in tumour invasion and metastasis they do so by avoiding and excluding the control systems [5]. Growth factors and other cytokines stored and cross-complexed at syndecan/perlecan low-affinity as well as PTKR-SF high-affinity binding sites interfere into these pathological scenarios (cf. chapters 3.2. and 3.3.).

The three-step development of the invasive phenotype of cancer cells comprises cell attachment, local proteolysis, and cell migration [265]. Adhesion is mediated by a contribution pattern of several classes of cell adhesion molecules such as vitronectin and laminin receptors amplified and dispersed over the entire cell surface. In addition, cytokine-inducible members of the immunoglobulin superfamily and the cell surface hyaluronan receptor facilitate the metastatic process in serving as tumour cell attachment sites to the vascular or lymphatic endothelium. Molecules of the cadherin family, however, suppress tumour invasion. Overexpression of E-cadherin in highly invasive clones resulted in a loss of invasive potency. Matrix metalloproteinases, constitutively overexpressed or induced by cytokines in tumour cell invasion, promote the extracellular matrix proteolysis. Growth factors such as EGF, TGFα, and PDGF up-regulate the transcription of interstitial collagenase and stromelysin [266]. Moreover, the balance of active enzymes and their inhibitors (TIMPs) has shifted in favour of proteolysis.

Tumour cell motility and metastatic spread are dominated by chemokinesis, chemotaxis, and haptotaxis [267,268]. Matrix proteolysis and directional migration are prerequisites for intravasation, extravasation, and propagation into the target tissue. While the initial stages of metastasis encompass haptotactic migration over insoluble matrix proteins, chemotactic responses to partially degraded matrix components characterize the migratory phenotype later [268]. Cell locomotion in eukaryotic cells resides in the cortical actin cytoskeleton which is interwoven with the cytoplasmic syndecan as well as the cell- and matrix-binding perlecan domains [265]. Therefore, the actin-based cytoskeletal proteins α-actinin, filamin, and desmin were adsorbed as monomolecular layers to a hydrophobic silica surface in order to investigate the effect of Ca^{2+} ions by ellipsometry [cf. 269]. Ca^{2+} ions in a concentration of 10^{-4}, 10^{-3} and 2.52 mmol/L had no effect on the adsorbed amount, refractive index and molecular length of these individual intermediate filament proteins.

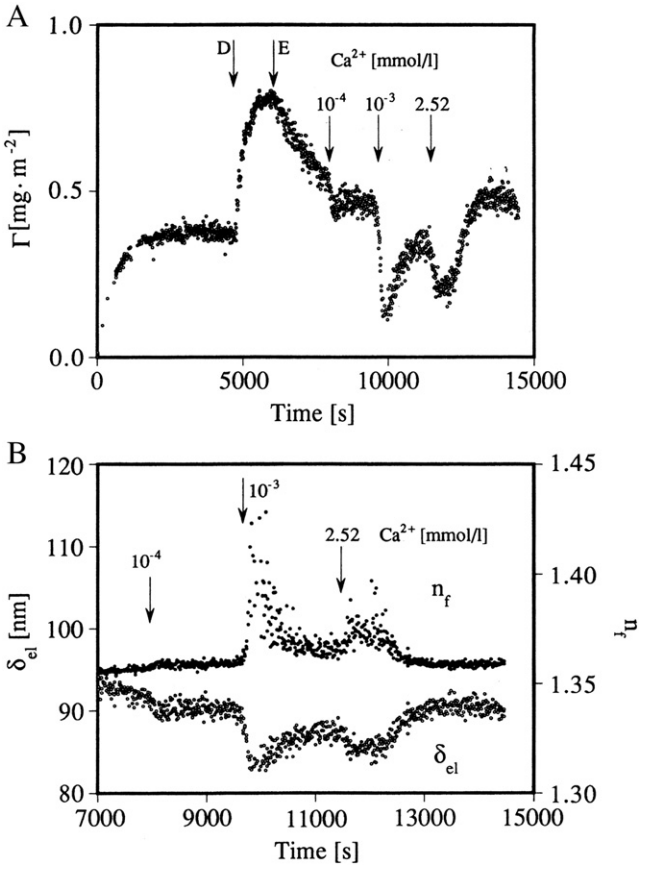

Fig. 39. (A) Amount of cross-linked filamin–desmin (0.05 mg/mL for filamin and desmin, respectively) adsorbed at hydrophobic silica from a Ca^{2+}-free K^+-Krebs solution as a function of time (pH 7.27). Arrow D indicates dilution by a factor of 10, arrow E equilibration. Ca^{2+} additions were 10^{-4}, 10^{-3}, and 2.52 mmol/L. (B) Adsorbed layer thickness (δ_{el}) and mean adsorbed layer refractive index (n_f) versus time (from [265]).

A completely different picture resulted when a mixed solution of filamin plus desmin was adsorbed to methylated silica (Fig. 39). The adsorbed amount was initially only 0.38 mg/m^2, doubled with dilution and decreased again with equilibration. Unlike to HS proteoglycan, with which Ca^{2+} ions initiate a promotion in adsorption, these ions caused here a reduction of the primary adsorbed amount by 25% already in a concentration of 10^{-4} mmol/L Ca^{2+}, however, by 85% with 10^{-3} and 2.52 mmol/L. The effects of Ca^{2+} ions on molecular length and refractive index of the filamin–desmin aggregates were dramatic (Fig. 39B). Whereas Ca^{2+} neither had an effect on the adsorption of the individual compounds to a hydrophobic silica surface nor on their conformation and molecular length, 10^{-4}, 10^{-3}, and 2.52 mmol/L Ca^{2+} effected a drastic change of refractive index as well as shortening of the 92.5 nm molecular complex of filamin–desmin by 2.5, 6.7, and 6.5 nm, respectively (−2.6%, −9.9%, −9.7%). The shortening triggered immediately by the Ca^{2+} addition lasted for 12 min.

In order to elucidate the linkage between the cytoplasmic and cell/matrix-binding domains of the HS-PGs and the cytoskeleton, the ellipsometric investigations at issue on the influence of Ca^{2+} ions on α-actinin, filamin, and desmin were conducted. Actin-based cytoskeletal and contractile proteins appear to be distributed in two domains [199]: (1) longitudinal intermediate filaments free of myosin, but containing desmin, vimentin, filamin, actin, and α-actinin, and (2)

contractile protein filaments containing actin, myosin, tropomyosin, and caldesmon. The tension developed by the contractile protein filaments of a myocyte is proportionately transmitted to the cell interior and exterior by the proteins of intermediate filaments. These latter appear not only in muscle cells but also in normal and cancerously transformed endo- and epithelial cells, neurons, and fibroblasts. The intermediate filaments build an intracellular network which is anchored in the dense bands and dense bodies corresponding functionally to the Z discs in obliquely striated musculature [270]. They might be their phylogenetic precursors since both structures contain α-actinin. In contrast to the dense bodies, dense bands contain the protein vinculin. As the intermediate filaments link dense bands and dense bodies throughout the cell, they form an actin-based cytoskeleton. Via vinculin and talin, but also via fibulin and α-actinin, this cytoskeleton is connected with transmembrane integrins. Their extracellular domains interact with proteoglycans (perlecan, decorin) and glycoproteins (laminin, fibronectin) of the basement membrane and extracellular matrices, which in turn communicate with extracellular collagen and elastin fibres (inside-out signalling) [271].

On the other hand, the cell-surface proteoglycans of the novel gene family of syndecans (Greek *syndein*, to bind together) are polymorphic, membrane-intercalated, proteoheparan/chondroitin sulfates abundant on epi/endothelial and induced mesenchymal cells during embryogenesis and in adult tissues [78,81]. Their highly conserved cytoplasmic protein sequence contains three tyrosine residues that may provide phosphorylation sites for protein kinases, which are key enzymes in many signal transduction pathways, or they may form the sites for cross-linkage with cytoskeletal elements [14]. This entodomain has protein-binding activity because the intact proteoglycan can bind directly or indirectly to F-actin and associates with the actin-containing cytoskeleton [272] when the ectodomain undergoes a conformational change whether by shear stress or by cross-linking at the cell surface (outside-in signalling [271]). Since a cell type can contain both syndecans and integrins as structurally and functionally distinct receptors, syndecan has been called a coreceptor collaborating with integrins in signal transduction [14]. Thus, this manifoldly interwoven structure of copolymers builds up a functional cytoskeletal organization and mechanical syncytium [199,273]. This aspect appears to be even more significant, as the dynamic regulation of the assembly and turnover of intermediate filaments takes place by means of the phosphorylation of desmin by cAMP-dependent protein kinase or protein kinase C [274].

The striking observation in our investigations was that Ca^{2+} ions contracted only filamin–desmin aggregates, whereas they had no effect on the single elements, i.e., filamin and desmin alone. Apparently, a cross-linkage of both molecules is the prerequisite to this contraction. Filamin has been described as a cross-linker and bundling protein [275,276]. The free Ca^{2+} concentration in a tumour cell is about 10^{-7} mol/L. Even this low concentration had a slightly contracting effect. The physiological elevation of $[Ca^{2+}]_i$ by a factor of 10 was followed by a contraction of approximately 10% of the molecular length on average. Comparably, a vascular smooth muscle cell contracts maximally with a rise in $[Ca^{2+}]_i$ by a factor of 2.5–9 [199]. The unphysiologic elevation of the Ca^{2+} concentration to its extracellular value (2.52 mmol/L; factor 2520) revealed no further shortening of the aggregates. Thus, the contraction curve exhibits saturation behaviour in dependence on the Ca^{2+} concentration. The maximum contraction is attained at 1 μmol/L Ca^{2+} or lower values. In contrast, the measurement of the adsorption Γ and thickness δ_{el} of α-actinin, filamin and desmin developed to be Ca^{2+}-independent. This is not surprising since α-actinin is a constituent of the dense bands and dense bodies, strategic anchoring sites of intermediate filament proteins. It may be mentioned that we determined with ellipsometric techniques the molecular length of α-actinin in physiological salt solution to be 106.7 nm, while electron microscopic images have revealed 40 nm long macromolecules [277].

Kjellén and Lindahl [15] reported on the functional significance of the intracellular domain of syndecan that it interacts with the actin cytoskeleton, resulting in the formation or elimination of focal cell adhesions. Therefore, syndecan is implicated in the cellular regulation of shape and tissue organization [79]. Structural association of the entodomain with actin-based intermediate filaments provides a network through which cytoskeletal contractile elements can apply tractile forces for subsequent cell movement or deformation [278]. Furthermore, the syndecans may participate in a variety of cellular phenomena as proliferation, differentiation, transformation, migration, and motility [78]. This multifunctionality might serve to integrate cellular behaviour in response to physical stimuli (shear stress, electrostatic attractions), growth factors (bFGF, TGFβ, IGF-1) and extracellular matrices (laminin, fibronectin, thrombospondin) [76,81].

In general, the finding of a Ca^{2+}-dependent contraction of the cross-linked intermediate filament proteins filamin–desmin stands for assistance of the contraction mechanisms in muscular cells. But nonmuscular cells, like tumour cells, can contract in this way as well. A Ca^{2+} increase could result in a retraction of the tumour cell via its effect on the cytoskeleton. Finally, the filamin–desmin contraction could be a trigger of nonmuscular cell locomotion, for example of the amoeboid migration, or the extra- and intravasation in inflammation or tumour invasion and metastasis.

7. Epilogue

This last section on tumorigenicity in particular will have reminded the reader that connective tissues are not only a matrix for cells, but that the extracellular matrix regulates the development and function of all cells in a multicellular organism. The term “connective tissue” goes beyond a descriptive static representation of the connections between tissues. Since it tries to define the cells and their matrices in a functional dynamic connection and interdependency, it includes the most important life processes that take place in connective tissue structures and their biomolecules. Although proteins and polysaccharides, along with their sequences, conformations, and interactions, are being discovered at a rapid pace, this plethora of information is still entirely insufficient to understand these many-body systems that are not simple but formed by subunits arranged in complexity and hierarchy.

References

[1] Fontane T. Wanderungen durch die Mark Brandenburg. Band 1 (Grafschaft Ruppin) “Rheinsberg”. Berlin: Hertz; 1862.
[2] Lindman B, Forsén S. Chlorine, bromine and iodine NMR: physico-chemical and biological applications. Heidelberg: Springer-Verlag; 1976.
[3] Kreis T, Vale R, editors. Guidebook to the extracellular matrix and adhesion proteins. Oxford: Oxford University Press; 1999.
[4] Berg JM, Tymoczko JL, Stryer L. Stryer Biochemie. Heidelberg: Springer Spektrum; 2012.
[5] Siegel G. Connective tissue: more than just a matrix for cells. In: Greger R, Windhorst U, editors. Comprehensive human physiology, vol. 1. Berlin, Heidelberg: Springer-Verlag; 1996. p. 173–224.
[6] Ebert G. Biopolymere. Darmstadt: Steinkopff; 1980.
[7] Siegel G, Walter A, Bostanjoglo M, Jans AWH, Kinne R, Piculell L, et al. Ion transport and cation–polyanion interactions in vascular biomembranes. J Membr Sci 1989;41:353–75.
[8] Buddecke E, Kröz W, Tittor W, Makromolekulare Polysaccharid-Proteine, I. Chondroitinsulfat-Protein aus Rindernasenknorpel – Beziehungen zwischen makromolekularen Eigenschaften und Funktion. Hoppe Seyler's Z Physiol Chem 1967;348:651–64.
[9] Gustavsson H, Siegel G, Lindman B, Fransson L-Å. $^{23}Na^{+}$ NMR in solutions of mucopolysaccharides. FEBS Lett 1978;86:127–30.
[10] Siegel G, Gustavsson H, Ehehalt R, Lindman B. The role of membrane potential in the regulation of vascular tone. Bibl Anat 1977;15:126–35.
[11] Siegel G, Ehehalt R, Gustavsson H, Fransson L-Å. Ion binding properties of vascular connective tissue. In: Casteels R, Godfraind T, Rüegg JC, editors. Excitation–contraction coupling in smooth muscle. Amsterdam, New York, Oxford: Elsevier/North-Holland Biomedical Press; 1977. p. 279–88.
[12] Malmsten M, Siegel G. Ellipsometry studies of lipoprotein adsorption in atherosclerosis and Alzheimer's. J Drug Del Sci Tech 2007;17:245–51.
[13] Buddecke E. Proteoglycans. In: Gabius H-J, editor. The sugar code. Fundamentals of glycosciences. Weinheim: Wiley-VCH Verlag; 2009. p. 199–216.

[14] Hardingham TE, Fosang AJ. Proteoglycans: many forms and many functions. FASEB J 1992;6:861–70.
[15] Kjellén L, Lindahl U. Proteoglycans: structures and interactions. Annu Rev Biochem 1991;60:443–75.
[16] Fransson L-Å. Structure and function of cell-associated proteoglycans. Trends Biochem Sci 1987;12:406–11.
[17] Atkins EDT. Molecular architecture of the animal and some microbial extracellular polysaccharides. In: Walton AG, editor. Proceedings of the first Cleveland symposium on macromolecules. Structure and properties of biopolymers. Amsterdam: Elsevier; 1977. p. 61–85.
[18] Malmsten M, Claesson P, Siegel G. Forces between proteoheparan sulfate layers adsorbed at hydrophobic surfaces. Langmuir 1994;10:1274–80.
[19] Mitra AK, Arnott S, Atkins EDT, Isaac DH. Dermatan sulfate: molecular conformations and interactions in the condensed state. J Mol Biol 1983;169:873–901.
[20] Brown DC, Vogel KG. Characteristics of the *in vitro* interaction of a small proteoglycan (PG II) of bovine tendon with type I collagen. Matrix 1989;9:468–78.
[21] Bidanset DJ, Guidry C, Rosenberg LC, Choi HU, Timpl R, Hook M. Binding of the proteoglycan decorin to collagen type VI. J Biol Chem 1992;267:5250–6.
[22] Danielson KG, Baribault H, Holmes DF, Graham H, Kadler KE, Iozzo RV. Targeted disruption of decorin leads to abnormal collagen fibril morphology and skin fragility. J Cell Biol 1997;136:729–43.
[23] Yamaguchi Y, Mann DM, Ruoslahti E. Negative regulation of transforming growth factor-β by the proteoglycan decorin. Nature 1990;346:281–4.
[24] Heremans A, de Cock B, Cassiman J-J, van den Berghe H, David G. The core protein of the matrix-associated heparan sulfate proteoglycan binds to fibronectin. J Biol Chem 1990;265:8716–24.
[25] Mörgelin M, Paulsson M, Hardingham TE, Heinegård D, Engel J. Cartilage proteoglycans. Assembly with hyaluronate and link protein as studied by electron microscopy. Biochem J 1988;253:175–85.
[26] Zimmermann DR, Ruoslahti E. Multiple domains of the large fibroblast proteoglycan, versican. EMBO J 1989;8:2975–81.
[27] Timpl R. Proteoglycans of basement membranes. Experientia 1993;49:417–28.
[28] Maimone MM, Tollefsen DM. Structure of a dermatan sulfate hexasaccharide that binds to heparin cofactor II with high affinity. J Biol Chem 1990;265:18263–71.
[29] Castellot Jr JJ, Choay J, Lormeau J-C, Petitou M, Sache E, Karnovsky MJ. Structural determinants of the capacity of heparin to inhibit the proliferation of vascular smooth muscle cells. II. Evidence for a pentasaccharide sequence that contains a 3-*O*-sulfate group. J Cell Biol 1986;102:1979–84.
[30] Lindahl U, Bäckström G, Thunberg L, Leder IG. Evidence for a 3-*O*-sulfated D-glucosamine residue in the antithrombin-binding sequence of heparin. Proc Natl Acad Sci U S A 1980;77:6551–5.
[31] Busch SJ, Sassone-Corsi P. Dimers, leucine zippers and DNA-binding domains. Trends Genet 1990;6:36–40.
[32] Jackson RL, Busch SJ, Cardin AD. Glycosaminoglycans: molecular properties, protein interactions, and role in physiological processes. Physiol Rev 1991;71:481–539.
[33] De Agostini AI, Watkins SC, Slayter HS, Youssoufian H, Rosenberg RD. Localization of anticoagulantly active heparan sulfate proteoglycans in vascular endothelium: antithrombin binding on cultured endothelial cells and perfused rat aorta. J Cell Biol 1990;111:1293–304.
[34] Ruoslahti E, Yamaguchi Y. Proteoglycans as modulators of growth factor activities. Cell 1991;64:867–9.
[35] Tanaka Y, Adams DH, Shaw S. Proteoglycans on endothelial cells present adhesion-inducing cytokines to leukocytes. Immunol Today 1993;14:111–5.
[36] Noble NA, Harper JR, Border WA. *In vivo* interactions of TGF-β and extracellular matrix. Prog Growth Factor Res 1992;4:369–82.
[37] Gordon MY, Riley GP, Watt SM, Greaves MF. Compartmentalization of a haematopoietic growth factor (GM-CSF) by glycosaminoglycans in the bone marrow microenvironment. Nature 1987;326:403–5.
[38] Howard M, Muchamuel T, Andrade S, Menon S. Interleukin 10 protects mice from lethal endotoxemia. J Exp Med 1993;177:1205–8.
[39] Wang X-F, Lin HY, Ng-Eaton E, Downward J, Lodish HF, Weinberg RA. Expression cloning and characterization of the TGF-β type III receptor. Cell 1991;67:797–805.
[40] Folkman J, Langer R, Linhardt RJ, Haudenschild C, Taylor S. Angiogenesis inhibition and tumor regression caused by heparin or a heparin fragment in the presence of cortisone. Science 1983;221:719–25.
[41] Saksela O, Rifkin DB. Release of basic fibroblast growth factor-heparan sulfate complexes from endothelial cells by plasminogen activator-mediated proteolytic activity. J Cell Biol 1990;110:767–75.
[42] Basilico C, Moscatelli D. The FGF family of growth factors and oncogenes. Adv Cancer Res 1992;59:115–65.
[43] Ishai-Michaeli R, Eldor A, Vlodavsky I. Heparanase activity expressed by platelets, neutrophils, and lymphoma cells releases active fibroblast growth factor from extracellular matrix. Cell Regul 1990;1:833–42.
[44] Yayon A, Klagsbrun M, Esko JD, Leder P, Ornitz DM. Cell surface, heparin-like molecules are required for binding of basic fibroblast growth factor to its high affinity receptor. Cell 1991;64:841–8.
[45] McCarthy JB, Chelberg MK, Mickelson DJ, Furcht LT. Localization and chemical synthesis of fibronectin peptides with melanoma adhesion and heparin binding activities. Biochemistry 1988;27:1380–8.
[46] Hautanen A, Gailit J, Mann DM, Ruoslahti E. Effects of modifications of the RGD sequence and its context on recognition by the fibronectin receptor. J Biol Chem 1989;264:1437–42.
[47] Preissner KT. Structure and biological role of vitronectin. Annu Rev Cell Biol 1991;7:275–310.
[48] Tomasini BR, Mosher DF. Conformational states of vitronectin: preferential expression of an antigenic epitope when vitronectin is covalently and noncovalently complexed with thrombin–antithrombin III or treated with urea. Blood 1988;72:903–12.
[49] Lawler J, Hynes RO. The structure of human thrombospondin, an adhesive glycoprotein with multiple calcium-binding sites and homologies with several different proteins. J Cell Biol 1986;103:1635–48.
[50] Sun X, Mosher DF, Rapraeger A. Heparan sulfate-mediated binding of epithelial cell surface proteoglycan to thrombospondin. J Biol Chem 1989;264:2885–9.
[51] Bork P. The modular architecture of vertebrate collagens. FEBS Lett 1992;307:49–54.
[52] Bornstein P. Thrombospondins: structure and regulation of expression. FASEB J 1992;6:3290–9.
[53] Ruggeri ZM, Zimmerman TS. von Willebrand factor and von Willebrand disease. Blood 1987;70:895–904.
[54] Yurchenco PD, Schittny JC. Molecular architecture of basement membranes. FASEB J 1990;4:1577–90.
[55] Ayad S, Boot-Handford RP, Humphries MJ, Kadler KE, Shuttleworth CA. The extracellular matrix factsbook. San Diego, London, Boston, New York, Sydney, Tokyo, Toronto: Academic Press/Harcourt Brace; 1998.
[56] Fahrig T, Landa C, Pesheva P, Kühn K, Schachner M. Characterization of binding properties of the myelin-associated glycoprotein to extracellular matrix constituents. EMBO J 1987;6:2875–83.
[57] Cole GJ, Loewy A, Cross NV, Akeson R, Glaser L. Topographic localization of the heparin-binding domain of the neural cell adhesion molecule N-CAM. J Cell Biol 1986;103:1739–44.
[58] Kadmon G, Kowitz A, Altevogt P, Schachner M. Functional cooperation between the neural adhesion molecules L1 and N-CAM is carbohydrate dependent. J Cell Biol 1990;110:209–18.
[59] Wassmann S, Laufs U, Bäumer AT, Müller K, Ahlbory K, Linz W, et al. HMG-CoA reductase inhibitors improve endothelial dysfunction in normocholesterolemic hypertension via reduced production of reactive oxygen species. Hypertension 2001;37:1450–7.
[60] Stein O, Stein Y, Eisenberg S. A radioautographic study of the transport of ^{125}I-labeled serum lipoproteins in rat aorta. Z Zellforsch 1973;138:223–37.
[61] Schaefer H-E. Ätiologie und Pathogenese arterieller Verschlußkrankheiten. In: Alexander K, editor. Gefäßkrankheiten. Munich: Urban and Schwarzenberg; 1993. p. 25–46.
[62] Steele RH, Wagner WD, Rowe HA, Edwards IJ. Artery wall derived proteoglycan–plasma lipoprotein interaction: lipoprotein binding properties of extracted proteoglycans. Atherosclerosis 1987;65:51–62.
[63] Alves CS, Mourão AS. Interaction of high molecular weight chondroitin sulfate from human aorta with plasma low density lipoproteins. Atherosclerosis 1988;73:113–24.
[64] Cardin AD, Randall CJ, Hirose N, Jackson RL. Physical–chemical interaction of heparin and human plasma low-density lipoproteins. Biochemistry 1987;26:5513–8.
[65] Camejo G, Olofsson S-O, Lopez F, Carlsson P, Bondjers G. Identification of Apo B-100 segments mediating the interaction of low density lipoproteins with arterial proteoglycans. Arteriosclerosis 1988;8:368–77.
[66] Iozzo RV. Basement membrane proteoglycans: from cellar to ceiling. Nat Rev Mol Cell Biol 2005;6:646–56.
[67] Iozzo RV. Heparan sulfate proteoglycans: intricate molecules with intriguing functions. J Clin Invest 2001;108:165–7.
[68] Trescony PV, Oegema Jr TR, Farnam BJ, Deloria LB. Analysis of heparan sulfate from the Engelbreth–Holm–Swarm (EHS) tumor. Connect Tissue Res 1989;19:219–42.
[69] Battaglia C, Aumailley M, Mann K, Mayer U, Timpl R. Structural basis of β_1 integrin-mediated cell adhesion to a large heparan sulfate proteoglycan from basement membranes. Eur J Cell Biol 1993;61:92–9.
[70] Noonan DM, Fulle A, Valente P, Cai S, Horigan E, Sasaki M, et al. The complete sequence of perlecan, a basement membrane heparan sulfate proteoglycan, reveals extensive similarity with laminin A chain, low density lipoprotein-receptor, and the neural cell adhesion molecule. J Biol Chem 1991;266:22939–47.
[71] Kallunki P, Tryggvason K. Human basement membrane heparan sulfate proteoglycan core protein: a 467-kD protein containing multiple domains resembling elements of the low density lipoprotein receptor, laminin, neural cell adhesion molecules, and epidermal growth factor. J Cell Biol 1992;116:559–71.
[72] Iozzo RV, Murdoch AD. Proteoglycans of the extracellular environment: clues from the gene and protein side offer novel perspectives in molecular diversity and function. FASEB J 1996;10:598–614.
[73] Olgemöller B, Schleicher ED, Schwaabe S, Guretzki H-J, Gerbitz KD. High concentrations of low density lipoprotein decrease basement membrane-associated heparan sulfate proteoglycan in cultured endothelial cells. FEBS Lett 1990;264:37–9.
[74] Chait A, Chang MY, Olin K, Wight T. Interaction of oxidized LDL with arterial proteoglycans. Atherosclerosis 1997;134:197.
[75] Siegel G, Malmsten M, Klüßendorf D, Walter A, Schmidt A. Chemistry, recognition and function of a natural shear stress biosensor. ACS Polym Mater Sci Eng 1997;76:573–5.
[76] Siegel G, Walter A, Kauschmann A, Malmsten M, Buddecke E. Anionic biopolymers as blood flow sensors. Biosens Bioelectron 1996;11:281–94.
[77] Kallunki P, Eddy RL, Byers MG, Kestilä M, Shows TB, Tryggvason K. Cloning of human heparan sulfate proteoglycan core protein, assignment of the gene (*HSPG2*) to 1p36.1 → p35 and identification of a *Bam*HI restriction fragment length polymorphism. Genomics 1991;11:389–96.
[78] Mali M, Jaakkola P, Arvilommi A-M, Jalkanen M. Sequence of human syndecan indicates a novel gene family of integral membrane proteoglycans. J Biol Chem 1990;265:6884–9.

[79] Bernfield M, Sanderson RD. Syndecan, a developmentally regulated cell surface proteoglycan that binds extracellular matrix and growth factors. Philos Trans R Soc Lond [Biol] 1990;327:171–86.
[80] Klagsbrun M. The affinity of fibroblast growth factors (FGFs) for heparin; FGF-heparan sulfate interactions in cells and extracellular matrix. Curr Opin Cell Biol 1990;2:857–63.
[81] Saunders S, Jalkanen M, O'Farrell S, Bernfield M. Molecular cloning of syndecan, an integral membrane proteoglycan. J Cell Biol 1989;108:1547–56.
[82] Isacke CM, Horton MA. The Adhesion Molecule FactsBook. San Diego, San Francisco, New York, Boston, London, Sydney, Tokyo: Academic Press; 2000.
[83] Bernfield M, Kokenyesi R, Kato M, Hinkes MT, Spring J, Gallo RL, et al. Biology of the syndecans: a family of transmembrane heparan sulfate proteoglycans. Annu Rev Cell Biol 1992;8:365–93.
[84] Rapraeger A. Transforming growth factor (type β) promotes the addition of chondroitin sulfate chains to the cell surface proteoglycan (syndecan) of mouse mammary epithelia. J Cell Biol 1989;109:2509–18.
[85] Hallmann R, Horn N, Selg M, Wendler O, Pausch F, Sorokin LM. Expression and function of laminins in the embryonic and mature vasculature. Physiol Rev 2005;85:979–1000.
[86] Oettinger HF, Streeter H, Lose E, Copeland NG, Gilbert DJ, Justice MJ, et al. Chromosome mapping of the murine syndecan gene. Genomics 1991;11:334–8.
[87] Couchman JR. Syndecans: proteoglycan regulators of cell-surface microdomains? Nat Rev Mol Cell Biol 2003;4:926–37.
[88] Bishop JR, Schuksz M, Esko JD. Heparan sulphate proteoglycans fine-tune mammalian physiology. Nature 2007;446:1030–7.
[89] Siegel G, Malmsten M, Lindman B. Flow sensing at the endothelium–blood interface. Colloids Surf A Physicochem Eng Asp 1998;138:345–51.
[90] Siegel G, Malmsten M, Klüßendorf D, Walter A, Schnalke F, Kauschmann A. Blood-flow sensing by anionic biopolymers. J Auton Nerv Syst 1996;57:207–13.
[91] Götte M. Syndecans in inflammation. FASEB J 2003;17:575–91.
[92] Alexopoulou AN, Multhaupt HAB, Couchman JR. Syndecans in wound healing, inflammation and vascular biology. Int J Biochem Cell Biol 2007;39:505–28.
[93] Schmidt A, Echtermeyer F, Alozie A, Brands K, Buddecke E. Plasmin- and thrombin-accelerated shedding of syndecan-4 ectodomain generates cleavage sites at Lys^{114}-Arg^{115} and Lys^{129}-Val^{130} bonds. J Biol Chem 2005;280:34441–6.
[94] Scott JE. Supramolecular organization of extracellular matrix glycosaminoglycans, in vitro and in the tissues. FASEB J 1992;6:2639–45.
[95] Alberts B, Johnson A, Lewis J, Raff M, Roberts K, Walter P. Molecular biology of the cell. New York: Garland Science; 2008.
[96] Keene DR, Sakai LY, Lunstrum GP, Morris NP, Burgeson RE. Type VII collagen forms an extended network of anchoring fibrils. J Cell Biol 1987;104:611–21.
[97] Siebold B, Deutzmann R, Kühn K. The arrangement of intra- and intermolecular disulfide bonds in the carboxyterminal, non-collagenous aggregation and cross-linking domain of basement-membrane type IV collagen. Eur J Biochem 1988;176:617–24.
[98] Yurchenco PD, Furthmayr H. Type IV collagen "7S" tetramer formation: aspects of kinetics and thermodynamics. Ann N Y Acad Sci 1986;460:530–3.
[99] Yurchenco PD, Ruben GC. Basement membrane structure in situ: evidence for lateral associations in the type IV collagen network. J Cell Biol 1987;105:2559–68.
[100] Siebold B, Qian R-Q, Glanville RW, Hofmann H, Deutzmann R, Kühn K. Construction of a model for the aggregation and cross-linking region (7S domain) of type IV collagen based upon an evaluation of the primary structure of the α1 and α2 chains in this region. Eur J Biochem 1987;168:569–75.
[101] Timpl R. Structure and biological activity of basement membrane proteins. Eur J Biochem 1989;180:487–502.
[102] Paulsson M, Saladin K, Landwehr R. Binding of Ca^{2+} influences susceptibility of laminin to proteolytic digestion and interactions between domain-specific laminin fragments. Eur J Biochem 1988;177:477–81.
[103] Farquhar MG. The glomerular basement membrane. A selective macromolecular filter. In: Hay ED, editor. Cell biology of extracellular matrix. New York: Plenum; 1983. p. 335–78.
[104] Charonis AS, Tsilibary EC, Yurchenco PD, Furthmayr H, Coritz A. Binding of laminin to type IV collagen: a morphological study. J Cell Biol 1985;100:1848–53.
[105] Battaglia C, Mayer U, Aumailley M, Timpl R. Basement-membrane heparan sulfate proteoglycan binds to laminin by its heparan sulfate chains and to nidogen by sites in the protein core. Eur J Biochem 1992;208:359–66.
[106] Aumailley M, Battaglia C, Mayer U, Reinhardt D, Nischt R, Timpl R, et al. Nidogen mediates the formation of ternary complexes of basement membrane components. Kidney Int 1993;43:7–12.
[107] Curry FE, Michel CC. A fiber matrix model of capillary permeability. Microvasc Res 1980;20:96–9.
[108] Robinson GB, Walton HA. Glomerular basement membrane as a compressible ultrafilter. Microvasc Res 1989;38:36–48.
[109] Timpl R, Dziadek M. Structure, development, and molecular pathology of basement membranes. Int Rev Exp Pathol 1986;29:1–112.
[110] Olgemöller B, Schwaabe S, Gerbitz KD, Schleicher ED. Elevated glucose decreases the content of a basement membrane associated heparan sulphate proteoglycan in proliferating cultured porcine mesangial cells. Diabetologia 1992;35:183–6.
[111] Stone NJ, Robinson J, Lichtenstein AH, Bairey Merz CN, Lloyd-Jones DM, Blum CB, et al. ACC/AHA guideline on the treatment of blood cholesterol to reduce atherosclerotic cardiovascular risk in adults. J Am Coll Cardiol 2013. http://dx.doi.org/10.1016/j.jacc.2013.11.002.
[112] Siegel G, Malmsten M, Klüßendorf D, Michel F. A receptor-based biosensor for lipoprotein docking at the endothelial surface and vascular matrix. Biosens Bioelectron 2001;16:895–904.
[113] Siegel G, Malmsten M, Michel F. A primary lesion model for arteriosclerotic microplaque formation. Int J Angiol 2000;9:129–34.
[114] Siegel G, Ermilov E, Pries AR, Winkler K, Schmidt A, Ringstad L, et al. The significance of lipid peroxidation in cardiovascular disease. Colloids Surf A Physicochem Eng Asp 2014;442:173–80.
[115] Malmsten M, Siegel G, Becker A. A model substrate for ellipsometry studies of lipoprotein deposition at the endothelium. J Colloid Interface Sci 2001;240:372–4.
[116] Abletshauser C, Klüßendorf D, Schmidt A, Winkler K, März W, Buddecke E, et al. Biosensing of arteriosclerotic nanoplaque formation and interaction with an HMG-CoA reductase inhibitor. Acta Physiol Scand 2002;176:131–45.
[117] Brown BG, Zhao X-Q, Sacco DE, Albers JJ. Lipid lowering and plaque regression. New insights into prevention of plaque disruption and clinical events in coronary disease. Circulation 1993;87:1781–91.
[118] Anber V, Millar JS, McConnell M, Shepherd J, Packard CJ. Interaction of very-low-density, intermediate-density, and low-density lipoproteins with human arterial wall proteoglycans. Arterioscler Thromb Vasc Biol 1997;17:2507–14.
[119] Sawamura T, Kume N, Aoyama T, Moriwaki H, Hoshikawa H, Aiba Y, et al. An endothelial receptor for oxidized low-density lipoprotein. Nature 1997;386:73–7.
[120] Gordon DJ, Rifkind BM. High-density lipoprotein: the clinical implications of recent studies. N Engl J Med 1989;321:1311–6.
[121] Ross R. Atherosclerosis — an inflammatory disease. N Engl J Med 1999;340:115–26.
[122] Siegel G, Malmsten M, Klüßendorf D, Leonhardt W. Physicochemical binding properties of the proteoglycan receptor for serum lipoproteins. Atherosclerosis 1999;144:59–67.
[123] Siegel G, Abletshauser C, Malmsten M, Schmidt A, Winkler K. Reduction of arteriosclerotic nanoplaque formation and size by fluvastatin in a receptor-based biosensor model. Cardiovasc Res 2003;58:696–705.
[124] Siegel G, Ermilov E. Omega-3 fatty acids: benefits for cardio–cerebro-vascular diseases. Atherosclerosis 2012;225:291–5.
[125] Malmsten M, Siegel G, Wood WG. Ellipsometry studies of lipoprotein adsorption. J Colloid Interface Sci 2000;224:338–46.
[126] Malmsten M, Lindström A-L, Wärnheim T. Electrostatic effects on interfacial film formation in emulsion systems. J Colloid Interface Sci 1996;179:537–43.
[127] Cockerill GW, Reed S. High-density lipoprotein: multipotent effects on cells of the vasculature. Int Rev Cytol 1999;188:257–97.
[128] Huetz P, Ball V, Voegel J-C, Schaaf P. Exchange kinetics for a heterogeneous protein system on a solid surface. Langmuir 1995;11:3145–52.
[129] Miller GJ, Miller NE. Plasma-high-density-lipoprotein concentration and development of ischaemic heart-disease. Lancet 1975;1:16–9.
[130] Ji Z-S, Dichek HL, Miranda RD, Mahley RW. Heparan sulfate proteoglycans participate in hepatic lipase and apolipoprotein E-mediated binding and uptake of plasma lipoproteins, including high density lipoproteins. J Biol Chem 1997;272:31285–92.
[131] Rodríguez M, Ringstad L, Schäfer P, Just S, Hofer HW, Malmsten M, et al. Reduction of atherosclerotic nanoplaque formation and size by *Ginkgo biloba* (EGb 761) in cardiovascular high-risk patients. Atherosclerosis 2007;192:438–44.
[132] Malmsten M, Lassen B. Competitive adsorption at hydrophobic surfaces from binary protein systems. J Colloid Interface Sci 1994;166:490–8.
[133] Malmsten M, Muller D, Lassen B. Sequential adsorption of human serum albumin (HSA), immunoglobulin G (IgG), and fibrinogen (Fgn) at HMDSO plasma polymer surfaces. J Colloid Interface Sci 1997;193:88–95.
[134] Siegel G, Rodríguez M, Sauer F, Abletshauser C, de Mey C, Schötz K, et al. Nanotechnologic biosensor ellipsometry and biomarker pattern analysis in the evaluation of atherosclerotic risk profile. Biosens Bioelectron 2009;24:1512–7.
[135] Makoveichuk E, Lookene A, Olivecrona G. Mild oxidation of lipoproteins increases their affinity for surfaces covered by heparan sulfate and lipoprotein lipase. Biochem Biophys Res Commun 1998;252:703–10.
[136] Siegel G, Ermilov E, Saunders R, Pries AR, Malmsten M. Nanotechnologic point-of-care ellipsometric device for arteriosclerotic diseases. Arterioscler Thromb Vasc Biol 2010;30:e210.
[137] Siegel G, Schmidt A, Schäfer P, Malmsten M, Ringstad L, Winkler K, et al. The importance of scavenging reactive oxygen species in anti-aging medicine. Eng Life Sci 2009;9:363–75.
[138] Siegel G, Overbeck B, Just S, Winkler K, Malmsten M, Ermilov E. Alkaline phosphatase lowering in metabolic syndrome patients utilizing a phytochemical approach. Am J Gastroenterol 2011;106(Suppl. 2):S130.
[139] Siegel G, Winkler K, Lubitz I, Ermilov E. Multiparametric biomarkers as determinants of insulin resistance. Diabetes 2012;61(Suppl. 1):A627.
[140] Siegel G, Malmsten M, Molecular model for athero/arteriosclerosis, patent EP 0 946 876, 2005.
[141] Vassalle C, Botto N, Andreassi MG, Berti S, Biagini A. Evidence for enhanced 8-isoprostane plasma levels, as index of oxidative stress *in vivo*, in patients with coronary artery disease. Coron Artery Dis 2003;14:213–8.
[142] Glorioso N, Troffa C, Filigheddu F, Dettori F, Soro A, Pinna Parpaglia P, et al. Effect of the HMG-CoA reductase inhibitors on blood pressure in patients with essential hypertension and primary hypercholesterolemia. Hypertension 1999;34:1281–6.
[143] Spósito AC, Mansur AP, Coelho OR, Nicolau JC, Ramires JA. Additional reduction in blood pressure after cholesterol-lowering treatment by statins (lovastatin or pravastatin) in hypercholesterolemic patients using angiotensin-converting enzyme inhibitors (enalapril or lisinopril). Am J Cardiol 1999;83:1497–9.
[144] Borghi C, Prandin MG, Costa FV, Bacchelli S, Degli Esposti D, Ambrosioni E. Use of statins and blood pressure control in treated hypertensive patients with hypercholesterolemia. J Cardiovasc Pharmacol 2000;35:549–55.
[145] Ichihara A, Hayashi M, Koura Y, Tada Y, Kaneshiro Y, Saruta T. Long-term effects of statins on arterial pressure and stiffness of hypertensives. J Hum Hypertens 2005;19:103–9.

[146] Kaesemeyer WH, Caldwell RB, Huang J, Caldwell RW. Pravastin sodium activates endothelial nitric oxide synthase independent of its cholesterol-lowering actions. JACC 1999;33:234–41.
[147] Nickenig G, Bäumer AT, Temur Y, Kebben D, Jockenhövel F, Böhm M. Statin-sensitive dysregulated AT1 receptor function and density in hypercholesterolemic men. Circulation 1999;100:2131–4.
[148] Glass CK, Witztum JL. Atherosclerosis: the road ahead. Cell 2001;104:503–16.
[149] Ridker PM. High-sensitivity C-reactive protein, inflammation, and cardiovascular risk: from concept to clinical practice to clinical benefit. Am Heart J 2004;148: S19–26.
[150] Libby P. Inflammation in atherosclerosis. Nature 2002;420:868–74.
[151] Hardy J, Selkoe DJ. The amyloid hypothesis of Alzheimer's disease: progress and problems on the road to therapeutics. Science 2002;297:353–6.
[152] Hansson GK. Inflammation, atherosclerosis, and coronary artery disease. N Engl J Med 2005;352:1685–95.
[153] Gorelick PB, Wong KS, Bae H-J, Pandey DK. Large artery intracranial occlusive disease. A large worldwide burden but a relatively neglected frontier. Stroke 2008;39:2396–9.
[154] Siegel G, Ableteshauser C, Malmsten M, Schmidt A, Buddecke E, Winkler K. Reduction of arteriosclerotic nanoplaque formation and size by fluvastatin in a receptor-based biosensor model. Perfusion 2003;16:85.
[155] Libby P. Molecular bases of the acute coronary syndromes. Circulation 1995;91: 2844–50.
[156] Davies MJ. Stability and instability: two faces of coronary atherosclerosis. The Paul Dudley White Lecture 1995. Circulation 1996;94:2013–20.
[157] Falk E, Shah PK, Fuster V. Coronary plaque disruption. Circulation 1995;92:657–71.
[158] Sloop CH, Dory L, Roheim PS. Interstitial fluid lipoproteins. J Lipid Res 1987;28: 225–37.
[159] Rubanyi GM, Vanhoutte PM, editors. Endothelium-derived relaxing factors. Basel, München, Paris, London, New York, New Delhi, Bangkok, Singapore, Tokyo, Sydney: Karger; 1990.
[160] Bevan JA, Joyce EH. Flow-induced relaxation in a resistance artery is associated with an amiloride-sensitive sodium dependent mechanism in vascular smooth muscle. J Vasc Med Biol 1991;2:281–8.
[161] Schwarz G, Droogmans G, Nilius B. Shear stress-induced membrane currents and calcium transients in human vascular endothelial cells. Pflugers Arch 1992;421:394–6.
[162] Furchgott RF, Zawadzki JV. The obligatory role of endothelial cells in the relaxation of arterial smooth muscle by acetylcholine. Nature 1980;288:373–6.
[163] Sperelakis N, Wood JD, editors. Frontiers in smooth muscle research. New York: Wiley-Liss; 1990.
[164] Sperelakis N, Kuriyama H, editors. Ion channels of vascular smooth muscle cells and endothelial cells. New York, Amsterdam, London, Tokyo: Elsevier; 1991.
[165] Bevan JA, Halpern W, Mulvany MJ, editors. The resistance vasculature. Totowa, New Jersey: Humana Press; 1991.
[166] Bevan JA. The role of flow-induced contraction and relaxation in the regulation of vascular tone. In: Bevan JA, Kaley G, Rubanyi G, editors. Flow-dependent regulation of vascular function. New York: Oxford University Press; 1995. p. 128–52.
[167] Harder DR, Gilbert R, Lombard JH. Vascular muscle cell depolarization and activation in renal arteries on elevation of transmural pressure. Am J Physiol 1987;253: F778–81.
[168] Keatinge WR, Harman MC. Local mechanisms controlling blood vessels. London, New York, Toronto, Sydney, San Francisco: Academic Press; 1980.
[169] Siegel G, Walter A, Rückborn K, Buddecke E, Schmidt A, Gustavsson H, et al. NMR studies of cation induced conformational changes in anionic biopolymers at the endothelium–blood interface. Polymer J 1991;23:697–708.
[170] Siegel G, Bevan JA. Anionic biopolyelectrolytes as sensors of blood flow. In: Bevan JA, Kaley G, Rubanyi G, editors. Flow-dependent regulation of vascular function. New York: Oxford University Press; 1995. p. 153–62.
[171] Khayutin VM, Nikolsky VP, Rogoza AN, Lukoshkova EV. Endothelium determines stabilization of the pressure drop in arteries. Acta Physiol Scand 1993;148: 295–304.
[172] Bevan JA, Siegel G. Blood vessel wall matrix flow sensor: evidence and speculation. Blood Vessels 1991;28:552–6.
[173] Schmidt A, Buddecke E. Cell-associated proteoheparan sulfate from bovine arterial smooth muscle cells. Exp Cell Res 1988;178:242–53.
[174] Buddecke E, Wollensak J. Biochemistry and pathobiochemistry of proteoglycans of the eye. Fortschr Ophthalmol 1989;86:502–8.
[175] Siegel G, Walter A, Buddecke E, Schmidt A, Gustavsson H, Lindman B. Membranous and extramembranous cation binding of vascular proteoglycans. Funktionsanalyse biologischer Systeme 1994;22:93–112.
[176] Gustavsson H, Siegel G, Lindman B, Fransson L-Å. $^{23}Na^{+}$-NMR studies of cation binding to multi-chain and single-chain glycosaminoglycan peptides. Biochim Biophys Acta 1981;677:23–31.
[177] Gustavsson H, Siegel G, Lindman B, Ehehalt R. Studies of cation binding to mucopolysaccharides by $^{23}Na^{+}$ NMR. In: Oosawa F, editor. Dynamic aspects of biopolyelectrolytes and biomembranes. Tokyo: Kodansha Ltd.; 1982. p. 3–18.
[178] Siegel G, Adler A, Mildenberger E, Walter A. The effect of external calcium on voltage-tension and ion binding in vascular smooth muscle. Coll INSERM/CNRS 1984;124:101–10.
[179] Siegel G, Walter A, Bostanjoglo M, Jans AWH, Kinne R. $^{23}Na^{+}$- and $^{39}K^{+}$-NMR studies of cation–polyanion interactions in vascular connective tissue. In: Tsuchiya M, Asano M, Mishima Y, Oda M, editors. Microcirculation — an update, vol. 1. Amsterdam, New York, Oxford: Excerpta Medica; 1987. p. 407–11.
[180] Siegel G, Walter A, Jans AWH, Kinne R. Binding of mono- and divalent cations to different components of the extracellular matrix. Abhandl Rhein-Westf Akad Wissensch 1989;82:155–70.
[181] Nagasawa M. Ion-binding phenomena of polyelectrolytes. In: Sélégny E, Mandel M, Strauss UP, editors. Charged and reactive polymers, Vol. I: Polyelectrolytes. Dordrecht: Reidel; 1974. p. 57–77.
[182] Einstein A. Eine neue Bestimmung der Moleküldimensionen. Ann Phys IV. Folge 1906;19:289–306.
[183] Einstein A. Eine neue Bestimmung der Moleküldimensionen. Ann Phys 1911;34: 591–2.
[184] Kuhn W. Über die Gestalt fadenförmiger Moleküle in Lösung. Kolloid Z 1934;68: 2–15.
[185] Siegel G, Rodríguez M, Schön T, Ableteshauser C, Schmidt A, Hetzer R, et al. Blood flow sensor susceptibility to lipoproteins in early arteriosclerosis and its clinical improvement by statin therapy — a nanoplaque study. Desalination 2006;191: 417–25.
[186] Malmsten M, Siegel G, Buddecke E, Schmidt A. Cation-promoted adsorption of proteoheparan sulphate. Colloids Surf B Biointerfaces 1993;1:43–50.
[187] Rodríguez M, Lindinger A, Pérez Lustres JL, Kovalenko SA, Ernsting NP, Wöste L, et al. Femtosecond dynamics of proteoheparan sulfate (HS-PG) after UV excitation — a readout for arteriosclerotic nanoplaque formation? Biochem Biophys Res Commun 2006;345:886–93.
[188] Rodríguez M, Lindinger A, Ernsting NP, Malmsten M, Siegel G. Towards biosensing of arteriosclerotic nanoplaque formation using femtosecond spectroscopy. Arch Biochem Biophys 2007;460:92–9.
[189] Siegel G, Malmsten M, Schmidt A. Flow sensing at the endothelial cell membrane — blood interface. J Membr Sci 1996;113:101–13.
[190] Manning GS. Polyelectrolytes. Annu Rev Phys Chem 1972;23:117–40.
[191] Siegel G, Malmsten M, Lindman B. Flow sensing by anionic biopolyelectrolytes at the endothelial cell membrane — blood interface. In: Mathieu HJ, Reihl B, Briggs D, editors. European Conference on Applications of Surface and Interface Analysis. Chichester, New York, Brisbane, Toronto, Singapore: John Wiley & Sons; 1996. p. 38–41.
[192] Korte S, Wiesinger A, Straeter AS, Peters W, Oberleithner H, Kusche-Vihrog K. Firewall function of the endothelial glycocalyx in the regulation of sodium homeostasis. Pflugers Arch — Eur J Physiol 2012;463:269–78.
[193] Siegel G, Schnalke F, Schaarschmidt J, Müller J, Hetzer R. Hypoxia and vascular muscle tone in normal and arteriosclerotic human coronary arteries. J Vasc Med Biol 1991;3:140–9.
[194] Gouy M. Sur la constitution de la charge électrique à la surface d'un électrolyte. J Phys Théor Appl Sér 4 (Paris) 1910;9:457–68.
[195] Chapman DL. A contribution to the theory of electrocapillarity. Phil Mag 1913;25: 475–81.
[196] Stern O. Zur Theorie der elektrolytischen Doppelschicht. Z Elektrochem 1924;30: 508–16.
[197] Borst-Pauwels GWFH. Ion transport in yeast. Biochim Biophys Acta 1981;650: 88–127.
[198] Siegel G, Walter A, Rückborn K, Schnalke F, Buddecke E, Schmidt A, et al. Maintenance of the Na^{+} distribution in the arterial wall. In: Kakihana H, Hardy Jr HR, Hoshi T, Toyokura K, editors. Seventh symposium on salt, vol. II. Amsterdam, London, New York, Tokyo: Elsevier Science Publ.; 1993. p. 395–407.
[199] Siegel G. Vascular smooth muscle. In: Greger R, Windhorst U, editors. Comprehensive human physiology, vol. 2. Berlin, Heidelberg: Springer-Verlag; 1996. p. 1941–64.
[200] Bülbring E, Brading AF, Jones AW, Tomita T, editors. Smooth muscle. London: Edward Arnold; 1970.
[201] Levick JR. An introduction to cardiovascular physiology. Boca Raton: CRC Press; 2009.
[202] Siegel G, Ebeling BJ, Hofer HW. Foundations of vascular rhythm. Ber Bunsenges Phys Chem 1980;84:403–6.
[203] Mulvany MJ, Aalkjær C. Structure and function of small arteries. Physiol Rev 1990;70:921–61.
[204] Siegel G, Hofer HW, Walter A, Rückborn K, Schnalke F, Koepchen HP. Autorhythmicity in blood vessels: its biophysical and biochemical bases. Springer Series in Synergetics 1991;55:35–60.
[205] Fewtrell C. Ca^{2+} oscillations in non-excitable cells. Annu Rev Physiol 1993;55: 427–54.
[206] Bassingthwaighte JB, King RB, Roger SA. Fractal nature of regional myocardial blood flow heterogeneity. Circ Res 1989;65:578–90.
[207] Haken H. Entwicklungslinien der Synergetik. I. Naturwissenschaften 1988;75: 163–72.
[208] Haken H. Entwicklungslinien der Synergetik. II. Naturwissenschaften 1988;75: 225–34.
[209] Bülbring E, Lüllmann H. The effect of metabolic inhibitors on the electrical and mechanical activity of the smooth muscle of the guinea-pig's taenia coli. J Physiol Lond 1957;136:310–23.
[210] Siegel G. Principles of vascular rhythmogenesis. Prog appl Microcirc 1983;3:40–62.
[211] Chance EM, Curtis AR, Jones IP, Kirby CR. FACSIMILE: a computer program for flow and chemistry simulation, and general initial value problems. Harwell: UK Atomic Energy Authority; 1977.
[212] Monod J, Wyman J, Changeux J-P. On the nature of allosteric transitions: a plausible model. J Mol Biol 1965;12:88–118.
[213] Siegel G, Roedel H, Hofer HW. Basic rhythms in vascular smooth muscle. INSERM Coll 1976;50:215–32.
[214] Evans PR, Hudson PJ. Three dimensional structure of phosphofructokinase from *Bacillus stearothermophilus*. In: Hofmann E, Pfeil W, Aurich H, editors. Protein:

structure, function and industrial applications. Oxford: Pergamon Press; 1979. p. 349–57.
[215] Marquardt DL. An algorithm for least squares estimates of non-linear parameters. J Siam 1963;11:431–41.
[216] Post RL. Seeds of sodium, potassium ATPase. Annu Rev Physiol 1989;51:1–15.
[217] Läuger P, Apell H-J. Transient behaviour of the Na^+/K^+-pump: microscopic analysis of nonstationary ion-translocation. Biochim Biophys Acta 1988;944:451–64.
[218] Blackman RB, Tukey JW. The measurement of power spectra. New York: Dover Publications; 1959.
[219] Lee YW. Statistical theory of communication. New York, London: John Wiley & Sons; 1960.
[220] Siegel G, Roedel H, Nolte J, Hofer HW, Bertsche O. Ionic composition and ion exchange in vascular smooth muscle. In: Bülbring E, Shuba MF, editors. Physiology of smooth muscle. New York: Raven Press; 1976. p. 19–39.
[221] Malmsten M, Siegel G. Electrostatic and ion-binding effects on the adsorption of proteoglycans. J Colloid Interface Sci 1995;170:120–7.
[222] Siegel G, Malmsten M, Klüßendorf D, Hofer H-W. Vascular smooth muscle, a multiply feedback-coupled system of high versatility, modulation and cell-signaling variability. Int J Microcirc Clin Exp 1997;17:360–73.
[223] Gordienko DV, Tsukahara H. Tetrodotoxin-blockable depolarization-activated Na^+ currents in a cultured endothelial cell line derived from rat interlobar artery and human umbilical vein. Pflugers Arch 1994;428:91–3.
[224] Knowles RG, Palacios M, Palmer RMJ, Moncada S. Formation of nitric oxide from L-arginine in the central nervous system: a transduction mechanism for stimulation of the soluble guanylate cyclase. Proc Natl Acad Sci U S A 1989;86:5159–62.
[225] Hayashi C. Nonlinear oscillations in physical systems. New York: McGraw-Hill; 1964.
[226] van der Pol B. On a type of oscillation hysteresis in a simple triode generator. Phil Mag 1922;43:177–93.
[227] Linkens DA. Analytical solution of large numbers of mutually coupled nearly sinusoidal oscillators. IEEE Trans Circ Syst CAS 1974;21:294–300.
[228] Rosenbrock HH. An automatic method for finding the greatest or least value of a function. Comput J 1960;3:175–84.
[229] Cohen I, Daut J, Noble D. The effects of potassium and temperature on the pacemaker current, i_{K2}, in Purkinje fibres. J Physiol Lond 1976;260:55–74.
[230] Comper WD, Laurent TC. Physiological function of connective tissue polysaccharides. Physiol Rev 1978;58:255–315.
[231] Rees DA. Stereochemistry and binding behaviour of carbohydrate chains. MTP Int Rev Sci 1975;5:1–42.
[232] Manning GS. Limiting laws and counterion condensation in polyelectrolyte solutions. I. Colligative properties. J Chem Phys 1969;51:924–33.
[233] Manning GS. Limiting laws and counterion condensation in polyelectrolyte solutions. II. Self-diffusion of the small ions. J Chem Phys 1969;51:934–8.
[234] Katchalsky A, Alexandrowicz Z, Kedem O. Polyelectrolyte solutions. In: Conway BE, Barradas RG, editors. Chemical physics of ionic solutions. New York: Wiley; 1966. p. 295–346.
[235] Angyal SJ. Complex formation between sugars and metal ions. Pure Appl Chem 1973;35:131–46.
[236] Angyal SJ, Davies KP. Complexing of sugars with metal ions. Chem Commun 1971:500–1.
[237] Hubbard PS. Nonexponential nuclear magnetic relaxation by quadrupole interactions. J Chem Phys 1970;53:985–7.
[238] Bull TE. Nuclear magnetic relaxation of spin-3/2 nuclei involved in chemical exchange. J Magn Reson 1972;8:344–53.
[239] Gustavsson H, Lindman B, Bull TE. Sodium-23 nuclear magnetic resonance in polyanion solution. Correlation times and quadrupole coupling constants of sodium(+) bound to poly(methacrylic acid). J Am Chem Soc 1978;100:4655–61.
[240] Siegel G, Bostanjoglo M, Walter A, Jans AWH, Kinne R. Cation interactions in connective tissue and their relation to regulation of vascular tone. In: Halpern W, Pegram BL, Brayden JE, Mackey K, McLaughlin MK, Osol G, editors. Resistance arteries. Ithaca, New York: Perinatology Press; 1988. p. 329–35.
[241] Ohnishi T, Imai N, Oosawa F. Interaction between rod-like polyelectrolytes. J Phys Soc Jpn 1960;15:896–905.
[242] Imai N. Interaction between polyions and low molecular ions. J Phys Soc Jpn 1961;16:746–60.
[243] Oosawa F. Polyelectrolytes. New York: Marcel Dekker; 1971.
[244] Fuoss RM, Katchalsky A, Lifson S. The potential of an infinite rod-like molecule and the distribution of the counter ions. Proc Natl Acad Sci U S A 1951;37:579–89.
[245] Lifson S, Katchalsky A. The electrostatic free energy of polyelectrolyte solutions. II. Fully stretched macromolecules. J Polym Sci 1954;13:43–55.
[246] Wennerström H, Jönsson B, Linse P. The cell model for polyelectrolyte systems. Exact statistical mechanical relations, Monte Carlo simulations, and the Poisson – Boltzmann approximation. J Chem Phys 1982;76:4665–70.
[247] Dunstone JR. Ion-exchange reactions between acid mucopolysaccharides and various cations. Biochem J 1962;85:336–51.
[248] Siegel G, Walter A, Gustavsson H, Lindman B. Magnesium and membrane function in vascular smooth muscle. Artery 1981;9:232–52.
[249] Mathews MB. Trivalent cation binding of acid mucopolysaccharides. Biochim Biophys Acta 1960;37:288–95.
[250] Gelman RA, Blackwell J. Interactions between mucopolysaccharides and cationic polypeptides in aqueous solution: Chondroitin 4-sulfate and dermatan sulfate. J Biopolymers 1973;12:1959–74.
[251] Öbrink B, Sundelöf L-O. Light scattering in the study of associating macromolecules. The binding of glycosaminoglycans to collagen. Eur J Biochem 1973;37:226–32.
[252] Siegel G, Walter A, Lindman B. Cation binding to anionic biopolymers of vascular connective tissue. J Phys (Paris) 1984;45: C2-595-8.
[253] Grant GT, Morris ER, Rees DA, Smith PJC, Thom D. Biological interactions between polysaccharides and divalent cations: the egg-box model. FEBS Lett 1973;32:195–8.
[254] Frensdorff HK. Stability constants of cyclic polyether complexes with univalent cations. J Am Chem Soc 1971;93:600–6.
[255] Gould RO, Rankin AF. Calcium complexes of uronic acid monomers. Chem Commun 1970:489–90.
[256] Anthonsen T, Larsen B, Smidsrød O. NMR-studies of the interaction of metal ions with poly(1,4-hexuronates). II. The binding of europium ions to sodium methyl α-D-galactopyranosiduronate. Acta Chem Scand 1973;27:2671–3.
[257] Atkins EDT, Mackie W, Parker KD, Smolko EE. Crystalline structures of poly-D-mannuronic and poly-L-guluronic acids. Polym Lett 1971;9:311–6.
[258] Rees DA. Shapely polysaccharides. Biochem J 1972;126:257–73.
[259] Haug A, Smidsrød O. Selectivity of some anionic polymers for divalent metal ions. Acta Chem Scand 1970;24:843–54.
[260] Kohn R, Larsen B. Preparation of water-soluble polyuronic acids and their calcium salts, and the determination of calcium ion activity in relation to the degree of polymerization. Acta Chem Scand 1972;26:2455–68.
[261] Kline RP, Kupersmith J. Effects of extracellular potassium accumulation and sodium pump activation on automatic canine Purkinje fibres. J Physiol Lond 1982;324:507–33.
[262] Baumgarten CM, Isenberg G. Depletion and accumulation of potassium in the extracellular clefts of cardiac Purkinje fibers during voltage clamp hyperpolarization and depolarization. Pflügers Arch Eur J Physiol 1977;368:19–31.
[263] Toole BP. Hyaluronan and its binding proteins, the hyaladherins. Curr Opin Cell Biol 1990;2:839–44.
[264] Piculell L, Lindman B. Association and segregation in aqueous polymer/polymer, polymer/surfactant, and surfactant/surfactant mixtures: similarities and differences. Adv Colloid Interf Sci 1992;41:149–78.
[265] Siegel G, Malmsten M. The role of the endothelium in inflammation and tumor metastasis. Int J Microcirc Clin Exp 1997;17:257–72.
[266] Matrisian LM. The matrix-degrading metalloproteinases. BioEssays 1992;14:455–63.
[267] Aznavoorian S, Stracke ML, Krutzsch H, Schiffmann E, Liotta LA. Signal transduction for chemotaxis and haptotaxis by matrix molecules in tumor cells. J Cell Biol 1990;110:1427–38.
[268] Stetler-Stevenson WG, Aznavoorian S, Liotta LA. Tumor cell interactions with the extracellular matrix during invasion and metastasis. Annu Rev Cell Biol 1993;9:541–73.
[269] Tiberg F, Jönsson B, Tang J, Lindman B. Ellipsometry studies of the self-assembly on nonionic surfactants at the silica–water interface: equilibrium aspects. Langmuir 1994;10:2294–300.
[270] Stephens NL. The biochemistry of smooth muscle. Baltimore: University Park Press; 1977.
[271] Hynes RO. Integrins: versatility, modulation, and signaling in cell adhesion. Cell 1992;69:11–25.
[272] Rapraeger A, Jalkanen M, Bernfield M. Cell surface proteoglycan associates with the cytoskeleton at the basolateral cell surface of mouse mammary epithelial cells. J Cell Biol 1986;103:2683–96.
[273] Izzard CS, Radinsky R, Culp LA. Substratum contacts and cytoskeletal reorganization of BALB/c 3T3 cells on a cell-binding fragment and heparin-binding fragments of plasma fibronectin. Exp Cell Res 1986;165:320–36.
[274] Kamm KE, Stull JT. Regulation of smooth muscle contractile elements by second messengers. Annu Rev Physiol 1989;51:299–313.
[275] Gorlin JB, Yamin R, Egan S, Stewart M, Stossel TP, Kwiatkowski DJ, et al. Human endothelial actin-binding protein (ABP-280, nonmuscle filamin): a molecular leaf spring. J Cell Biol 1990;111:1089–105.
[276] Hartwig JH, Kwiatkowski DJ. Actin-binding proteins. Curr Opin Cell Biol 1991;3:87–97.
[277] Blanchard A, Ohanian V, Critchley D. The structure and function of α-actinin. J Muscle Res Cell Motil 1989;10:280–9.
[278] Watson PA. Function follows form: generation of intracellular signals by cell deformation. FASEB J 1991;5:2013–9.